ENERGY LEVELS OF ^{117}In AND ^{171}Lu

ENERGY LEVELS OF ^{117}In AND ^{171}Lu

By

PHILIP ROBERT GREGORY, B.Sc., M.Sc.

A Thesis

Submitted to the School of Graduate Studies

in Partial Fulfilment of the Requirements

for the Degree

Doctor of Philosophy

McMaster University

November 1972

DOCTOR OF PHILOSOPHY
(Physics)

McMASTER UNIVERSITY
Hamilton, Ontario

TITLE: Energy Levels of ^{117}In and ^{171}Lu

AUTHOR: Philip Robert Gregory, B.Sc. (University of Sussex)
M.Sc. (McMaster University)

SUPERVISOR: Professor M. W. Johns

NO. OF PAGES: ix, 152

SCOPE AND CONTENTS:

The energy levels of ^{117}In populated in the beta decay of ^{117}Cd and ^{117m}Cd have been studied with the aid of Ge(Li) gamma ray detectors singly and in coincidence mode. A decay scheme based on the present results is proposed and speculation is made concerning a possible interpretation of some of the levels as a rotational band based on the 1/2+[431] Nilsson orbital.

The energy levels of ^{171}Lu populated by single particle transfer reactions have been studied using an Enge spectrograph and a number of Nilsson assignments are made. These results have been complemented by a study of the gamma rays and conversion electrons following the reaction $^{169}Tm(\alpha,2n)^{171}Lu$, using Ge(Li) detectors and an on line Orange spectrometer. Assignments were made to high spin for rotational bands based on five Nilsson orbitals. In addition some interesting K forbidden interband transitions were observed and discussed in terms of Nilsson model branching ratio predictions.

ACKNOWLEDGEMENTS

My thanks are due to the supervisory committee who guided this work. They are Dr. M. W. Johns (Supervisor), Dr. D. G. Burke (member from the Department of Physics) and Dr. D. J. Kenworthy (member from the Department of Applied Mathematics).

The ^{117}Cd problem was suggested by W. B. Cook and the ^{171}Lu problem was suggested by Dr. D. G. Burke. The assistance of Dr. J. C. Waddington and Dr. Z. Preibisz for help with experiments and analysis during the course of the ^{171}Lu study is gratefully acknowledged, as are many useful discussions with R. A. O'Neil and G. Frank concerning the use of the Nilsson model program.

Thanks are also due to Dr. Horoshko and Dr. Harar of the Nuclear Structure Laboratory at Rochester for permission to make extensive use of their (^{3}He,d) and (α,t) reaction data, to levels in ^{117}In, prior to publication.

Scholarship support was made available through the Province of Ontario.

TABLE OF CONTENTS

LIST OF FIGURES

LIST OF TABLES

CHAPTER 1

THEORETICAL CONSIDERATIONS

1.1 Introduction

The nuclear physicist faces two basic problems; he does not know the form of the nucleon-nucleon interaction and he can not handle the number of degrees of freedom involved in a calculation of the nuclear wave function. These two problems are inextricably linked in our use of models as a means of simplification.

A model is a method of transferring some relationship or process from its actual setting to a setting where it is more conveniently studied.

Mathematics is a model kit. There are pieces which fit together according to certain rules. Using the standard pieces one can represent a real life situation. Once the transformation has been made the model is allowed to work according to its own rules. If successful, its predictions will be in agreement with experimental results.

There have been a great number of models proposed to describe nuclear properties. Each is limited in scope. Some are successful only for certain nuclear mass regions, others describe only specific aspects of nuclear behaviour .

One of the most widely used is the shell model which is based on a quasi-atomic approach to the nuclear system. Its surprising success is based on two basic properties of nuclear matter. The first, saturation, describes the observation that all nucleons have the same binding energy and density. Nuclear matter theory shows that these characteristics arise from the specifics of the strength and shape of the nucleon-nucleon potential together with the consequences of the exclusion principle. The second key empirical fact is that the mean free path of a low energy nucleon moving through nuclear matter is relatively long compared to a nuclear radius. It appears that the nucleus is a very cold Fermi system. Most states below the Fermi level are occupied, so that only a nucleon with initial energy above the Fermi level can scatter from another nucleon.

The remainder of this chapter deals with specific aspects of some nuclear models and roughly traces their historical development.

1.2 The Nuclear Shell Model

The basic idea of the nuclear shell model is that the interaction of any one nucleon within the nucleus with the remaining nucleons can be mainly represented by a static potential well whose shape and spatial extension is expected to be similar to that of the nuclear density distribution. In such a potential well there will be a series of single

particle energy levels characterized by the quantum numbers n, ℓ, j.

In the atomic case a similar procedure successfully predicts "closed shell" configurations characterized by a lack of low-lying excited states. Physically these occur at the noble gases (Ne, A, Kr, X). Such closed shell effects exist in nuclei at the so called "magic nucleon numbers" 2, 8, 20, 28, 50, 82 and 126. However it was found that there is no reasonable form for the central potential which leads to these numbers. This impasse was surmounted by Mayer (1949, 1950) and independently by Haxel, Jensen and Suess (1949, 1950) by postulating a coupling between the spin of the nucleon and its orbital angular momentum. It is necessary that this force be about 20 times stronger and of opposite sign to the force expected from a consideration of the magnetic spin-orbit interaction experienced by an electron in an atom. Thus it is due to nuclear forces, and not to electromagnetic phenomena or small relativistic effects. Its effect is to raise those states for which $j = \ell - \frac{1}{2}$ and depress those for which $j = \ell + \frac{1}{2}$, thus causing some high spin levels to be depressed into the next lowest shell. Figure 1.1 shows the ordering of the shell model levels using a simple harmonic oscillator potential with the $\ell \cdot s$ force. Each level is labelled by $n\ell j$ and may contain $2j+1$ neutrons or protons corresponding to different values of the orientation of the

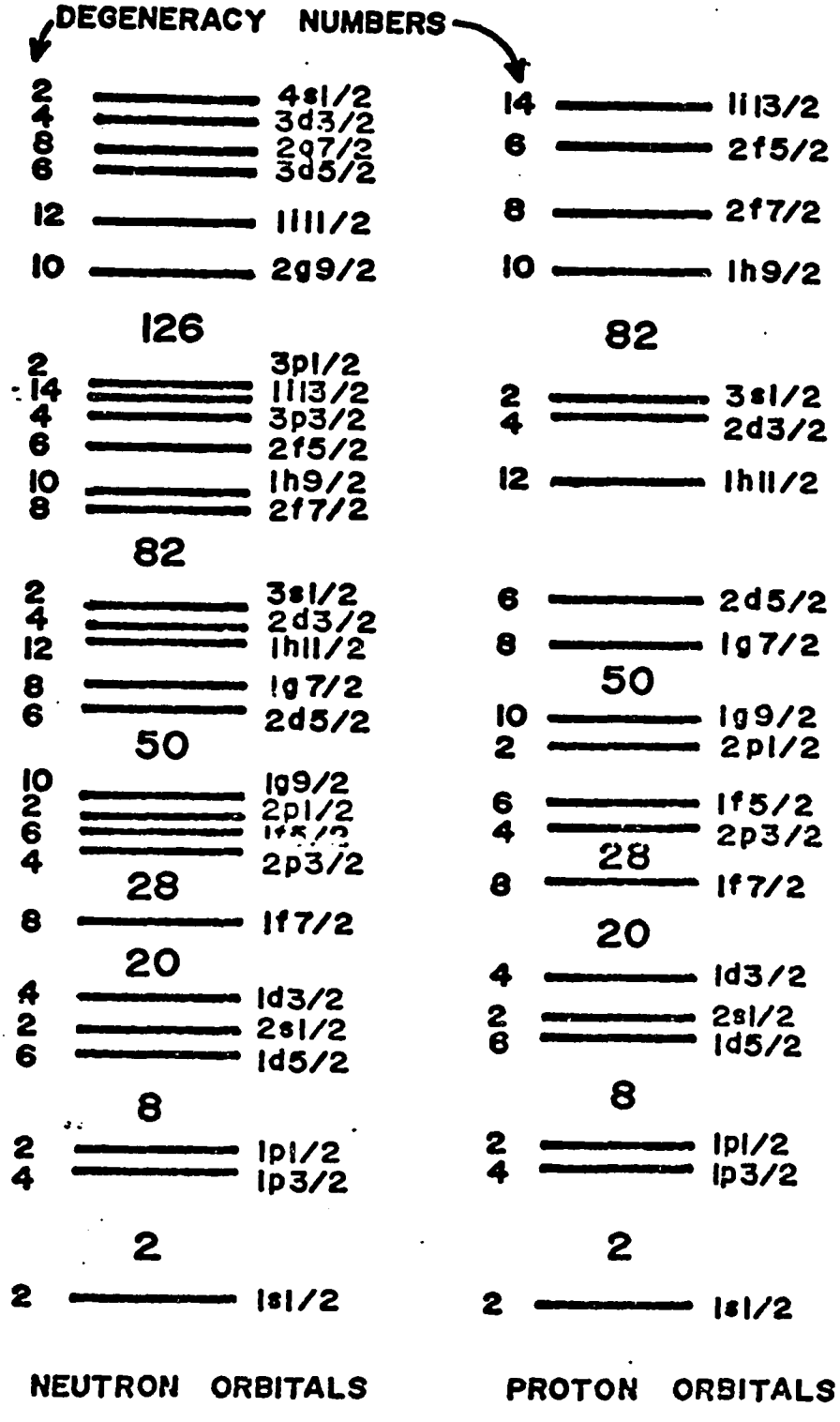

Figure 1.1 Ordering of shell model levels arising from a simple harmonic oscillator potential plus a spin orbit interaction.

spin quantum number j. It appears also that pairs of particles having equal and opposite values of this spin orientation quantum number find it energetically favourable to couple, so that the resultant angular momentum is zero. For a nucleus containing even numbers of neutrons and protons, all coupled pair wise, the total angular momentum is zero, and since the pairs are symmetric under inversion the system has positive parity. However, for an odd A nucleus, in the last neutron or proton energy level to be filled there is either an odd neutron or an odd proton which is unpaired. In its simplest form, the shell model predicts that the spin and parity of the nucleus will be that of the unpaired nucleon. More sophisticated calculations consider all possible couplings of the extra core nucleons, assuming some simple form for the "residual interaction".

Such procedures have been very successful for nuclei with nucleon numbers close to the magic numbers, however there is a large body of experimental evidence which suggests that in certain mass regions ($A \sim 20$, $150 < A < 190$, and $A > 220$) away from closed shells nuclei have a non spherical stable shape. This shape can be explained in terms of the quadrupole interaction between nucleons. Pairing forces tend to produce a spherical equilibrium shape whereas the quadrupole force gives rise to a tendency for each nucleon to align its orbit with the average field produced by all the other nucleons, thus producing a deformed equilibrium shape.

When the field becomes deformed the angular momentum of a particle orbital ceases to be a good quantum number and the particle wave functions are spread over a number of j orbitals. States of good total angular momentum are generated by coupling the intrinsic angular momentum with a rotational angular momentum.

Before continuing to a discussion of the rotational Hamiltonian it is appropriate to consider a little more closely the effects of the short-range pairing forces. It is noted above that it is the balance between the pairing force and the quadrupole force which determines the equilibrium shape of the nucleus. In addition, the pairing force tends to destroy the independent particle structure, which is a basic assumption of the shell model approach, and causes a diffuseness of the Fermi surface. This difficulty is best overcome by introducing the concept of quasi-particles. The quasi-particle can be considered as a conjugate pair (j,m) and (j-,m), that is as a particle in the state (j,m) and a hole in the state (j,-m). The correlation produced by the interaction between pairs of particles is such that the levels of the simple shell model are no longer filled or empty in the usual sense. Instead particle hole pairs or quasi-particles are distributed amongst these levels in a correlated fashion. Thus in a given state of the nucleus a particular shell model level (n,ℓ,j) has a probability $V^2_{n\ell j}$ of being occupied and $U^2_{n\ell j}$ of being empty.

Under a simple transformation from particles to quasi-particles the energies of the shell model levels ($\varepsilon_{nj\ell}$) become

$$E_{n\ell j} = [(\varepsilon_{nj\ell} - \lambda)^2 + \Delta^2]^{\frac{1}{2}} - \Delta$$

where λ is a parameter for the position of the Fermi level and Δ, the diffuseness, is a measure of the pairing strength.

The formalism for handling correlated pairs of particles was originally developed by Bardeen, Cooper and Schreiffer (1957) in dealing with the problem of superconductivity. The application to nuclear physics was made by Bohr, Mottelson and Pines (1958).

1.3 Collective Motion in Nuclei

The collective properties of a many body system are, as the name implies, those in which a large number of nucleons are involved, moving in a more or less correlated fashion. Since the shell model contains in principle a full description of nuclear properties it is theoretically capable of handling all collective properties. However it is found that not only is the calculation prohibitively large but that a greater insight may be achieved by approaching the problem from a completely different direction.

In the liquid drop model individual nucleons are completely ignored. Nuclear properties are calculated using a semi-classical procedure based on an analogy with a fluid droplet. When applied in detail to the low-lying excited

levels of nuclei, the liquid drop model is inadequate. It predicts too few levels, and these are far too widely spaced. However it does predict large quadrupole moments and the strong enhancement of E2 transitions which are characteristic features of many deformed nuclei. Bohr (1952) and Bohr and Mottelson (1953) fused the individual-particle and liquid-drop aspects of the nuclear system into a successful "unified" model.

If the collective motions, vibrations and rotations, of the deformed nucleus are slow compared with the frequency of particle motions then the nuclear wave function may be separated and written as a simple product. In the highly deformed nuclear mass region vibrational motion does not play a very important role in odd A nuclei. Accordingly it will be omitted from the following discussion. The separated wave function may be written as

$$\psi = D_{rot}\chi_{int}$$

where D_{rot} describes the orientation of the nuclear shape, and χ_{int} the motion of the nucleons in a distorted potential well. This was first suggested by Bohr (1952) and is known as the adiabatic assumption. Non adiabatic effects are treated as small pertubations.

The nuclear Hamiltonian may be written in the form

$$H = H_{int} + T_{rot} + H_{coupl}$$

where H_{int} is the intrinsic or particle Hamiltonian, T_{rot} is the kinetic energy operator of the rotational motion and H_{coupl} couples the rotation and intrinsic motions. Of course for the adiabatic assumption to be valid it is necessary that H_{coupl} be small relative to H_{int} and H_{rot}.

Now for a rigid body with body fixed axes x', y', z'

$$T_{rot} = \frac{\hbar^2}{2\mathcal{J}_{x'}} R_{x'}^2 + \frac{\hbar^2}{2\mathcal{J}_{y'}} R_{y'}^2 + \frac{\hbar^2}{2\mathcal{J}_{z'}} R_{z'}^2$$

This may be simplified by assuming axial symmetry, for which $\mathcal{J}_{x'} = \mathcal{J}_{y'} = \mathcal{J}_o$ and $R_{z'} = 0$. $\mathcal{J}_o$ may be regarded as a variable parameter to allow for non rigid nuclei. Thus

$$T_{rot} = \frac{\hbar^2}{2\mathcal{J}} R^2 .$$

Figure 1.2 shows the quantum numbers appropriate for rotations coupled to particle motion.

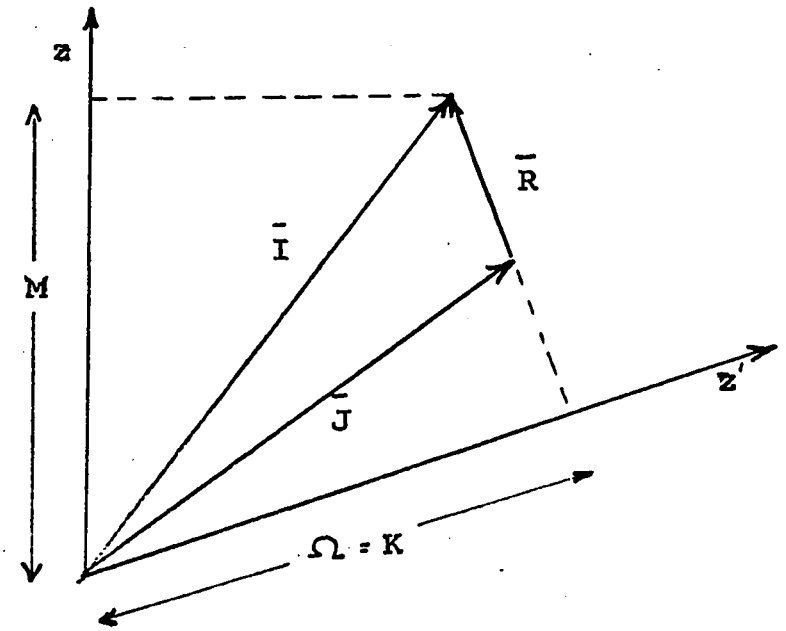

Figure 1.2. Coupling scheme in the rotational wave function

The projection of the intrinsic spin J on the body fixed axis is labelled Ω, for the case of axial symmetry this is equal to K, the projection of the total spin I. The space fixed axis is denoted by z.

Using the relationship $\bar{R} = \bar{I} - \bar{J}$, the rotational term in the Hamiltonian may be written

$$T_{rot} = \frac{\hbar^2}{2\mathcal{J}} [I^2 - 2(\bar{I}\cdot\bar{J}) + J^2]$$

the term $\frac{\hbar^2}{2\mathcal{J}} J^2$ is a function only of the intrinsic motion and may be incorporated into H_{int}. Accordingly the total Hamiltonian becomes

$$H = H_{int} + \frac{\hbar^2}{2\mathcal{J}} I^2$$

where the term H_{coupl} is neglected and the the term $\frac{\hbar^2}{\mathcal{J}} (\bar{I}\cdot\bar{J})$ is omitted for the time being. The appropriate definite parity normalized eigenfunction may be derived (Elliott 1958) using the rotational eigenfunctions $D^I_{MK}(\theta)$ derived by Bohr (1952). The result is

$$\psi(IKM) = \left[\frac{2I+1}{16\pi^2}\right]^{\frac{1}{2}} \{D^I_{MK}(\theta)\chi_K(\lambda') + (-1)^{I-J} D^I_{M-K}(\theta)\chi_{-K}(\lambda')\} .$$

A set of states, all of which involve the same intrinsic function $\chi_K(\lambda')$ but have different values of I is called a rotational band. From the properties of D^I_{MK} functions

$$\frac{\hbar^2}{2\mathcal{J}} I^2 \psi(IKM) = \frac{\hbar^2}{2\mathcal{J}} I(I+1)\psi(IKM) .$$

Hence the familiar I(I+1) energy spacing of rotational bands.

The term $\frac{\hbar^2}{\mathcal{J}}(\bar{I}\cdot\bar{J})$ is called the decoupling term as it measures the decoupling of the intrinsic motion $\bar{J}$ from the body fixed symmetry axis. Its effect is to mix the wavefunctions of bands for which $\Delta K = 1$. This is referred to as Coriolis coupling. In general the energy spacing between rotational bands is much greater than the off diagonal matrix elements linking these bands and so the effect on the rotational spectrum may be considered as a perturbation. In one case, however, the coupling term does have diagonal matrix elements. This occurs for $K = \frac{1}{2}$ bands and is a consequence of the symmetry of the wavefunction for $K = \pm\frac{1}{2}$. That is the Coriolis interaction may couple the two parts of the total wave function with $K = +\frac{1}{2}$ and $K = -\frac{1}{2}$.

The correction term may be easily derived (Elliott 1958) with the result that the energy spectrum of a rotational band may be given by

$$E_K(I) = E_K + \frac{\hbar^2}{2\mathcal{J}}\left[I(I+1)+a(-1)^{I+\frac{1}{2}}(I+\tfrac{1}{2})\delta_{K,\frac{1}{2}}\right].$$

The term a is called the decoupling parameter; like $\mathcal{J}$ it is usually regarded as a variable parameter.

When rotational bands for which $\Delta K = 1$ lie close together in energy, Coriolis mixing has to be explicitly taken into account. Its importance was first emphasized by Kerman (1956).

For levels of spin I in rotational bands K and K+1

we have unperturbed energies $E_K(I)$ and $E_{K+1}(I)$. To find the perturbed energies it is necessary to diagonalize a 2×2 matrix

$$\begin{vmatrix} E_K(I) & C \\ C & E_{K+1}(I) \end{vmatrix}$$

where C is the matrix element

$$(IMK+1| -\frac{\hbar^2}{\mathcal{J}} (\bar{I}\cdot\bar{J}) |IMK)$$

$$= [(I-K)(I+K+1)]^{\frac{1}{2}} A_K \quad \text{(Elliott 1958)}$$

where A_K must be calculated from some specific model of the intrinsic motion.

The solutions to the secular equation are expanded as a power series in the parameter

$$\varepsilon = \frac{2|A_K|[(I-K)(I+K+1)]^{\frac{1}{2}}}{E_{K+1}(I)-E_K(I)}$$

which leads in first order to the expression for the perturbed rotational energies (Rowe 1970)

$$E(I) = E_K^{\,o} + \frac{\hbar^2}{2\mathcal{J}}[I(I+1)+a(-1)^{I+\frac{1}{2}}(I+\tfrac{1}{2})\delta_{K,\frac{1}{2}}]$$

$$+ \frac{A_K^{\,2}}{E_K(I)-E_{K+1}(I)}[I(I+1)-K(K+1)] \ .$$

Provided the moments of inertia are the same for both bands the denominator of the perturbation term is independent of I. Thus the effect of the band mixing is a renormalization of the inertial parameter. The band lower in energy gets de-

pressed while the upper band is expanded.

The effect of band mixing most strongly affects the transition rates for transitions between bands of different K where the change in K is greater than the multipolarity of the transition. The pure rotational model forbids such transitions so even small admixtures of the wavefunctions, brought about by stepwise coupling of bands for which $\Delta K = 1$, produce drastic changes in the branching rates.

Finally it may be noted that the assumption of axial symmetry made above is generally found to be a reasonable one. However the non axially symmetric case has been considered (Davydov and Filippov 1958) and is found to have some success, particularly in the transition regions between spherical and strongly deformed nuclei.

CHAPTER 2

FURTHER COMMENTS ON NUCLEAR MODELS

2.1 The Nilsson Model

Single particle states in the deformed region are described very well by using the shell model approach but with an axially-symmetric deformed potential such as the one proposed by Nilsson (1955). The single-particle Hamiltonian to be used is,

$$H = H_o + C\bar{\ell}\cdot\bar{s} + D\ell^2 \ .$$

The first term is a deformed harmonic oscillator potential, and the second term is the spin-orbit force discussed in Chapter 1. The term $D\ell^2$ is introduced to simulate the main difference between the oscillator and square well potentials, the effect of the latter potential being to depress states with high ℓ. This is necessary since the tendency of the square well is to favour prolate deformed shapes, as opposed to oblate, and it is found in the region of large deformation that all nuclei have prolate shapes. The result is to perturb the (2j+1) fold degeneracy of a spherical potential state of spin j, as shown in figure 2.1. Each state is labelled by $K\pi[Nn_3\Lambda]$, where N is the major oscillator quantum number, n_3 its projection on the symmetry axis and Λ the projection on the symmetry axis. These are known as the asymptotic quantum

numbers since they are only constants of motion in the limit of large deformation. The figure shows energy dependence of each state with the deformation parameter δ.

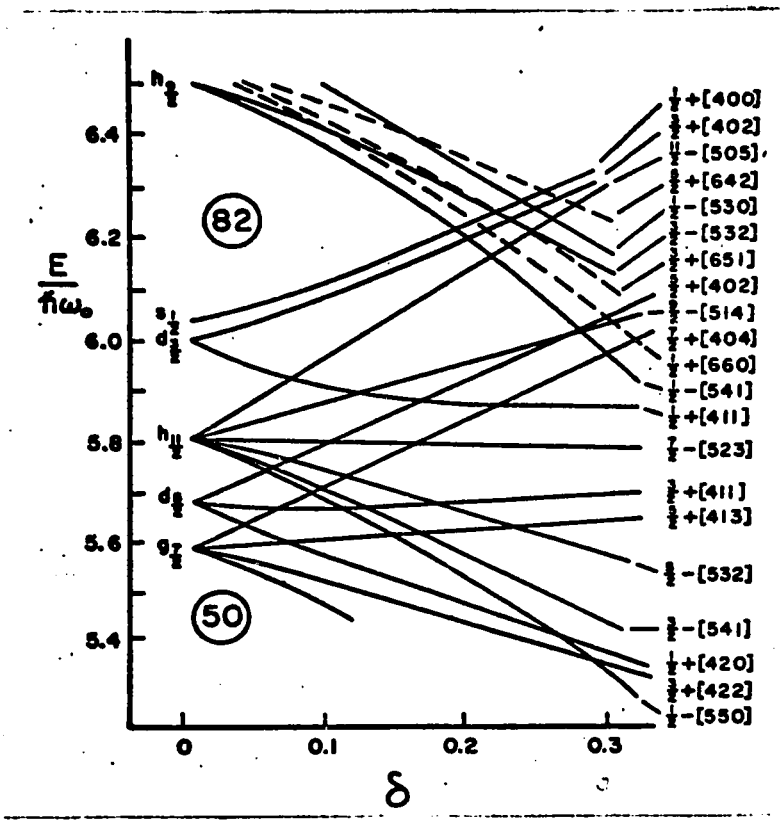

Figure 2.1 Partial Nilsson diagram for proton states in the rare earth region

In its simplest form for odd A nuclei the Nilsson model assumes only axially symmetric nuclei and allows only the last particle to have any intrinsic motion. A convenient representation chosen by Chi (1967) uses isotopic harmonic oscillator eigenvectors as the set of base vectors. Then the Nilsson wave functions χ_K may be written

$$\chi_K = \sum_j C_{j\ell} |N\ell jK\rangle$$

Thus the expansion of a state such as the $1/2^+[411]$ will contain five terms corresponding to the $1/2$ projections of the $g_{9/2}$, $g_{7/2}$, $d_{5/2}$, $d_{3/2}$ and $s_{1/2}$ shell model states which occur in the N = 4 oscillator shell. The expansion coefficients $C_{j\ell}$ which can be calculated for a given nuclear deformation can be experimentally extracted from pickup and stripping reaction cross sections.

Nilsson model calculations were made during the course of the present work using a computer program that was due originally to Chi (1967) and was modified by O'Neil (1970). In this program the quasiparticle energies are given by

$$E^K_{qp} = [(\epsilon_K - \lambda)^2 + \Delta^2]^{1/2} - \Delta$$

where ϵ_K is the Nilsson single particle energy, λ is the energy of the Fermi surface and 2Δ the pairing energy. The members of the unperturbed bands are assumed to have energies given by

$$E_K(I) = E^K_{qp} + A\left[I(I+1)-K^2\right] + a(-1)^{I+1/2}(I+1/2)\delta_{K,1/2}\Big) .$$

The Coriolis matrix element between orbitals with quantum numbers K and K+1 is given by

$$V^{K,K+1} = -\alpha A_{av} \sum_j C^K_{j\ell} C^{K+1}_{j\ell} \sqrt{(j-K)(j+K+1)} \quad \sqrt{(I-K)(I+K+1)}$$

$$\times (U_K U_{K+1} + V_K V_{K+1})$$

where A_{av} is the average of A_K and A_{K+1}. The occupational amplitudes U_K and V_K may be expressed in terms of the single particle energies ε_K, the Fermi level λ, and the pairing gap Δ as

$$U_K^2 = \frac{1}{2}\left(1 + \frac{\varepsilon_K-\lambda}{\sqrt{(\varepsilon_K-\lambda)^2+\Delta^2}}\right) \quad , \quad V_K^2 = \frac{1}{2}\left(1 - \frac{\varepsilon_K-\lambda}{\sqrt{(\varepsilon_K-\lambda)^2+\Delta^2}}\right).$$

The term α is an attenuation factor which is used as an adjustable parameter to adjust the strength of the Coriolis interaction. It is found in general that an attenuation factor between 0.6 and 1 is required (Lovhøiden et al. 1972).

The rotational energy matrix is thus constructed and diagonalized in the space of all the Nilsson orbitals which lie within one or two MeV of the Fermi surface.

2.2 Non-Adiabatic Effects

When higher order terms in the expansion describing the Coriolis term are taken we may write for K = 0 bands

$$E_o = AI(I+1) + BI^2(I+1)^2 + CI^3(I+1)^3 + \ldots$$

while for $K \neq 0$ we obtain in addition some decoupling terms due to the fact that the rotational wave function contains one part in which the projection of the spin on the body fixed axis is K and one where it is -K. Thus we have (Nathan

and Nilsson 1965)

$$\Delta E_{\frac{1}{2}} = (-1)^{I+\frac{1}{2}}(I+\tfrac{1}{2})[A_1+B_1 I(I+1)+ \ldots]$$

$$\Delta E_{\frac{3}{2}} = (-1)^{I+\frac{3}{2}}(I-\tfrac{1}{2})(I+\tfrac{1}{2})(I+3/2)[B_3+C_3 I(I+1)\ldots]$$

etc.

Calculations (Chan 1966 and Hamamoto and Udagawa 1969) based on the cranking model and the Nilsson model including the pairing force have been quite successful in predicting values of the B parameter. Other studies have ascribed the observed $I^2(I+1)^2$ energy dependence to centrifugal stretching(Stephens et al 1965).

Thus in general rotational bands are described well by the expression (Hamamoto and Udagawa 1969)

$$E_{rot} = A[I(I+1)-K^2] + B[I(I+1)^2-K^2]^2 + \ldots.$$

$$+ (-1)^{I+K} \prod_{i=1-K}^{K} (I+i)[A_{2K}+B_{2K}[I(I+1)-K^2]+\ldots.]$$

where the parameters A, B, A_{2K}, B_{2K} etc. are determined by making a least squares fit to the level energies. However this procedure is unsuccessful for rotational bands which are appreciably Coriolis mixed because a large number of terms are required in the expansion to obtain a fit. On the other hand most Coriolis mixing calculations do not include in the energy expression any of the higher order terms of the expansion. In the present work it is found that the rotational energy

spacings can be reproduced with the introduction of just one extra parameter. Thus the unperturbed energy levels in the Coriolis mixing calculation are given by

$$E_K(I)=E^K_{q,p}+[A+B(I(I+1)-K^2)]\times[I(I+1)-K^2+a(-1)^{I+\frac{1}{2}}(I+\tfrac{1}{2})\delta_{K,\frac{1}{2}}]$$

When written in this way the form of the expression suggests a rotational parameter which varies with spin. The reason for this emphasis is that the variable moment of inertia model (Mariscotti et al 1968) has been extended to include odd A nuclei and has been shown to be very successful in describing the ground state band of ^{171}Lu (Gregory and Taylor 1972) Appendix A.

2.3 Rotational Model Predictions of Transition Rates

Analysis of the angular momentum properties of the radiation field leads to the well known classification into electric and magnetic multipoles. For deformed nuclei the appropriate operators may be simply transformed from the laboratory system to a coordinate system fixed in the nucleus. Upon writing out the reduced matrix element (Nathan and Nilsson 1965) it becomes apparent that the matrix element vanishes if the multipole order λ is less than the change in K value. The so called K forbiddenness. Moreover for $|K_i-K_f| \leq \lambda < K_i+K_f$ the branching from an arbitrary state to any two members of one rotational band is independent of any intrinsic matrix element and depends only on a ratio of two Clebsch-Gordon coefficients (Alaga et al. 1955). That is

$$\frac{B(\lambda, I_i \to I_f')}{B(\lambda, I_i \to I_f)} = \frac{\langle I_i \lambda K_i (K_f - K_i) | I_f, K_f \rangle^2}{\langle I_i \lambda K_i (K_f - K_i) | I_f K_f \rangle^2} .$$

In practice K forbidden transitions are frequently observed. It is found that they are generally hindered by $\sim 100\times(\Delta K-\lambda)$ over allowed transitions.

According to the rotational model (Nathan and Nilsson 1965) the reduced transition probabilities for gamma transitions within a rotational band are given by

$$B(E2, KI_i \to KI_f) = \frac{5}{16\pi} e^2 Q_o^2 \langle I_i, 2, K, 0 | I_f, K \rangle^2$$

$$B(M1, KI_i \to KI_f) = \frac{3}{16\pi} e^2 \lambda^2 (g_K - g_R)^2 K^2 F(U_i, I_f, K)^2$$

with $F = (I_i, I_f, K) = \langle I_i, 1, K, 0 | I_f, K \rangle (1+\delta_{K,\frac{1}{2}} b_o (-1)^{I_g + \frac{1}{2}})$

where e is the charge of an electron, Q is the quadrupole moment, g_K and g_R are the gyromagnetic factors of particle motion and rotational motion respectively, λ is the Compton wavelength of the proton and I_g is the greater of I_i and I_f.

From the above formulae one can derive the M1/E2 mixing parameter

$$\frac{1}{\delta^2} = I_\gamma(M1, I \to I-1) / I_\gamma(E2, I \to I-1)$$

$$= \frac{1.148}{E_\gamma (I \to I-1)^2_{MeV}} \left[\frac{g_K - g_R}{Q_o}\right]^2 (I+1)(I-1)(1+(-)^{I+\frac{1}{2}} b_o \delta_{K,\frac{1}{2}})^2 .$$

The cascade to crossover gamma intensity ratio can be expressed

in terms of this mixing ratio (Winter et al. 1970)

$$\frac{I_\gamma(I\to I-1)}{I_\gamma(I\to I-2)} = \frac{E(I\to I-1)^5}{E(I\to I-2)^5}\,\frac{2K^2(2I-1)}{(I+1)(I+K-1)(I-K-1)}\,\left(1+\frac{1}{\delta^2}\right)$$

so that for $K \neq \frac{1}{2}$

$$\left(\frac{g_K-g_R}{Q_o}\right)^2 = \frac{E(I\to I-1)^2_{MeV}}{1.148(I+1)(I-1)}\left(\frac{I_\gamma(I\to I-1}{I_\gamma(I\to I-2)}\,\frac{E(I\to I-2)^5}{E(I\to I-1)^5}\,\frac{(I+1)(I+K-1)(I-K-1)}{2K^2(2I-1)}\right.$$

$$\left.-1\right)$$

In the absence of Coriolis mixing this term is considered a constant for the band; the spin dependence of the relative B(M1) and B(E2) is almost exactly cancelled by the spin dependence of the rotational energies.

2.4 The Statistical Model and (ion,xnγ) Reactions

As was mentioned at the beginning of Chapter 1, certain models are appropriate only for very specific aspects of nuclear behaviour. Such is the statistical model which describes the evaporation of particles from a compound nucleus.

The type of reaction where the incoming projectile forms a compound nucleus with the target and then proceeds to evaporate several neutrons or charged particles has been known for a number of years. With light nuclei where the Coulomb barrier is small a variety of reactions occur and, for example, protons and alpha particles as well as neutrons are emitted; with medium and heavy nuclei the Coulomb barrier strongly inhibits charged particle emission so that the dominant mode

of decay is evaporation of neutrons. Under these circumstances the reaction has the great virtue that, by choosing the appropriate bombarding energy, it is possible to make one final product nucleus almost uniquely and with large cross section. Initially, Moringa and Gugelot (1963) studied the ground state bands of even-even nuclei using the (α,xn) reaction, since then the method has been extended to odd A nuclei using a number of heavier ions as projectiles.

The first step in any calculation for these reactions is to evaluate the angular momentum brought into the system. This is done with an optical model program. Next it is necessary to consider how the compound nucleus will decay. According to the statistical model, the relative probability of neutron and alpha decay depends on the transmission coefficients and the available phase space. Thus the relative probabilities depend directly on the relative level densities in the final nuclei. For emission of particles of zero angular momentum the transmission coefficients will be roughly unity for neutrons of all energies, but only for alpha particles having energies above the Coulomb barrier. This energy difference gives rise to a large difference in level density which causes neutron emission to dominate. Measured and calculated (α,xn) cross sections (Kurz et al. 1971) are shown in fig. 2.2.

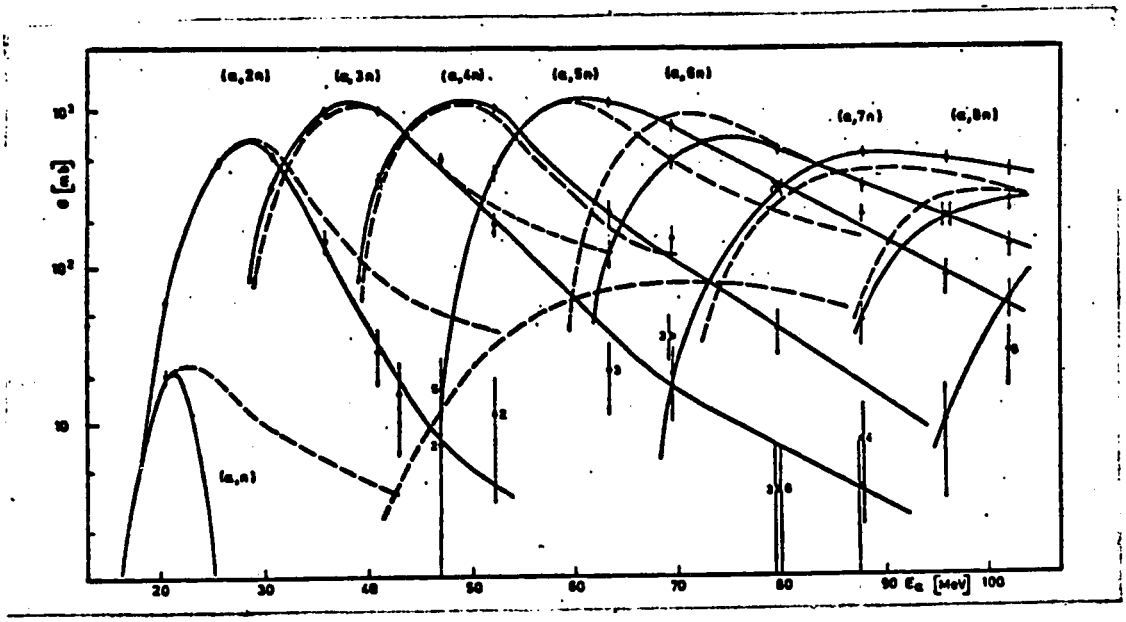

Figure 2.2 Measured (dashed curves) and calculated (full curves) $^{197}Au(\alpha,xn)$ cross sections (Kurz et al.1971)

Grover and Gilat (1967) introduced the very useful concept of the Yrast line. The energy taken up by the rotation of the nucleus is given by

$$E_I = \frac{\hbar^2}{2\mathcal{J}} I(I+1) \quad .$$

One would not expect to find any levels of spin I below $E = E_I$. The level of spin I with the lowest energy is known as the yrast level as shown schematically in figure 2.3.

In the region above the yrast line the gamma rays will cascade down by electric dipole transitions until they reach the yrast line, giving rise to a very large number of

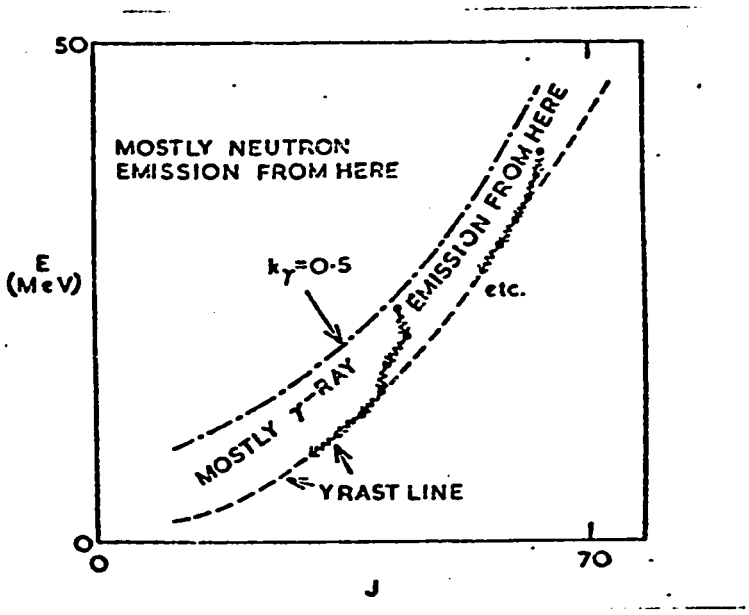

Figure 2.3 Schematic diagram illustrating the region of excitation energy and angular momentum in which most de-excitation is by γ radiation (Grover and Gilat 1967).

unresolved gamma rays. Once the yrast line is reached gamma de-excitation is along it, at some point the yrast line becomes a distinct rotational band in the final nucleus. In general this is the ground state band since this is most likely to have the lowest energy levels of a given I. Thus, although the ground state band may be present in the gamma spectrum up to high spin sidebands may be only weakly fed.

One feature of reactions of the type (ion,xn) which has proved to be quite useful in making assignments of gamma transitions is the anisotropy of the emitted gamma rays and conversion electrons. The excited state in the compound nucleus has a strong spin alignment in the plane perpendicular to the beam direction. The evaporated neutrons with low energy and

low angular momentum do not disturb this alignment very much. consequently the angular distribution of the de-exciting gamma rays in the final nucleus is found to depend on the spins of the excited levels and the transition. This feature was first exploited in (ion,xn) reactions by Ejiri et al (1966). Their work gives an outline of the statistical model calculation used to analyze the angular distributions.

2.5 Single Particle Transfer Reactions

Single particle transfer reactions are a class of direct reactions. That is reactions in which the nucleons of the target nucleus are thought to remain undisturbed. One nucleon is simply transferred, with the outgoing particals bearing information about the populated state.

The method of calculating such reactions uses a number of approximations but nevertheless is quite successful. The target potential, described by the optical model, distorts the incoming plane waves, described by the distorted wave Born approximation. A particle is transferred, and the scattered particle moves away from the residual nucleus.

For an even even target nucleus and a stripping reaction the differential cross section is given by

$$\frac{d\sigma}{d\Omega} = 2N\sigma_{\ell}(\theta)C_{j\ell}{}^{2}U^{2}$$

The terms $C_{j\ell}$ and U have been previously defined. The intrinsic single particle cross sections $\sigma_{\ell}(\theta)$ contain no

nuclear structure information. A full expression for this term and details of the calculation are given by O'Neil (1972).

The expression $\frac{d\sigma}{d\Omega} / 2N\sigma_{\ell}(\theta)$ is known as the spectroscopic factor and may be compared with the term $C_{j\ell}^2 U^2$ calculated from the Nilsson model. The normalization factor N is a calculated term which is found to be only approximately accurate. To allow a comparison of spectroscopic factors the usual procedure is to renormalize for a prominent state for which the spectroscopic factor is thought to be known from a nuclear model.

As another aid to the identification of states it may be noted that the "strength" of the reaction is spread to several members of the rotational band built on a particular Nilsson orbital. Since a given single particle Nilsson wave function is characterized by the expansion coefficients, $C_{j\ell}$, the relative cross sections of the different rotational members will form a distinctive pattern. Also, since there is just one coefficient, $C_{j\ell}$, from each of the shell model states which appear in the oscillator shell there will be a limited number of members of a rotational band which can be populated by the reaction. That is, members of the band will be populated to $j = N+1/2$.

CHAPTER 3

INSTRUMENTS AND TECHNIQUES

3.1 Introduction

A number of techniques are available for the study of nuclei. Those used in this work are described below.

The facilities at McMaster for nuclear studies include a pool type, enriched fuel, nuclear reactor. The neutron flux at the irradiation position is 1.3×10^{13} neutrons/cm^2/sec. One particular feature which proved useful for the ^{117}Cd decay study is a pneumatic sample irradiation and delivery system.

The other main facility is a High Voltage FN type tandem Van de Graaf ion accelerator. Some of the features of this machine and the experimental areas are shown in fig. 3.1. A duo-plasmatron ion source offers a large variety of available ion beams from protons to carbon. The maximum terminal voltage is 9 MV, energy stability is good to 1 part in 10,000. Stabilization is by means of a feed back system from slits just after the analyzing magnet to the corona points near the terminal. The system is capable of holding stable beams as small as 0.5 namps. This last feature is especially important for the present on line gamma studies where it was found that the optimum peak to background ratio was achieved with the

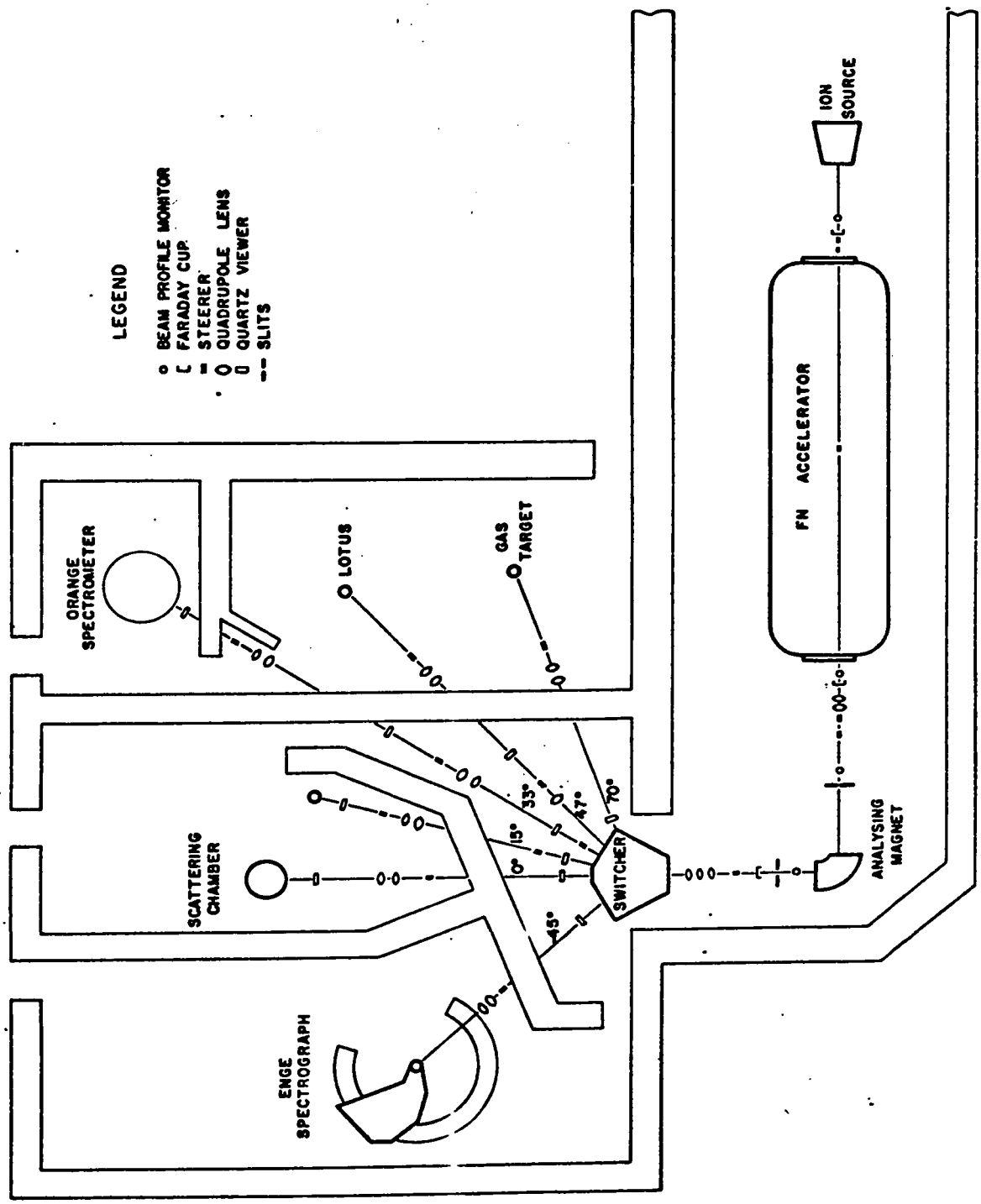

Figure 3.1 The McMaster F.N. tandem accelerator and experimental areas

detectors very close to the target thus requiring a corresponding reduction in beam current. It is also important to avoid oscillations in current as these produce an effective dead time in the analyzer much greater than is recorded, with a consequent degradation in detector energy resolution.

3.2 Germanium Semiconductor Spectrometers

The high data accumulation rate of a pulse amplitude analyzer fed by a detector which totally absorbs photons or charged particles to produce a signal linearly proportional to the energy absorbed has made such techniques very useful for nuclear measurements.

At the present time lithium drifted germanium semiconductor (Ge(Li)) detectors are almost exclusively used for measuring gamma radiation. They consist of a single crystal of high purity p doped germanium in which a region containing no free charge carriers is created by drifting lithium ions into the crystal. An incident photon, absorbed in the depleted region, creates electron hole pairs. These are swept out, by applying a reverse bias voltage to the crystal, to produce a charge pulse proportional to the energy of the incident photon.

The first stage of amplification is by means of a charge sensitive pre-amplifier. This is mounted as close as possible to the detector to minimize input capacitance, thus optimizing signal-to-noise ratio. The main amplifier stage includes pulse shaping networks and can be followed by a base

line restoration device which prevents high count rates from degrading the resolution.

The unipolar voltage pulses are digitized in the analogue to digital converter of a multichannel analyzer. This and other components of the whole system are indicated schematically in fig. 3.2.

The gamma ray spectra were stored on magnetic tape and were analyzed, following experiments, using the McMaster CDC 6400 computer. The positions and areas of the peaks in these spectra were obtained by means of a nonlinear, least-squares, curve-fitting program (Williams and McPherson 1968). In this program peaks are fitted by least squares to the function.

$$I(x) = \alpha+\beta x + \sum_{i=1}^{\leq 6} I_i \int_{-\infty}^{x_i} \exp[\varepsilon(y-x_i)]\exp-[\delta(x-y)^2]dy$$

where $I(x)$ is the number of counts in channel x, α and β are parameters determining the background and I_i and x_i are the intensity and position of the i^{th} peak whose width and skewness are defined by δ and ε. The program permitted the fitting of up to six peaks in the fitted region. The parameters ε and δ are slowly varying functions of energy, the procedure used was to have the program determine values from strong peaks and then interpolate for values of these parameters for the weaker peaks.

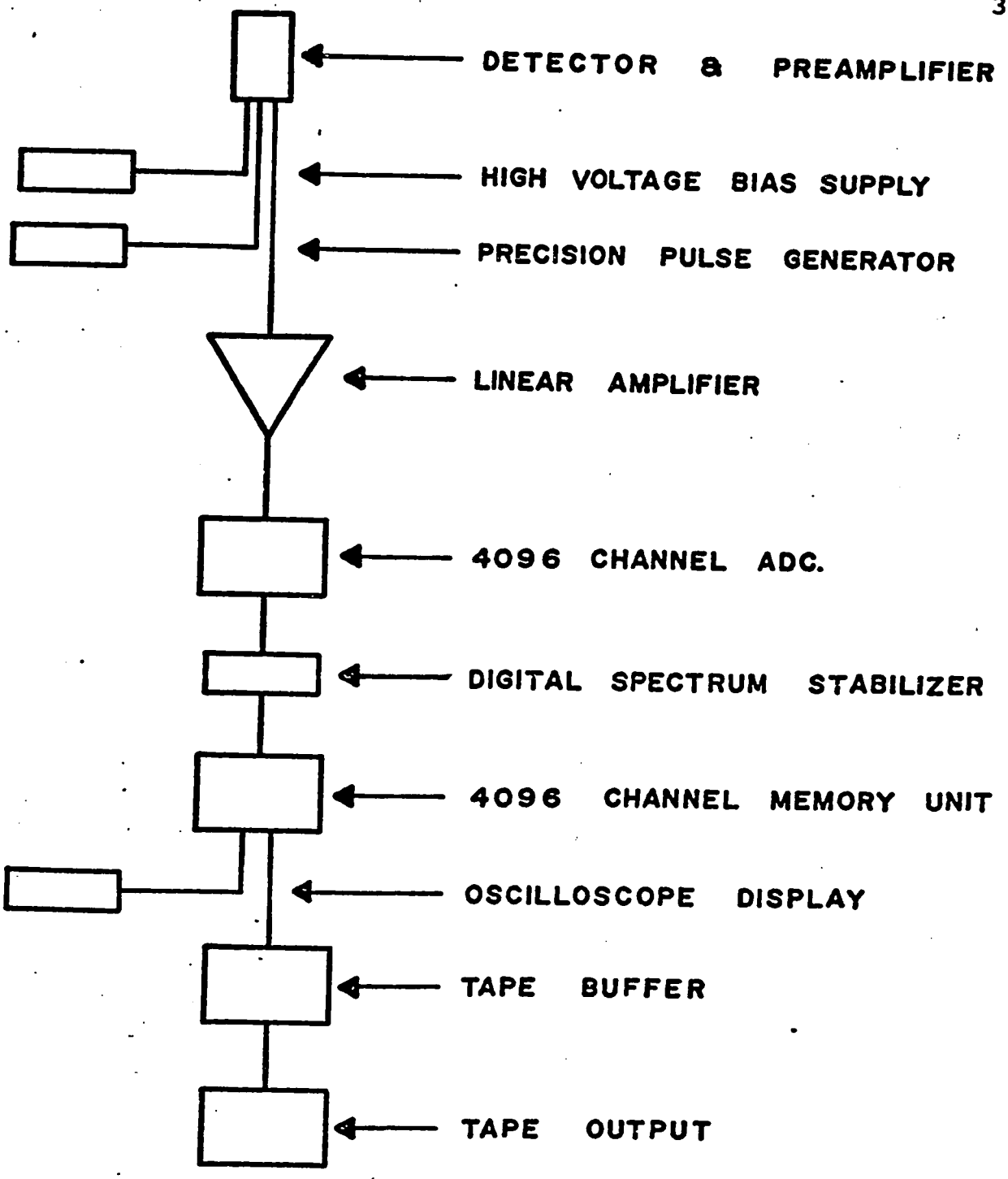

Figure 3.2 Components of a gamma spectrometer system

The energies of the stronger transitions were determined by accumulating a composite spectrum with sources having transitions whose energies are known to high precision. These strong transitions were then used as internal standards to find the energies of the weaker lines. The program fits by least squares the energy calibration to a polynomial function.

The efficiencies of the detectors for chosen geometries were measured as a function of gamma ray energy through the use of standard sources with known disintegration rates (I.A.E.A.) and with sources having transitions of well known relative intensities.

The use of Ge(Li) detectors in accelerator experiments presents some special problems. It was realized, after some period of trials, that attempts to shield the detectors from room background cannot be successful. Much of the room background consists of neutrons which produce gamma rays in any heavy mass shielding in the vicinity of the detector. Light mass shielding to stop the neutrons is too bulky to be useful. The solution was to position the detectors as closely as possible to the target position and to use a beam which was small and well focussed. Fortunately the ceilings in the accelerator lab are very high and the beam line is carried a reasonable distance from the floor (5'). A second discovery was that in the presence of a large background photo-peak sensitivity is not necessarily proportional to detector volume.

It was found that the sensitivity for measuring gamma rays up to an energy of 500 keV was greatest for very small planar detectors of high resolution, so called X-ray detectors, in spite of the very rapid decrease in efficiency for these detectors for gamma ray energies above 100 keV.

Another severe problem associated with the use of Ge(Li) detectors for on line experiments is that of neutron damage. Fast neutrons cause defects in germanium which act as hole traps. The effect of these traps is to cause incomplete charge collection and thus skewing of the low energy side of the peak. Because of the cost of germanium diodes there are very few available studies on this problem. Those studies which have been done differ widely in their estimate of total neutron flux at which damage is noticed. This is because the degradation in peak shape depends on the energy of γ-ray, and on the geometry of the detector. Thus Chasman et al (1965) report no deterioration of resolution for a small planar detector for a flux of 10^{11} fast neutrons. Stelson et al (1972) report a 50% increase in the peak width at 2.6 MeV following an irradiation by 6×10^{8} neutrons of a large coaxial device. It appears that degradation of performance will be observed at lower neutron dose levels for those detectors whose geometry favors collection of holes, such as the commonly used coaxial type, and for those detectors which are initially of the highest quality. Also the change in peak shape is noticeable earlier for high energy gamma rays

(Stelson et al 1972).

When neutrons scatter inelastically from ^{72}Ge nuclei they excite them with high probability to the 0^+ first excited state. The decay to the ground state is 100% by EO electron conversion and consequently is detected at virtually 100% efficiency. This line at 693 keV is a characteristic feature of all spectra taken with a Ge(Li) detector exposed to a fast neutron flux. It has a distinctive shape because the recoil energy of the germanium atom adds a high energy shoulder. The number of counts in this peak may be used as a rough measure of the neutron flux incident on the detector. Thus according to an expression due to Robinson (1969)

$$\text{Total neutron flux}(\text{neutrons}/\text{cm}^2) = \frac{300 \times (\text{total counts in 693 keV peak})}{\text{detector volume } (\text{cm}^3)}$$

A rough survey has been made for those types of experiments which are commonly done at McMaster and it is found that whatever beam current and energy is used the incident flux of neutrons is roughly 10^8/day. That is all experiments appear to be almost equally damaging. Thus a Coulomb excitation experiment which might use a beam of only 5 MeV α's requires a current perhaps 200 times as great as an $(\alpha,2n)$ experiment which requires 24 MeV α's and the neutron flux is comparable.

It is found that, by redrifting, a neutron damaged detector can be repaired at a cost of about 15% of the original cost of the detector. It has been found necessary to return detectors for a redrift after a total incident

flux of approximately 10^{10} neutrons.

3.3 Gamma-Gamma Coincidences with Ge(Li) Detectors

As an aid to establishing the level structure of a given nucleus experiments may be performed to establish gamma cascade relationships using two detectors. Pulse height information for two gamma rays is recorded if the two pulses occur within the resolving time of the circuit. Thus it is necessary to have precise time information for each pulse. This is limited by the variation in rise time of pulses originating in different positions in the germanium diode. This problem is minimized by using an extrapolated zero strobe device to generate the time markers. This device uses leading edge timing and generates a time pulse at a point extrapolated to zero from two points on the pulse rise time curve. Thus eliminating the problem of walk, that is the variation with pulse amplitude of the time at which a leading edge discriminator fires. The time markers from one detector were used to start a time-to-amplitude converter (T.A.C.) and those from the second detector were used to stop it. The output of the TAC was then a pulse with an amplitude proportional to the time difference between start and stop pulses. For coincident gamma rays the amplitude is constant and a window may be set with upper and lower discriminators on this pulse height. A window of equal size set on a different part of the TAC spectrum records those events for which the TAC was stopped by chance. The spread in TAC pulses is such that the window was

required to be $\sim$ 60 nsec wide. The components comprising a coincidence experiment circuit are shown schematically in fig. 3.3.

The linear pulses from each detector were digitized by ADC's interfaced to a PDP 9 computer. Pairs of A.D.C. address outputs form the coordinates of a coincidence event in a two dimensional (4096×4096) matrix, whose axes represent the energy detected by each detector. These address pairs were collected in blocks of 2048 and then written on magnetic tape. The tapes were analyzed on the CDC 6400 computer. First the events were summed to give the projections along two sides of the matrix. These projections were then used to set gates of interest and all counts contained in the "slice" through the matrix defined by a gate are extracted. Thus the whole matrix never had to be explicitly sorted.

The spectra generated by these gates were then analyzed to obtain the coincidence probability between any pair gamma rays. This is given by

$$C_{ij} = N_{ij}/(\varepsilon\omega)_i (\varepsilon\omega)_j N_o f$$

where N_{ij} is the number of coincidence events occurring between the full energy peaks of the i^{th} and j^{th} gamma rays, $(\varepsilon\omega)_i$ and $(\varepsilon\omega)_j$ are the corresponding efficiencies and f is the fraction of the peak in the gate. The constant N_o was determined from a well known cascade. The experimental coincidence probabilities were compared with those extracted from the proposed decay scheme

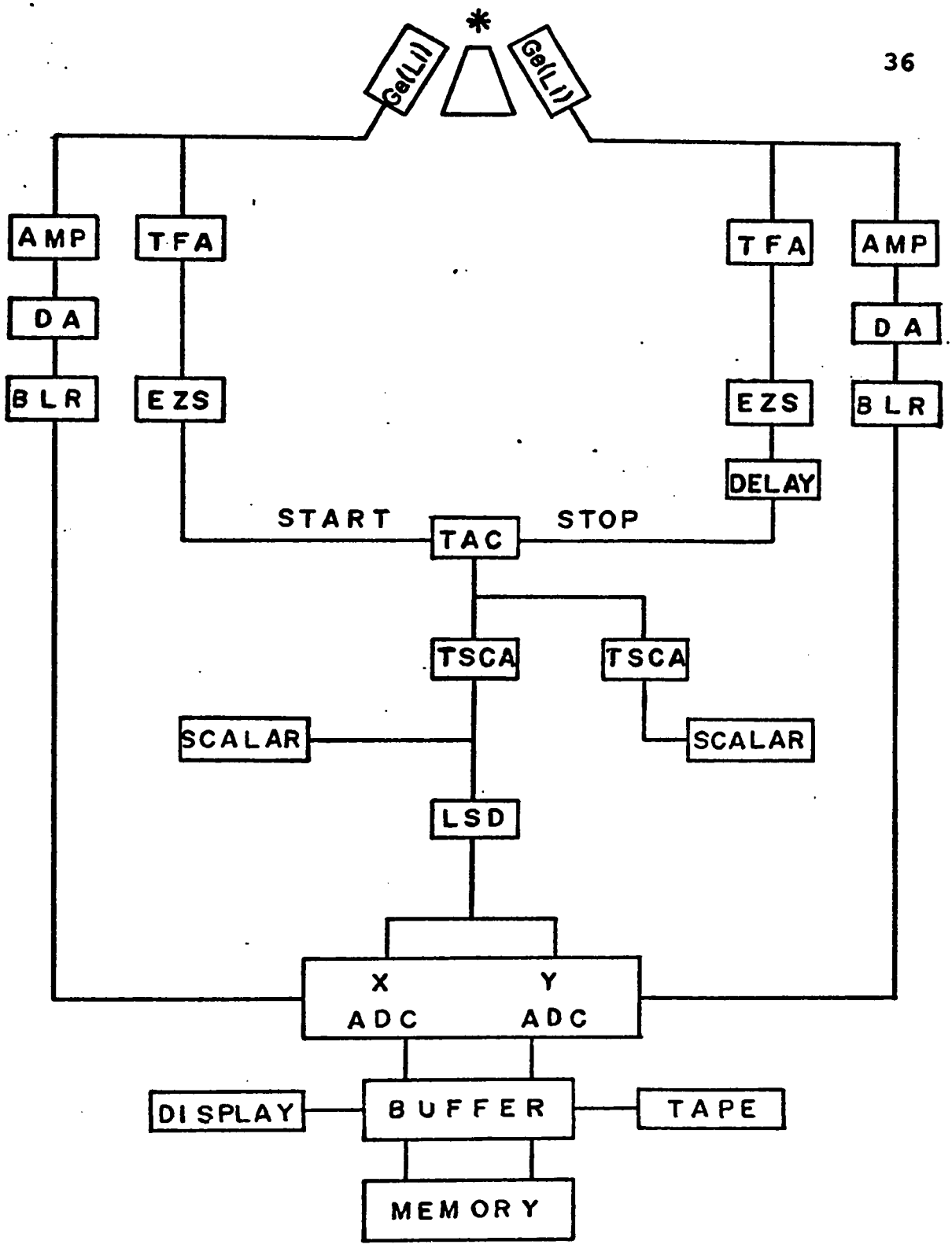

TFA: timing filter amplifier, BLR: base line restorer, DA: delay amplifier, EZS: extrapolated zero strobe, TSCA: timing single channel analyzer, LSD: logic shaper and delay, TAC: time to amplitude converter.

Figure 3.3 Components comprising a system for measuring γ-γ coincidences

according to

$$C_{ij} = \frac{I_i I_j}{\Sigma I_k}$$

where I_i represents the gamma intensity of the incoming transition and I_j, that of the outgoing transition of interest, ΣI_k represents the sum of the intensities of transitions de-exciting the level. More complex expressions can be derived for pairs of gamma rays when several intermediate levels are involved.

3.4 The Orange Spectrometer

The Orange double focussing electron spectrometer has an unusually high transmission coefficient which makes it especially suitable for on line applications. The McMaster seven gap instrument was made by Whitehead Engineering and is patterned after the Chalk River design (Geiger 1965). It consists of seven sector or wedge type spectrometers (Koefoed-Hansen et al. 1950 and Nielson and Koefoed-Hansen) arranged with rotational symmetry so that they share the same source and detector positions which lie on a central vertical axis as shown in fig. 3.4.

The focussed electrons enter the cylindrical plastic detector through a gap between two brass rings, the lower of which can be moved. Optimum momentum resolution (0.5%) is obtained, at a cost in transmission, with a gap between the rings of 1 mm. In order to reduce background the detector

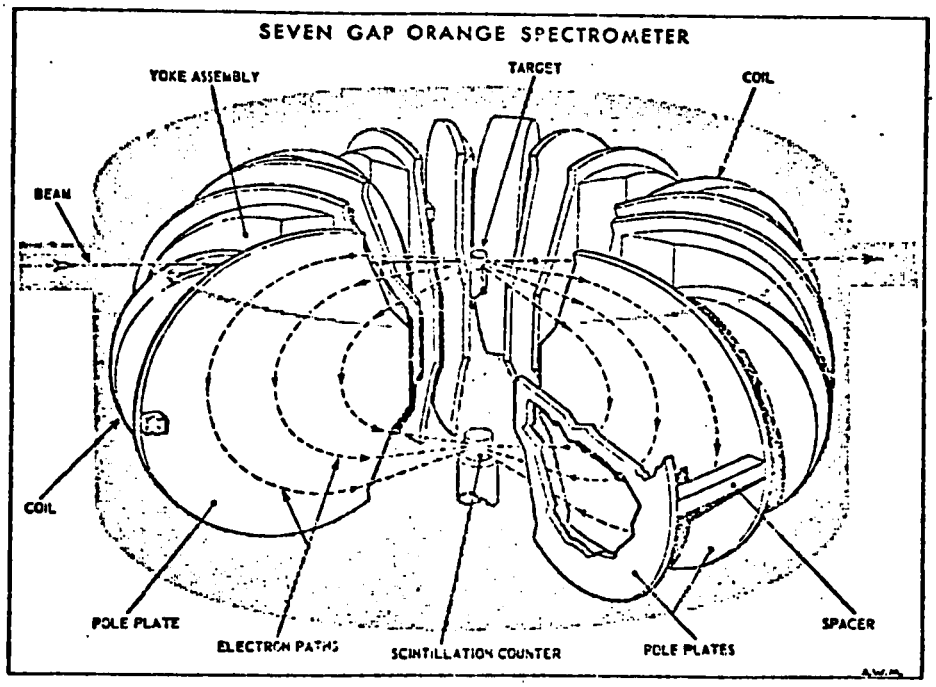

Figure 3.4 Schematic illustration of the "Orange" beta ray spectrometer. (From Geiger 1965).

was machined as small as was consistent with reasonable detection efficiency (1 cm diameter, 0.5 cm high).

The wedge spectrometers consist of water cooled copper windings around a soft iron core. The current to each can be adjusted independently to facilitate tuning the spectrometer. The magnetic field is measured with a Rawson probe, positioned in one of the gaps between the coils, and held constant to within 5 parts in 10^5 by means of a feedback network. The system is prevented from hunting by means of a rate coil in the gap beneath the Rawson probe. Electrons are focussed by means of the magnetic field ($H = H_o/r$) in each of the remaining six gaps. Features of the spectrometer are shown

in fig. 3.5.

For on line use it was necessary to overcome a severe background problem. Little could be done about the background due to scattered neutrons, or the low energy δ rays originating in the target, but the main background contribution came from scattered gamma-rays and to reduce this a number of modifications were made. For optimum resolution it is necessary to have a well defined beam spot at the target position, consequently a set of four independent and insulated Ta slits which define a 2mm × 3mm aperture were installed near the beam entrance port. The current to each could be measured, and minimized so that typically the current to the slits was 1% of the total. In order to remove the background arising from reactions on the Ta the assembly was rotatable, through a vacuum seal, to a position clear of the beam. During a long run the slits could be moved back into position to check that the beam had not wandered. A significant portion of the beam suffered small angle scattering in the target. By enlarging the exit part of the spectrometer, and the size of the beam pipe to the Faraday cup, two meters away, beam particles, scattered through angles up to 2½°, reached the shielded cave before hitting the beam pipe. In addition a number of lead baffles were placed in the spectrometer, each covered with aluminum to prevent electrons from being scattered by the lead and to attenuate the lead X-rays. The last section of the

ORANGE SPECTROMETER

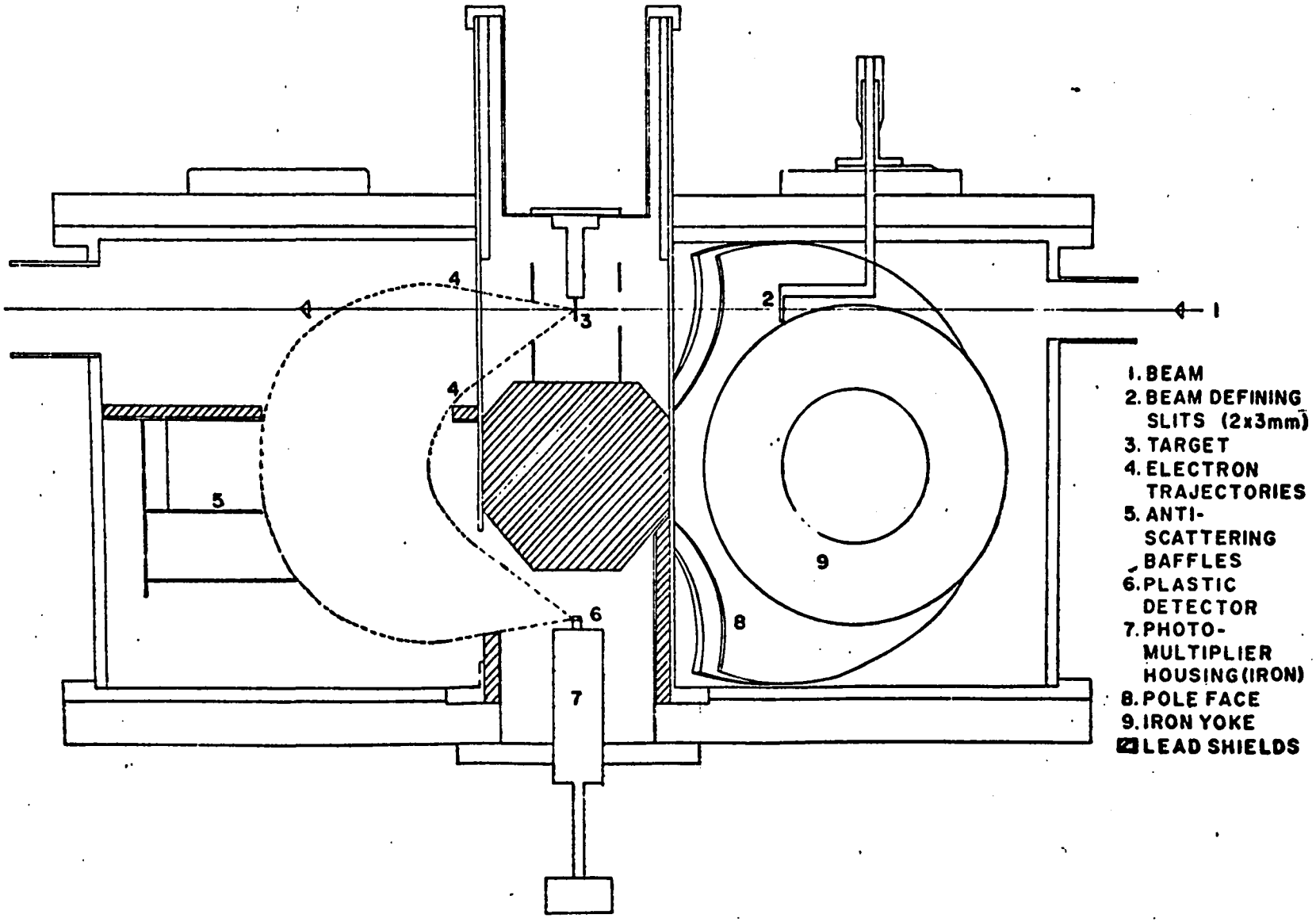

Figure 3.5 Features of the 'Orange' beta ray spectrometer

33° beam line, including the Orange spectrometer is shown in fig. 3.6. It was found, for reasons of low background, that the best position for on line gamma measurements was at the end of the 33° beam line. Accordingly the 8" diameter beam pipe between the Orange and the cave was constructed in such a way that a section could be removed and replaced with a special section with a gamma target position. The arrangement shown in the insert of fig. 3.6 was designed to allow the Ge(Li) detectors to be moved very close to the target. This is very important for coincidence experiments. Other target chambers incorporated features for changing targets, thin windows, and angular distributions. The whole of the last section of beam line, inside the cave, is insulated from ground and forms the Faraday cup.

To facilitate long runs the operation of the spectrometer was fully automated. During a cycle scalers recorded the number of focussed electrons, the charge to the Faraday cup, time elapsed, and the number of beam particles elastically scattered into a plastic scintillation detector mounted in one of the ports of the spectrometer. Normalization was achieved by this last count. At a pre-determined number, counting would stop, the scaler contents would be typed out along with the $B\rho$ value, and the spectrometer field would be stepped along a preset amount; following a pause of four seconds to allow for field stabilization the cycle was repeated.

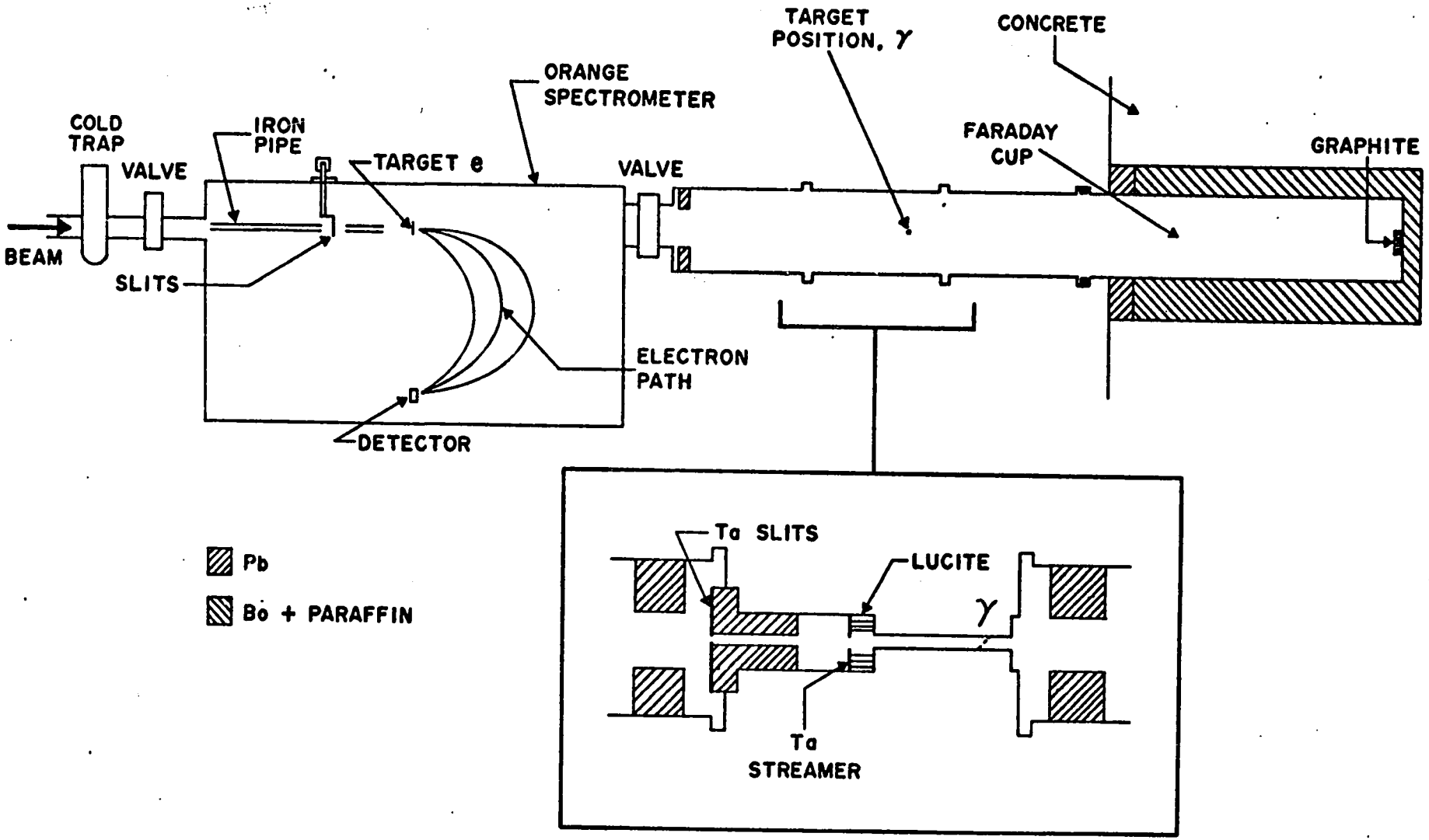

Figure 3.6

Target area of the 33° beam line. The target positions for electron and gamma ray measurements are indicated by e and γ, respectively

In general it was found that charge, elapsed time and the normalization count were strictly proportional, a change in this situation indicated an intermittent beam or a deteriorating target. These conditions were either rectified, or in the case of isolated points the data rejected.

3.5 The Enge Split-Pole Spectrograph

The level density in nuclei of the rare earth region demands the highest degree of resolution in all types of instrumentation. The study of transfer reactions in deformed nuclei is intimately connected to the advent of electrostatic accelerators and high-resolution magnetic spectrographs.

The tandem Van der Graaff accelerator can provide a beam of charged ions with an energy stability of the order of one part in 10,000. To take advantage of this high beam stability the Enge spectrometer (Enge 1964 and Spencer and Enge 1967) was designed to combine the inherent high resolution of magnetic analyzing devices with large collecting power over a broad energy range which is necessary for "on line" instruments. Unlike the Orange spectrometer which has a fixed radius and must therefore be stepped along through different field settings, the Enge spectrometer focusses particles of different magnetic rigidity onto a long focal plane.

The McMaster instrument is of the Enge split-pole

type built by AB Scanditronics of Sweden. A schematic plan, together with some of its features,is shown in fig. 3.7. The purpose of the split between the pole pieces is to provide second order double focussing over a large energy range ($E_{max}/E_{min} \sim 8$). Vertical focussing, the main purpose of which is to increase the collecting power of the instrument, is achieved in the fringing field areas, particularly at the entrance to the first gap.

The angle of the spectrometer with respect to the beam direction is chosen after consideration of the yields/angle of the light mass impurities and the particles of interest.

Particles which have been magnetically analyzed and focussed by the spectrograph were recorded in nuclear emulsions mounted along the focal plane. For the present work Eastman Kodak NTB nuclear emulsions were used. They were 50 microns thick and mounted on glass plates. Following developing the plates were scanned for particle tracks in $\frac{1}{4}$ mm wide strips across the plate width using a travelling microscope. In general itwas possible to eliminate unwanted reaction products by covering the plates with aluminum absorbers during exposure.

A proton N.M.R. probewas used to measure the strength of the magnetic field. Energy relationships may be calculated from the known characteristics of the instrument.

A semi-conductor detector can be placed in the target

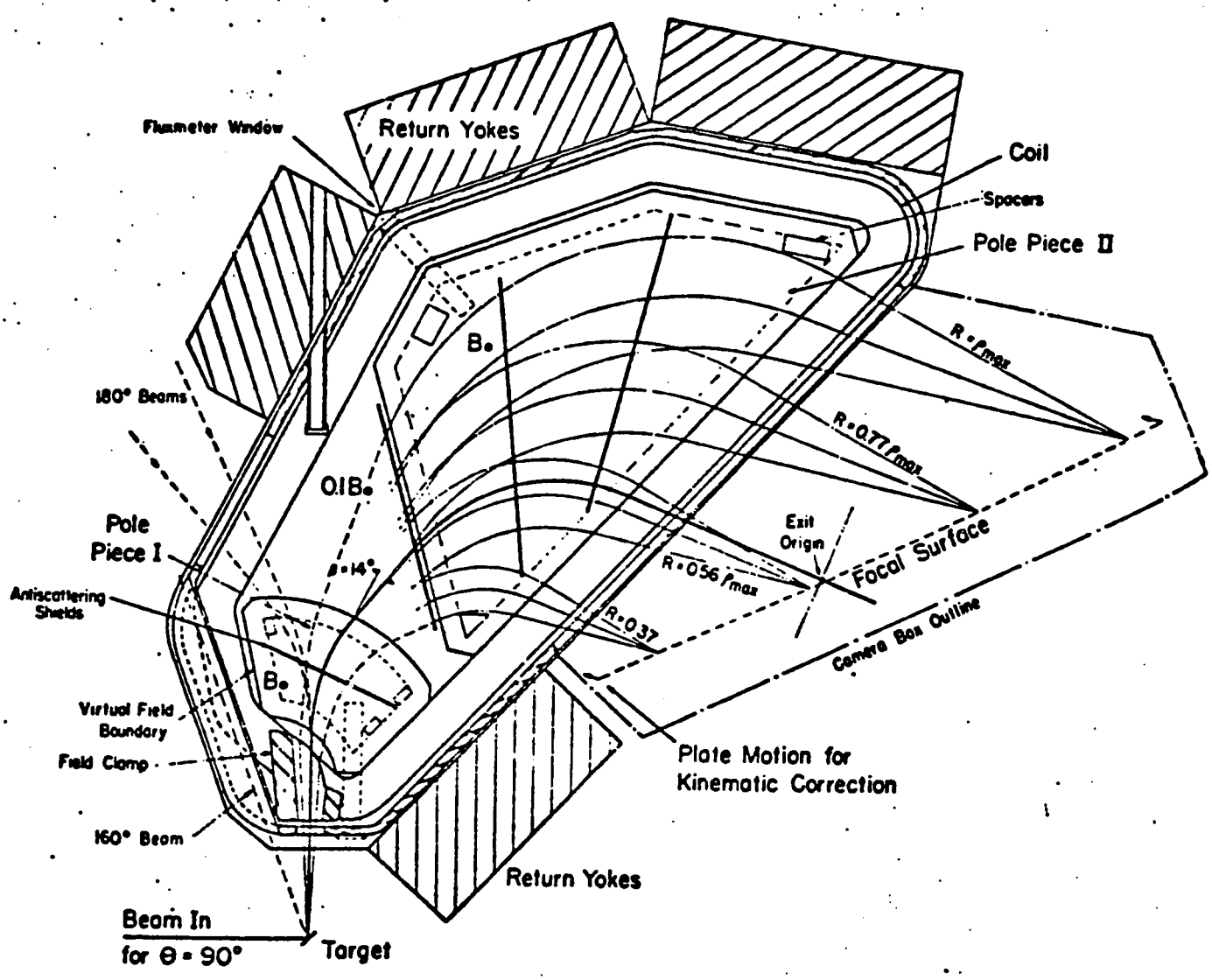

Figure 3.7 Schematic plan view of the "Enge" split pole spectrograph (Spencer and Enge 1967)

chamber to count particles elastically scattered from the beam. The number of course is used to calculate cross sections for the spectra on the emulsions. The energy of levels may be derived from the plate position using the known characteristics of the magnet (O'Neil 1972).

CHAPTER 4

The Decay of ^{117}Cd and ^{117m}Cd

4.1 Introduction

The nucleus ^{117}Cd undergoes β-decay with a half life of 2.5 hours from the $1/2^+$ ground state and with a half life of 3.4 hours from the $11/2^-$ isomer. These states can be described in terms of the spherical shell model as $s_{1/2}$ and $h_{11/2}$ states. The levels in ^{117}In thus populated and, in particular the low lying states, have been carefully studied (Backlin et al, 1967; Pandharipande et al, 1968; Chilosi et al, 1968). However, there are still problems involved in understanding the level scheme. Like the other odd mass Indium isotopes, ^{117}In has a $9/2^+$ ground state, a low lying $1/2^-$ isomeric state, and a number of low energy, low spin positive parity states.

Backlin et al (1967) made the suggestion that the positive parity states are the lowest members of the K = 1/2 rotational band based on the $1/2^+[431]$ Nilsson orbital. Pandharipande et al (1968) supported this interpretation and proposed the levels at 660, 748, 881, 1249 and 1715 keV as the $3/2^+$, $1/2^+$, $7/2^+$, $11/2^+$ and $9/2^+$ levels of such a band. R. Moret (1969) also proposed a $1/2^+$ rotational band but with levels at somewhat different energies from those of Pandharipande

et al. The present work, undertaken to establish energies, spins, and parities for levels above 750 keV, leads to a new proposal for the members of this band. In addition to the determination of gamma ray energies and an extensive series of γ-γ coincidence measurements, the half life and hence the parentage of each of the stronger transitions was established. Harar and Horoshko (1972) have made available to us unpublished data from $^{116}Cd(\alpha,t)^{117}In$ and $^{116}Cd(^{3}He,d)^{117}In$ reaction studies. These data, which complement ours, have proved to be of great value in assigning spins and parities.

4.2 Experimental Techniques

Cadmium oxide, enriched to 97.2% in ^{116}Cd, was irradiated for 4 to 5 minutes in the reactor at a flux of $\sim 10^{13}$ neutrons/cm^2/sec and delivered from the reactor core to the laboratory by a pneumatic rabbit system. The active material was transferred to gelatin capsules for counting in standard geometries. No chemical purification was carried out.

The gamma ray singles spectra were investigated with two Ge(Li) spectrometers. One employed a 50 cm^3 co-axial detector with a resolution of 2.3 keV (FWHM) at 1332 keV while the other involved a 0.9 cm^3 planar detector with a resolution of 0.7 keV at 122 keV.

Two-parameter gamma-gamma coincidence experiments were carried out using two 40 cm^3 Ge(Li) detectors which had reso-

lutions of 3.3 keV (FWHM) at 1332 keV. They were oriented at 60° and had a wedge shaped lead shield between them to minimize intercrystal scattering. Source strengths were chosen to maintain true to chance ratios of the order of better than 20:1. The coincidence events were recorded on magnetic tape using an address-recording technique, and were later sorted and analyzed using a CDC 6400 computer.

In order to determine the half life of each of the gamma lines, two separate experiments were performed. In both the intent was to determine the characteristic feeding (ie. isomer or ground state) rather than an absolute value for the half life, although this was obtained for some of the stronger transitions.

In the first experiment the decay of the stronger photopeaks from a single source was followed through four half lives, this being repeated for three sources and the results summed in order to improve the statistics. For the second experiment pairs of samples were irradiated together. The relative amounts of material in these was chosen in such a way that the total activity of the smaller sample counted immediately after irradiation was approximately equal to that of the larger sample counted 16.3 hours later. However, the ratio of the activities associated with the two decays had changed by a factor of four in the interval between the two measurements. In order to build up statistics, four such pairs

of sources were studied, to uniquely establish the origin of sixty-eight of the stronger transitions. In addition, transitions with a mixed feeding and long lived impurities were identified.

4.3 Gamma-ray Measurements

The low energy region of the ^{117g}Cd and ^{117m}Cd gamma ray spectrum as recorded with the 0.9 cm^3 thin window detector with no absorber is shown in fig. 4.1. The weak peak labelled es. pk. is the Ge X-ray escape peak (Ungrin and Johns 1969) resulting from the strong peak at 158 keV. Fig. 4.2 shows the gamma ray spectrum taken with the 50 cm^3 Ge(Li) detector shielded with a graded absorber of Pb, Cd and Cu, which had a total thickness of 5 mm, and a half inch thick plastic beta stopper. The lines shown at 158 and 552 keV belong to the decay of ^{117}In and those at 336 and 527 keV are associated with the decay of 43 day ^{115}Cd. Fig. 4.3 shows a portion of the results from the second half life experiment. Those transitions with a 3.4 hour half life have equal intensity in both spectra. The line at 748 keV is of special interest as it is seen to be a transition of mixed parentage. By following the decay of some of the stronger transitions values of 2.5±0.2 hours and 3.4±0.2 hours were obtained for the half lives of the ground state and isomer respectively, in excellent agreement with the previous determinations (Tang et al. 1965, Moret 1969).

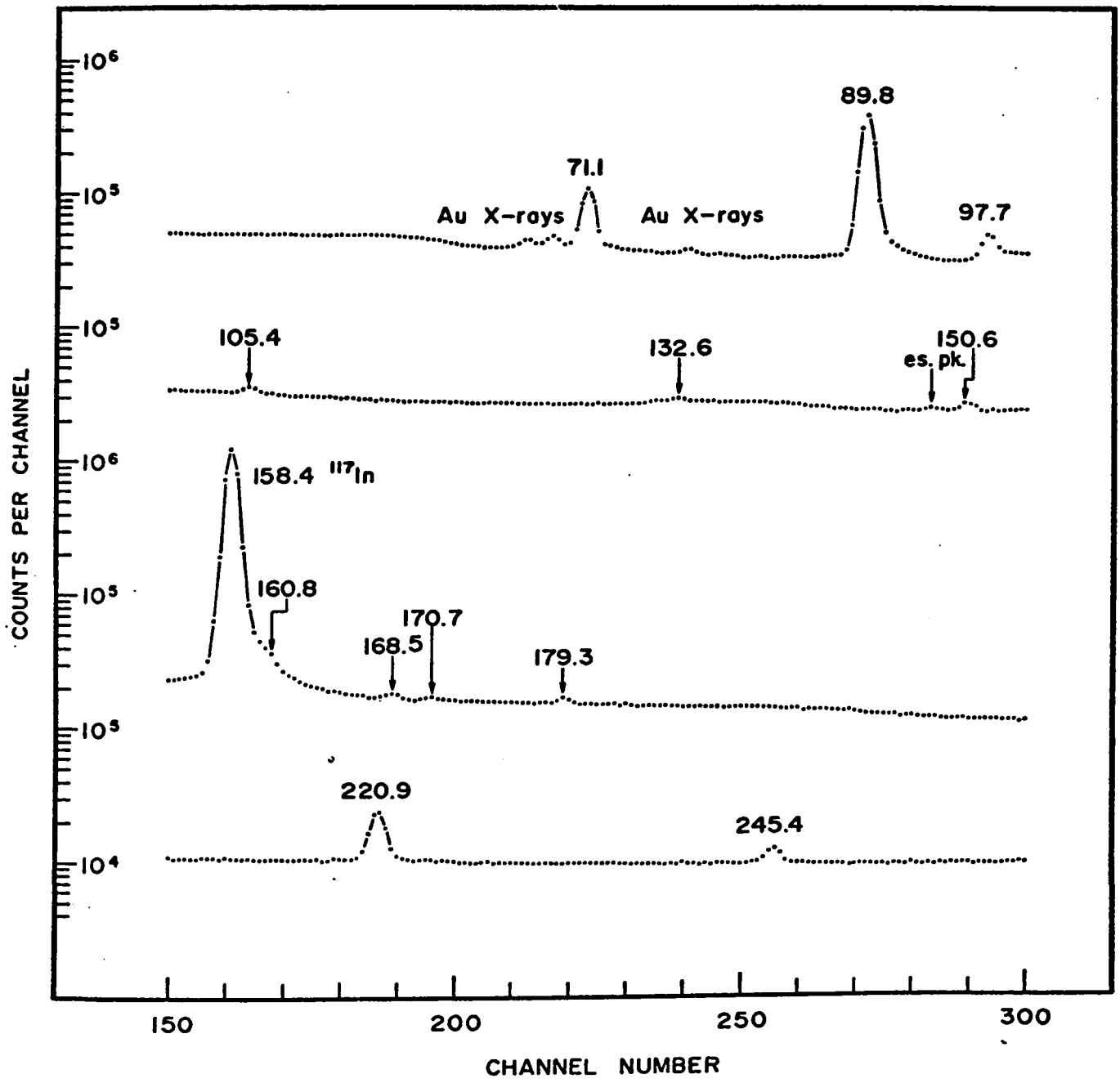

Figure 4.1 Low energy gamma spectrum of ^{117}Cd and ^{117m}Cd decay

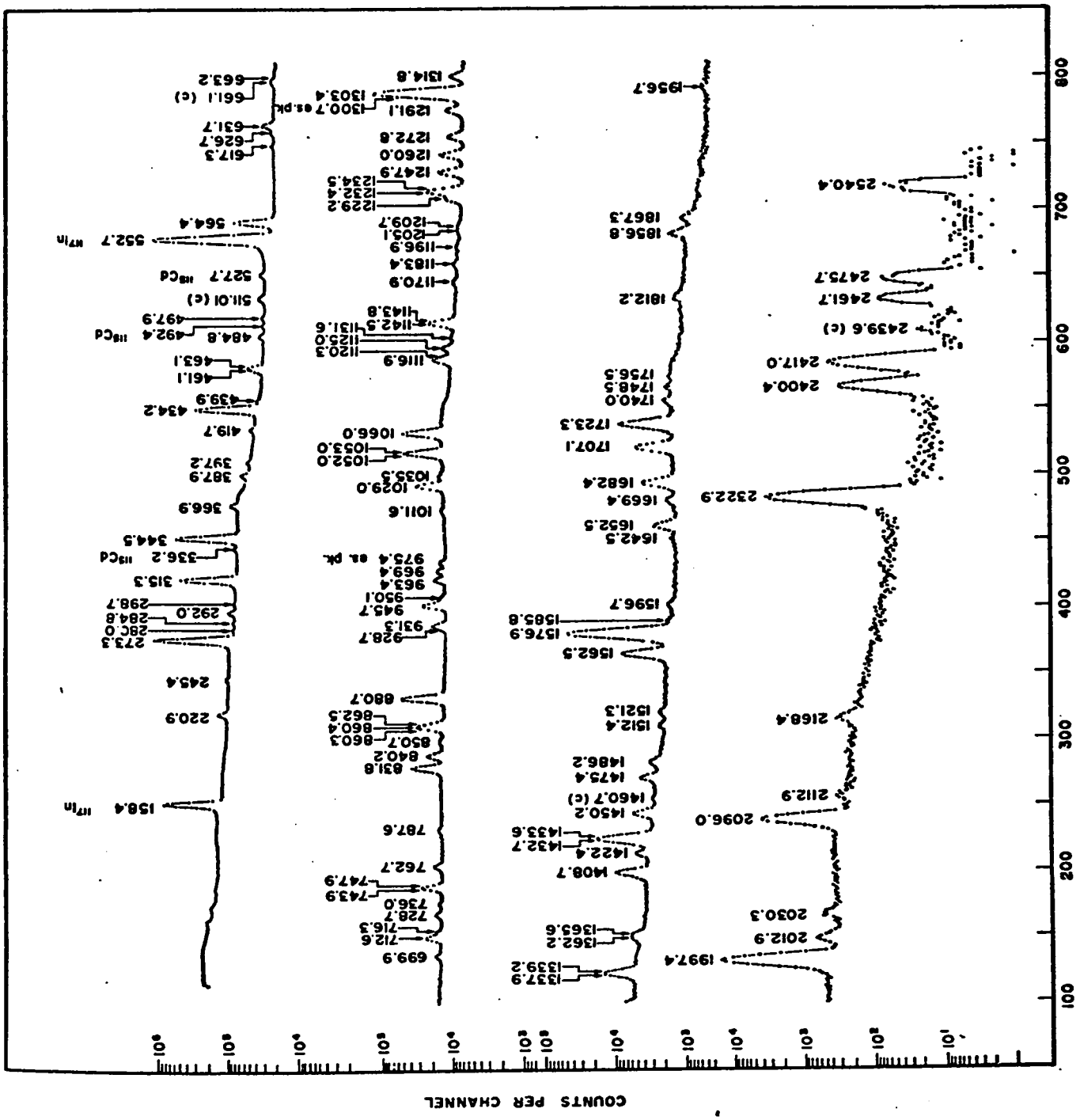

Gamma spectrum of ^{117}Cd and ^{117m}Cd decay

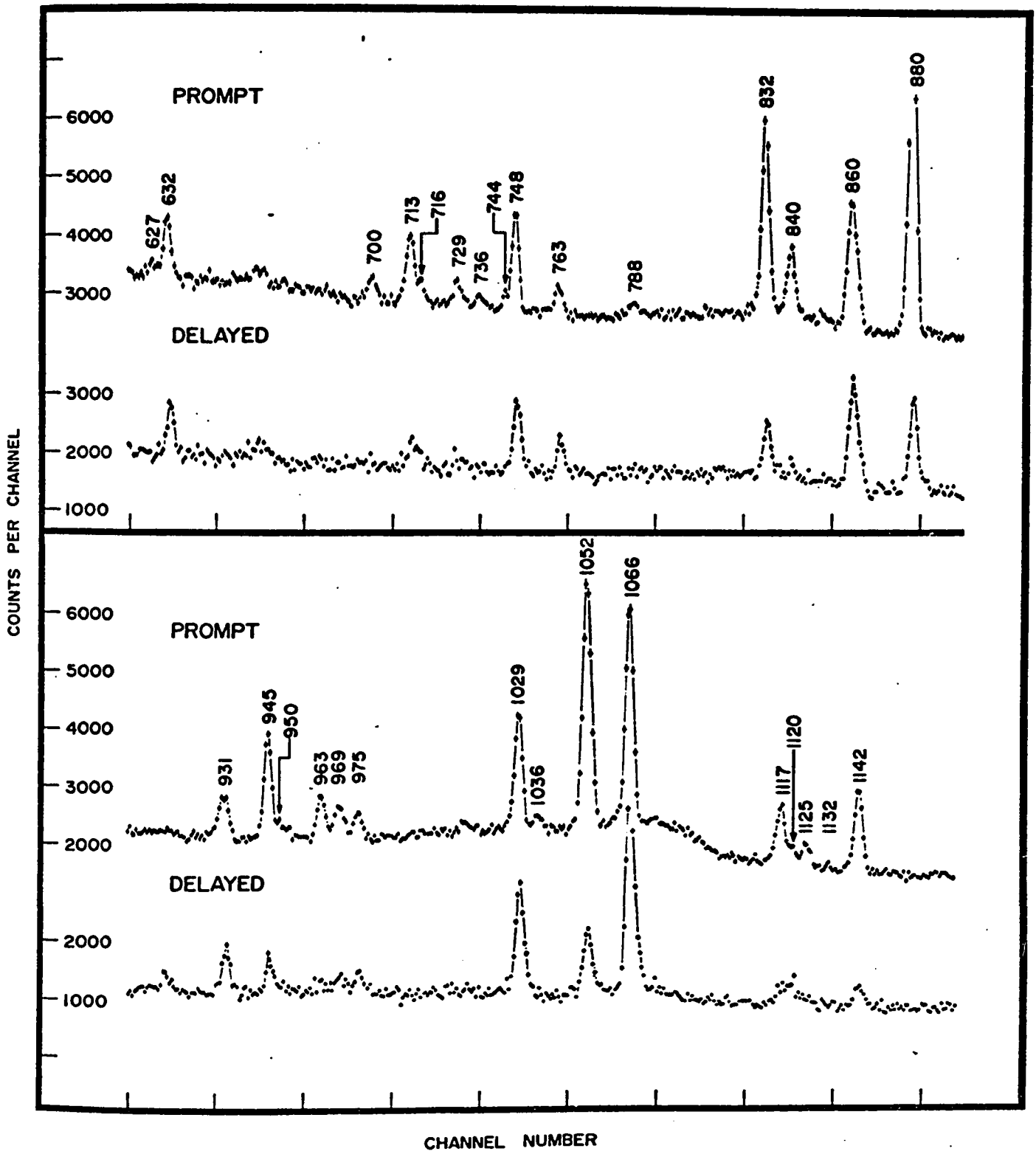

Figure 4.3 Section of the results from the half life experiment

The weighted averages of the energies and relative intensities of the gamma rays taken with the two detectors in several geometries are tabulated in the first and second columns of Table 4.1. In the case of close doublets and triplets, the relative intensities of the transitions have been determined from the coincidence probabilities. Column 5 gives the classification of each transition in the decay scheme in figs. 4.11 and 4.12. The parentage, where determined, is shown in column 3 and the evidence on which the gamma ray was fitted in the decay scheme in column 4. The transition parentage measurements of the present work are more extensive than those of Moret (1969).

4.4 Gamma-Gamma Coincidence Measurements

In the two parameter coincidence experiment, $\sim 5 \times 10^6$ pairs of coincidence events were recorded. A selection of the coincidence spectra associated with the sixty gates set on the spectrum is presented in figs. 4.4 to 4.10. Events due to background underlying the gating photopeak have been subtracted off in each case. No correction was made for chance, but the excellent signal to background ratio ensured that the chance peaks were not troublesome.

Fig. 4.4 presents the coincidence spectrum associated with a gate set on the 273 keV photopeak. The peaks in this spectrum define a large number of states, as shown in the partial decay scheme of the figure. Gates set on most of

TABLE 4.1

Gamma Ray Transitions in ^{117}In

Photon Energy (keV)	Photon Intensity[a]	Parentage[b]	Basis of Fit	Classification
71.11 ± 0.06	2.8 ± 0.3	g	E,γ-γ	659.7→588.6
89.71 ± 0.05	14.7 ± 1	g	E,γ-γ	749.4→659.7
97.67 ± 0.06	1.0 ± 0.1		E,γ-γ	2095.6→1997.2
105.4 ± 0.2	0.2 ± 0.06		E,γ-γ	1997.5→1892.0
132.6 ± 0.2	0.1 ± 0.04		E	880.7→747.9
150.6 ± 0.2	0.3 ± 0.1		E	1360.0→1209.0
160.8 ± 0.3	0.2 ± 0.1		E,γ-γ	749.4→659.7
168.5 ± 0.3	0.2 ± 0.06		E,γ-γ	1234.5→1066.0
170.7 ± 0.4	0.1 ± 0.02		E	1051.9→880.7
179.3 ± 0.4	0.1 ± 0.04		E	1892.0→1712.7
220.90 ± 0.07	5.1 ± 0.2	g	E,γ-γ	880.7→659.7
245.4 ± 0.2	0.7 ± 0.1	g		
273.31 ± 0.06	100	g	E,γ-γ	588.6→315.3
280.0 ± 0.3	0.3 ± 0.03		E	2171.9→1892.0
284.8 ± 0.3	0.2 ± 0.02		E,γ-γ	1997.5→1712.7
292.0 ± 0.1	2.0 ± 0.08	g	E,γ-γ	880.7→588.6
298.7 ± 0.03	0.20 ± 0.07		E	1365.5→1066.0
315.26 ± 0.06	78.7 ± 5 [c]		E	315.3→0
344.51 ± 0.06	62.7 ± 3.8	g	E,γ-γ	659.7→315.3
366.94 ± 0.08	2.6 ± 0.2	i	E,γ-γ	1432.7→1066.0
387.93 ± 0.07	1.5 ± 0.1	g	E,γ-γ	1997.5→1609.6
397.2 ± 0.1	0.5 ± 0.04			
419.71 ± 0.09	0.76 ± 0.06	g	E,γ-γ	2311.9→1892.0
434.23 ± 0.05	37.8 ± 2.6	g	E,γ-γ	749.4→315.3
439.9 ± 0.2	0.3 ± 0.08		E,γ-γ	1028.1→588.6
461.1 ± 0.1	0.9 ± 0.3	i	E,γ-γ	1209.0→747.9
463.09 ± 0.08	2.9 ± 0.3	g	E,γ-γ	1051.9→588.6
484.8 ± 0.1	0.8 ± 0.06	i	E,γ-γ	1365.5→880.7
497.9 ± 0.1	0.4 ± 0.04		E,γ-γ	1360.0→862.5
552.8 ± 0.1	0.44 ± 0.2		E,γ-γ	1432.7→880.7

Photon Energy (keV)	Photon Intensity[a]	Parentage[b]	Basis of Fit	Classification
564.4 ± 0.1	11.04 ± 0.76	i	E,γ-γ	1997.2→1432.7
617.3 ± 0.2	0.35 ± 0.11	i		
626.7 ± 0.2	0.4 ± 0.09	g	E,γ-γ	1376.1→749.4
631.7 ± 0.1	2.13 ± 0.14	i	E,γ-γ	1997.2→1365.5
663.2 ± 0.3	0.5 ± 0.1		γ-γ	1729.1→1066.0
699.9 ± 0.2	0.8 ± 0.07	g	E,γ-γ	1360.0→659.7
712.6 ± 0.2	2.86 ± 0.18	g		1028.1→315.3
716.3 ± 0.2	0.8 ± 0.12		E,γ-γ	1376.1→659.7
728.7 ± 0.2	0.9 ± 0.08	g	E,γ-γ	1609.6→880.7
736.0 ± 0.2	0.3 ± 0.09		E	2345.6→1609.6
743.9 ± 0.6	0.3 ± 0.1		E	2456.2→1712.7
747.2 ± 0.4	0.3 ± 0.2		γ-γ	1609.6→862.5
747.9 ± 0.2	4.6 ± 0.3	i	E,γ-γ	747.9→0
762.7 ± 0.1	1.3 ± 0.09	i	E,γ-γ	1997.5→1234.5
787.6 ± 0.2	0.5 ± 0.1	g	E	1376.1→588.6
831.79 ± 0.05	8.1 ± 0.5	g	E,γ-γ	1712.7→880.7
840.22 ± 0.05	2.9 ± 0.3	g	E,γ-γ	1892.0→1051.9
850.7 ± 0.5	0.4 ± 0.1		E	1712.7→862.5
860.3 ± 0.5	0.9 ± 0.4		γ-γ	1609.6→749.4
860.4 ± 0.5	6.6 ± 1.0	i	E,γ-γ	2095.6→1234.5
862.5 ± 0.2	1.8 ± 0.4		E,γ-γ	862.5→0
880.75 ± 0.05	14.6 ± 0.9	g	E,γ-γ	880.7→0
928.7 ± 0.5	0.9 ± 0.4		E,γ-γ	1957.1→1028.1
931.3 ± 0.3	2.2 ± 0.2	i	E,γ-γ	1997.2→1066.0
945.7 ± 0.1	5.4 ± 0.35	g	E,γ-γ	1997.5→1051.9
950.1 ± 0.2	1.04 ± 0.22	g	E,γ-γ	1609.6→659.7
963.4 ± 0.2	2.01 ± 0.17	g	E,γ-γ	1712.7→749.4
969.4 ± 0.2	1.81 ± 0.14		E,γ-γ	1997.5→1028.1
1011.6 ± 0.5	0.52 ± 0.07		E	1892.0→880.7
1029.0 ± 0.1	7.62 ± 0.43	i	E,γ-γ	2095.6→1066.0
1035.5 ± 0.1	0.8 ± 0.2	g	E,γ-γ	1784.8→749.4
1052.0 ± 0.1	11.5 ± 2.0	g	E,γ-γ	1051.9→0
1053.0 ± 0.2	2.5 ± 0.6	g	E,γ-γ	1712.7→659.7
1066.0 ± 0.1	15.2 ± 0.8	i	E,γ-γ	1066.0→0
1116.9 ± 0.2	3.5 ± 0.3	g	E,γ-γ	1997.5→880.7

Photon Energy (keV)	Photon Intensity[a]	Parentage[b]	Basis of Fit	Classification
1120.3 ± 0.5	0.6 ± 0.2	g	E,γ-γ	2171.9→1051.9
1125.0 ± 0.2	1.2 ± 0.2	g	E,γ-γ	1784.8→659.7
1131.6 ± 0.5	0.14 ± 0.06			
1142.5 ± 0.1	4.5 ± 0.3	g	E,γ-γ	1892.0→749.4
1143.8 ± 0.2	0.5 ± 0.3		E,γ-γ	2171.9→1028.1
1170.9 ± 0.4	0.55 ± 0.07		E	2405.3→1234.5
1183.4 ± 0.4	0.6 ± 0.06		E,γ-γ	2064.1→880.7
1196.9 ± 0.4	0.36 ± 0.06		E	1784.8→588.6
1205.1 ± 0.5	0.3 ± 0.1			
1209.7 ± 0.5	0.2 ± 0.1		E	1209.0→0
1229.2 ± 0.3	2.05 ± 0.17	g	E,γ-γ	2109.9→880.7
1232.4 ± 0.5	1.5 ± 0.5		E,γ-γ	1892.0→659.7
1234.5 ± 0.3	35.9 ± 4.0	i	E,γ-γ	1234.5→0
1247.9 ± 0.1	4.0 ± 0.2	g	E,γ-γ	1997.5→749.4
1260.0 ± 0.1	3.6 ± 0.2	g	E,γ-γ	2311.9→1051.9
1272.8 ± 0.1	2.4 ± 0.2	g	E,γ-γ	2022.1→749.4
1291.1 ± 0.1	2.6 ± 0.5	g	E,γ-γ	2171.9→880.7
1303.4 ± 0.1	62.7 ± 3.4	g	E,γ-γ	1892.0→588.6
1314.8 ± 0.3	2.3 ± 0.6	g	E,γ-γ	2064.1→749.4
1337.9 ± 0.1	4.5 ± 0.7	g	E,γ-γ	1997.5→659.7
1339.2 ± 0.5	1.6 ± 0.5		E,γ-γ	2405.3→1066.0
1362.2 ± 0.4	0.8 ± 0.2	g	E,γ-γ	2022.1→659.7
1365.6 ± 0.4	1.2 ± 0.2	i	E,γ-γ	1365.5→0.0
1408.7 ± 0.2	4.5 ± 0.3	g	E,γ-γ	1997.5→588.6
1422.4 ± 0.3	1.0 ± 0.09	g	E,γ-γ	2171.9→749.4
1431.2 ± 0.3	3.7 ± 0.5		E,γ-γ	2311.9→880.7
1432.7 ± 0.3	7.5 ± 1.0	i	E,γ-γ	1432.7→0
1433.6 ± 0.3	0.6 ± 0.3		E,γ-γ	2022.1→588.6
1450.2 ± 0.2	2.0 ± 0.1	g	E,γ-γ	2109.9→659.7
1475.4 ± 0.4	1.5 ± 0.1	g	E,γ-γ	2064.1→588.6
1486.2 ± 0.4	0.7 ± 0.1			
1512.4 ± 0.5	0.2 ± 0.05		E	2171.9→659.7
1521.3 ± 0.6	0.2 ± 0.06	g	E,γ-γ	2109.9→588.6
1562.5 ± 0.1	5.3 ± 0.48	g	E,γ-γ	2311.9→749.4
1576.9 ± 0.1	38.1 ± 2.1	g	E,γ-γ	1892.0→315.3
1585.8 ± 1.0	0.2 ± 0.1			

Photon Energy (keV)	Photon Intensity[a]	Parentage[b]	Basis of Fit	Classification
1596.7 ± 0.7	0.2 ± 0.06		E	2345.6→749.4
1642.5 ± 1.0	0.1 ± 0.04		E	1957.1→315.3
1652.5 ± 0.3	1.1 ± 0.1	g	E,γ-γ	2311.9→659.7
1669.4 ± 0.3	0.4 ± 0.1		E	2328.7→659. 7
1682.4 ± 0.3	2.5 ± 0.2	g	E	1997.5→315.3
1707.1 ± 0.1	3.5 ± 0.3	g	E	2022.1→315.3
1723.3 ± 0.1	6.4 ± 0.4	g	E,γ-γ	2311.9→588.6
1740.0 ± 0.6	0.2 ± 0.05		E,γ-γ	2328.7→588.6
1748.5 ± 0.7	0.2 ± 0.07		E	2064.1→315.3
1756.5 ± 0.9	0.1 ± 0.06		E,γ-γ	2345.6→588.6
1812.2 ± 0.3	0.04 ± 0.02			
1856.8 ± 0.2	0.7 ± 0.09		E	2171.9→315.3
1867.3 ± 0.3	0.3 ± 0.04		E,γ-γ	2456.0→588.6
1956.7 ± 2.0	0.06 ± 0.02			
1997.4 ± 0.02	18.2 ± 1.0	i	E,γ-γ	1997.2→0
2012.9 ± 0.4	0.4 ± 0.1		E	2328.7→315.3
2030.3 ± 0.5	0.3 ± 0.04		E	2345.6→315.3
2096.0 ± 0.2	0.5 ± 0.06	i	E	2095.6→0
2112.5 ± 0.7	0.07 ± 0.03			
2168.4 ± 0.9	0.2 ± 0.05			
2322.9 ± 0.3	5.2 ± 0.3	i	E	2322.9→0
2400.4 ± 0.3	0.5 ± 0.1	i	E	2400.4→0
2417.0 ± 0.3	0.7 ± 0.1	i	E	2417.0→0
2461.7 ± 0.4	0.2 ± 0.03			
2475.7 ± 0.4	0.2 ± 0.03			
2540.4 ± 0.4	0.1 ± 0.03			

a) The photon intensities are normalized to the strength of the 273 keV transition as determined from a six hour counting period immediately following a three minute irradiation.

b) Indicates measured feeding, g for ground state fed transitions and i for isomer fed transitions.

c) The 315 keV state is isomeric, the quoted intensity of the gamma ray represents its percentage of the 273 keV gamma ray when the two transitions are in equilibrium.

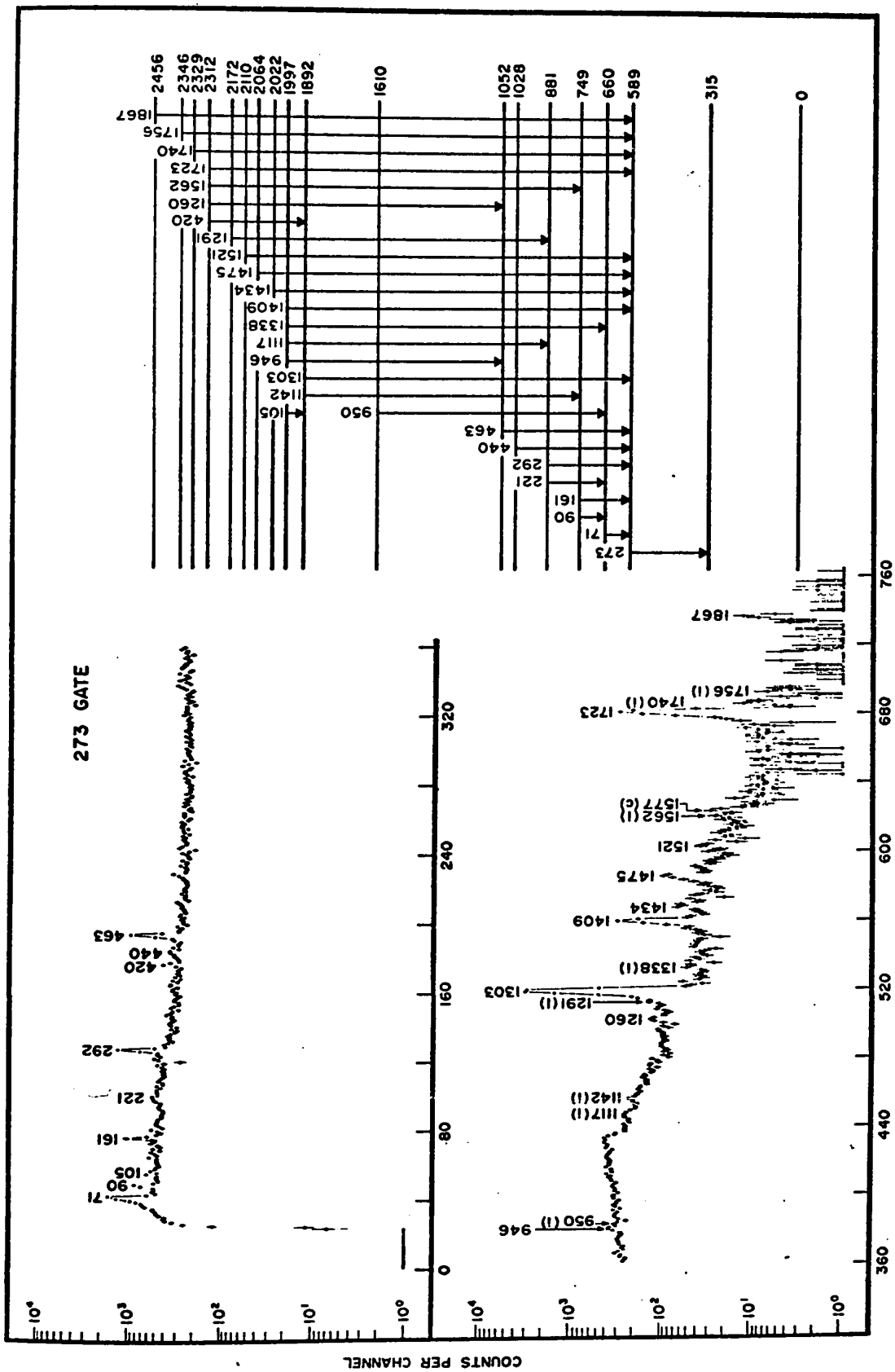

Figure 4.4 Coincidence spectrum associated with the 273 keV gate. The symbol (i) indicates clearer evidence in the reverse gate, lies marked (c) are due to chance

the peaks in this spectrum show the 273 keV line. In the singles spectrum the 161 keV transition is masked by the intense 158 keV transitions of ^{117}In; the intensity quoted for this gamma ray in table 4.1 has been deduced from coincidence probabilities derived from peaks seen in fig. 4.4 and fig. 4.8.

The spectrum in coincidence with the 344 keV gamma ray which de-excites the 660 keV state is shown in fig. 4.5. This gate provides evidence for many new levels as shown in the insert. Strong 158-552 keV coincidences occur in ^{117}Sn, and the imperfect subtraction of the Compton background in the gate brings up a large 158 keV peak. The weak 553 keV peak in fig. 4.5 is masked by the strong 552 keV transitions of the ^{117}In decay.

The 461-463 keV gate, shown in fig. 4.6 and the 434-440 keV gate (not shown) provide further support for many of the levels seen in the partial decay schemes of Figs. 4.4 and 4.5. The spectrum in coincidence with the strong 748 keV gamma ray Fig. 4.6 , containing nothing but a 461 keV peak and indicates that the 748 keV radiation feeds either the 315 keV isomeric state or the ground state. Since the 461 and 748 keV lines both decay with a 3.4 hr half-life, the second choice is mandatory. These data thus define two new levels at 748 and 1209 keV, the ordering being determined by the fact that the 748 keV transition is the stronger of the pair. Some support for these levels is provided by a very

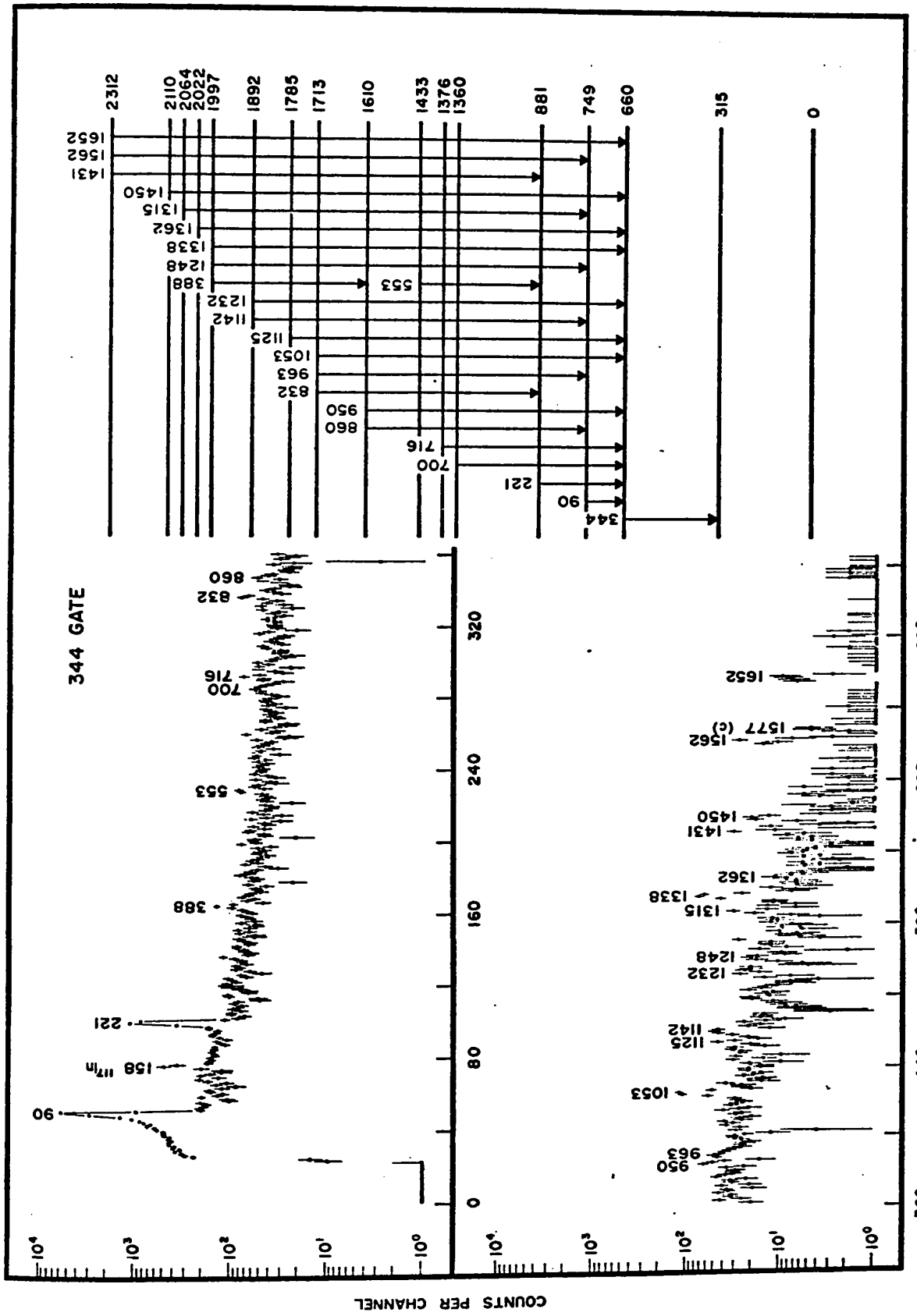

Figure 4.5 Coincidence spectrum associated with the 344 keV gate

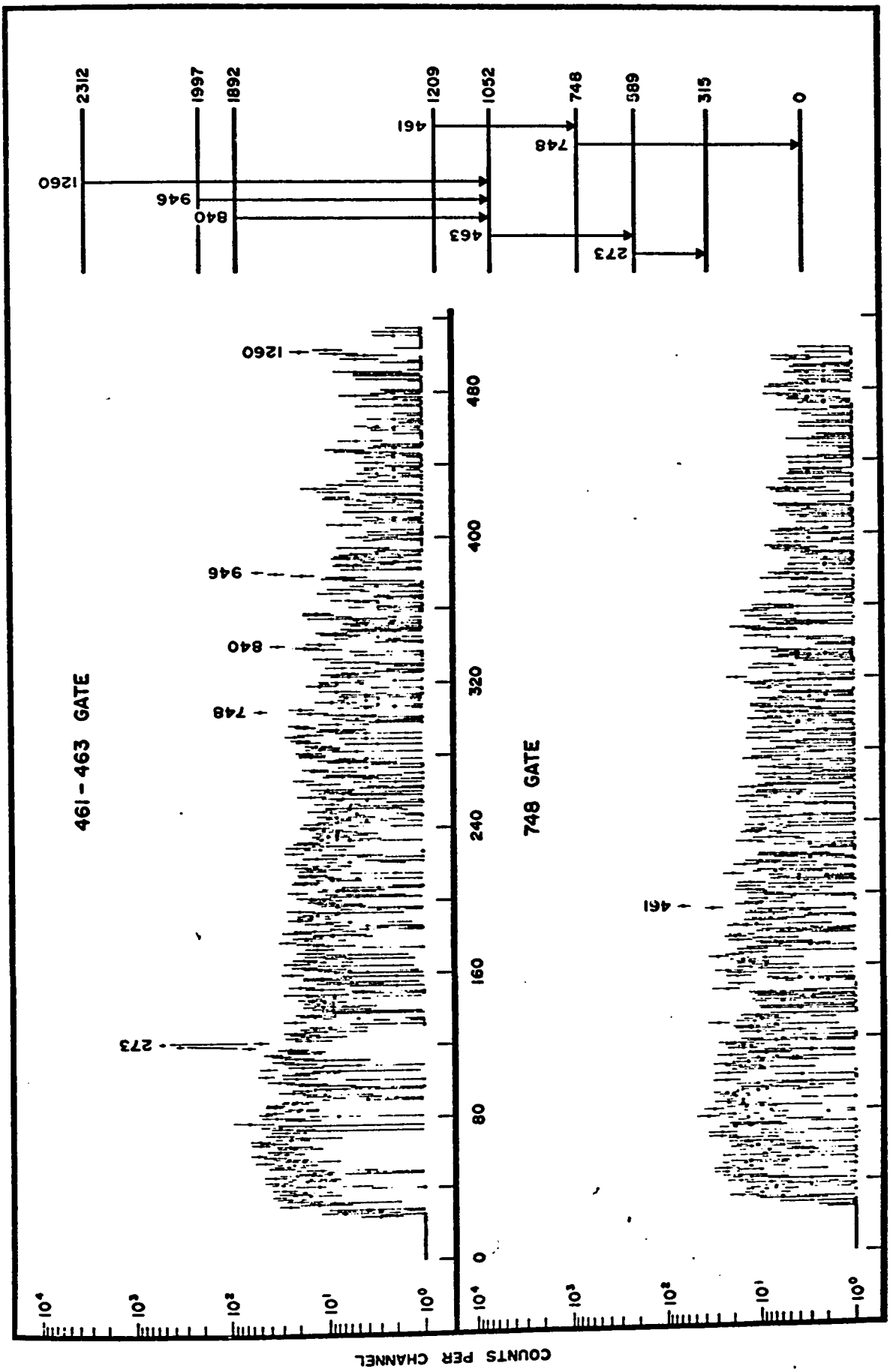

Figure 4.6 Coincidence spectra associated with the 461-463 keV and 748 keV gates

weak 1209 keV cross over transition.

Fig. 4.7 shows spectra associated with gates set on the 832 keV peak and on the composite peak including the 860.3-860.4-862.5 keV transitions. In the latter gate the peak at 1234 keV is due to 800-1234 keV coincidences involving two strong lines which decay with the 3.4 hour half life. The peaks at 90, 161, 273, 344 and 434 keV require the presence of an otherwise unobserved 860.3 keV transition of intensity 0.9. Finally, the 498 keV peak arises from the 489-862 cascade to the ground state. The order of this cascade is determined by relative intensities and defines the level at 862 keV.

Fig. 4.8 shows the lines in coincidence with the 881 keV gate. The 485 and 632 keV transitions have a 3.4 hr half life and deexcite a high spin 1997 keV state; the 285, 388 and 1117 keV gamma rays decay from a low spin 1997 keV level. The 881 keV state is noteworthy in that it is fed from both the ground state and isomer.

Fig. 4.9 presents the 1066 keV gated spectrum, which, together with the spectra in coincidence with the 564 and 1433-1434 keV gates (not shown) provide strong support for the partial decay scheme of the figure. The weak peak at 663 keV in Fig. 4.9 and a better defined 1066 keV peak in the 663 keV gate are evidence for a level at 1729 keV. The 1366 keV state in Fig. 4.8 is similarly defined by 485 and 1366 keV peaks in the 632 keV gate and a 632 keV peak in the 1366 keV

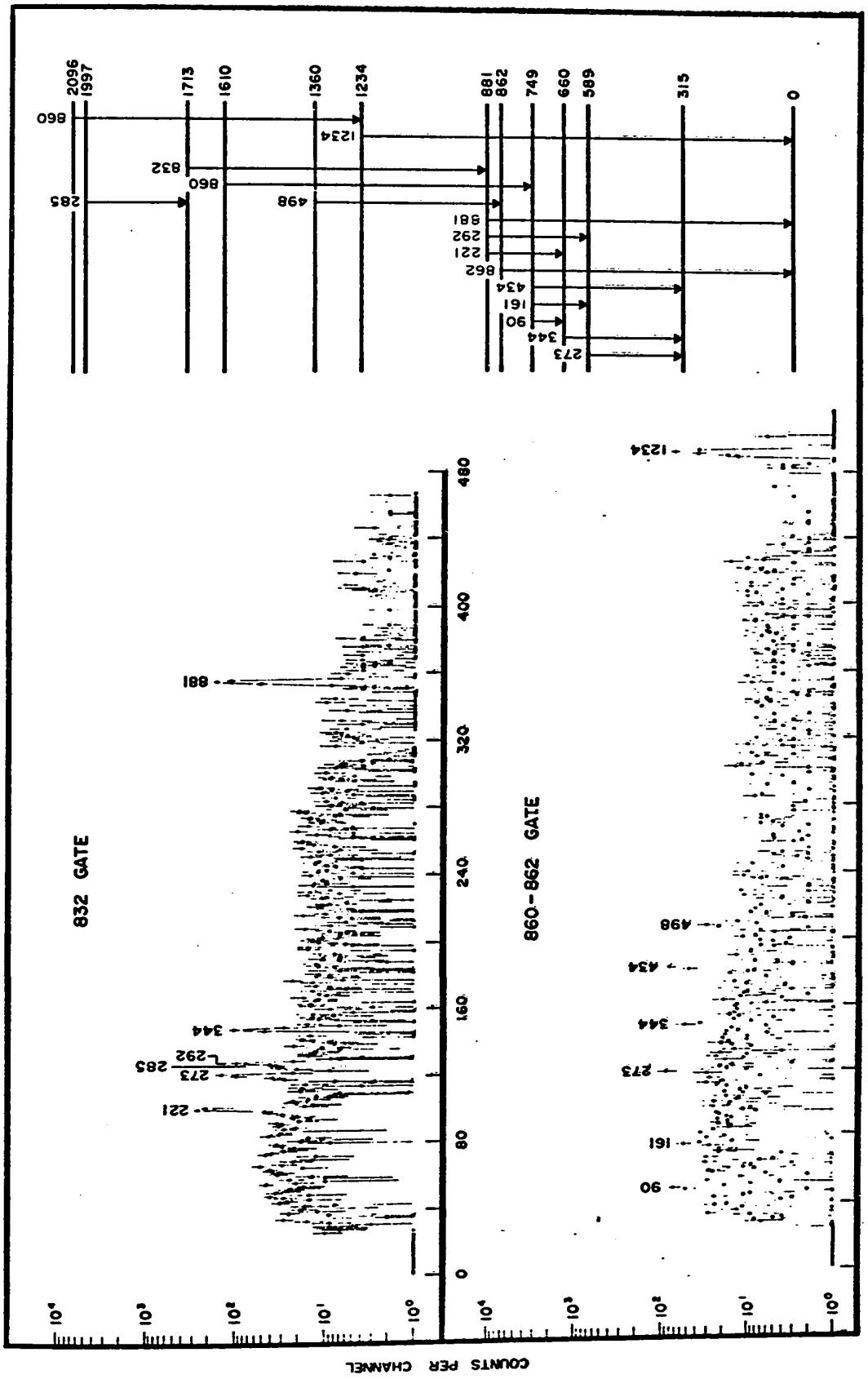

Figure 4.7 Coincidence spectra associated with the 832 keV and 860-862 keV gates

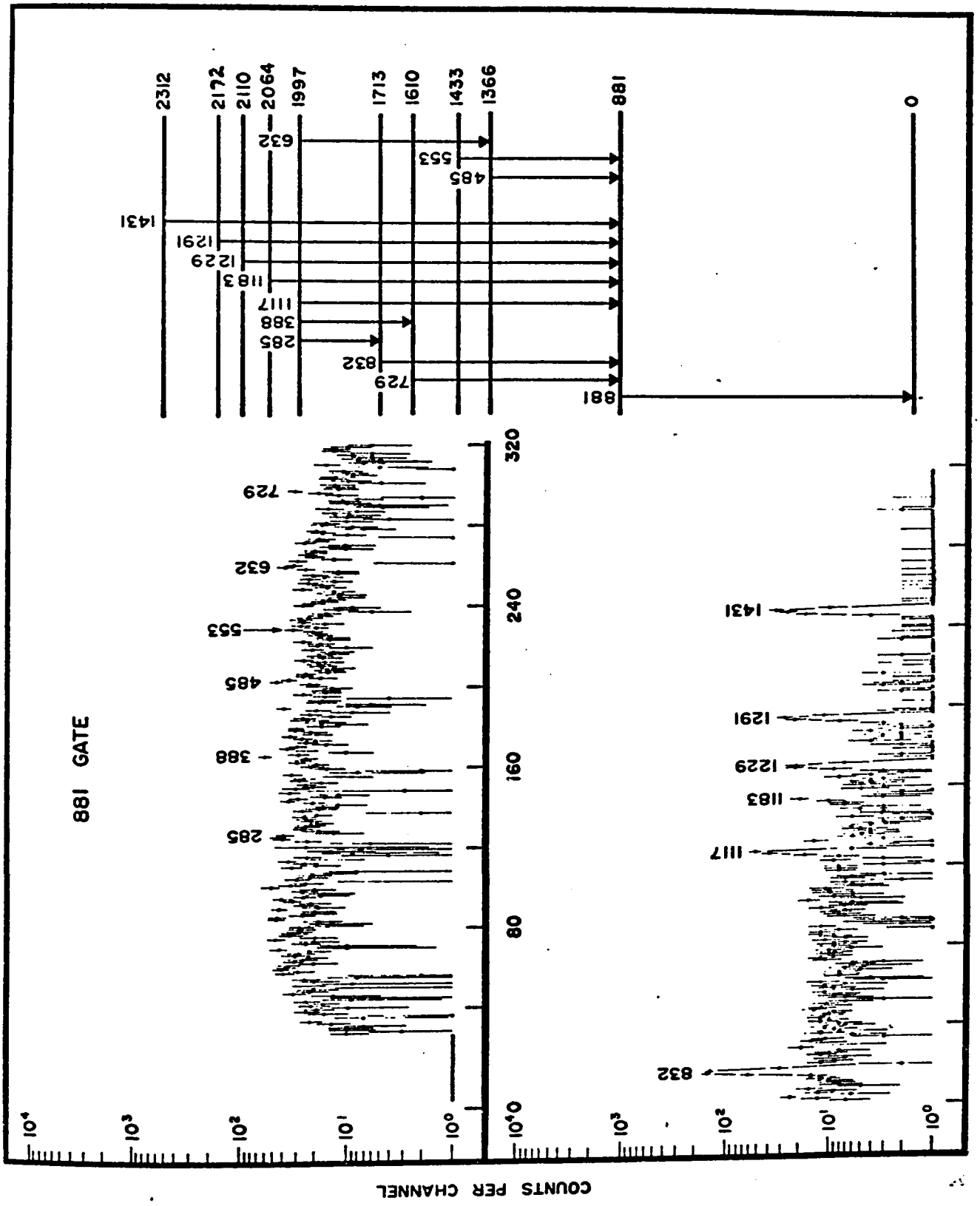

Figure 4.8 Coincidence spectrum associated with the 881 keV gate

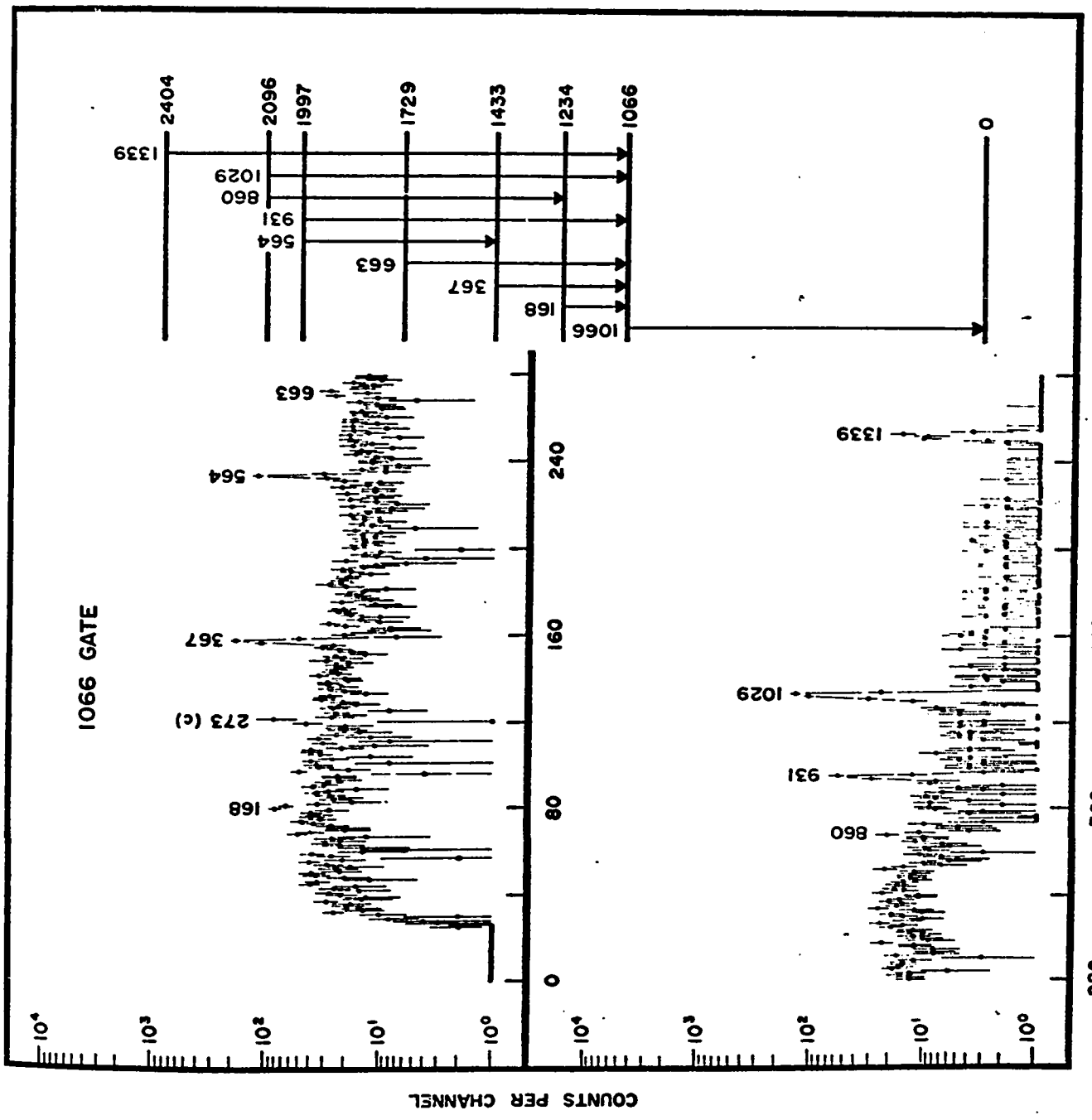

Figure 4.9 Coincidence spectrum associated with the 1066 keV gate

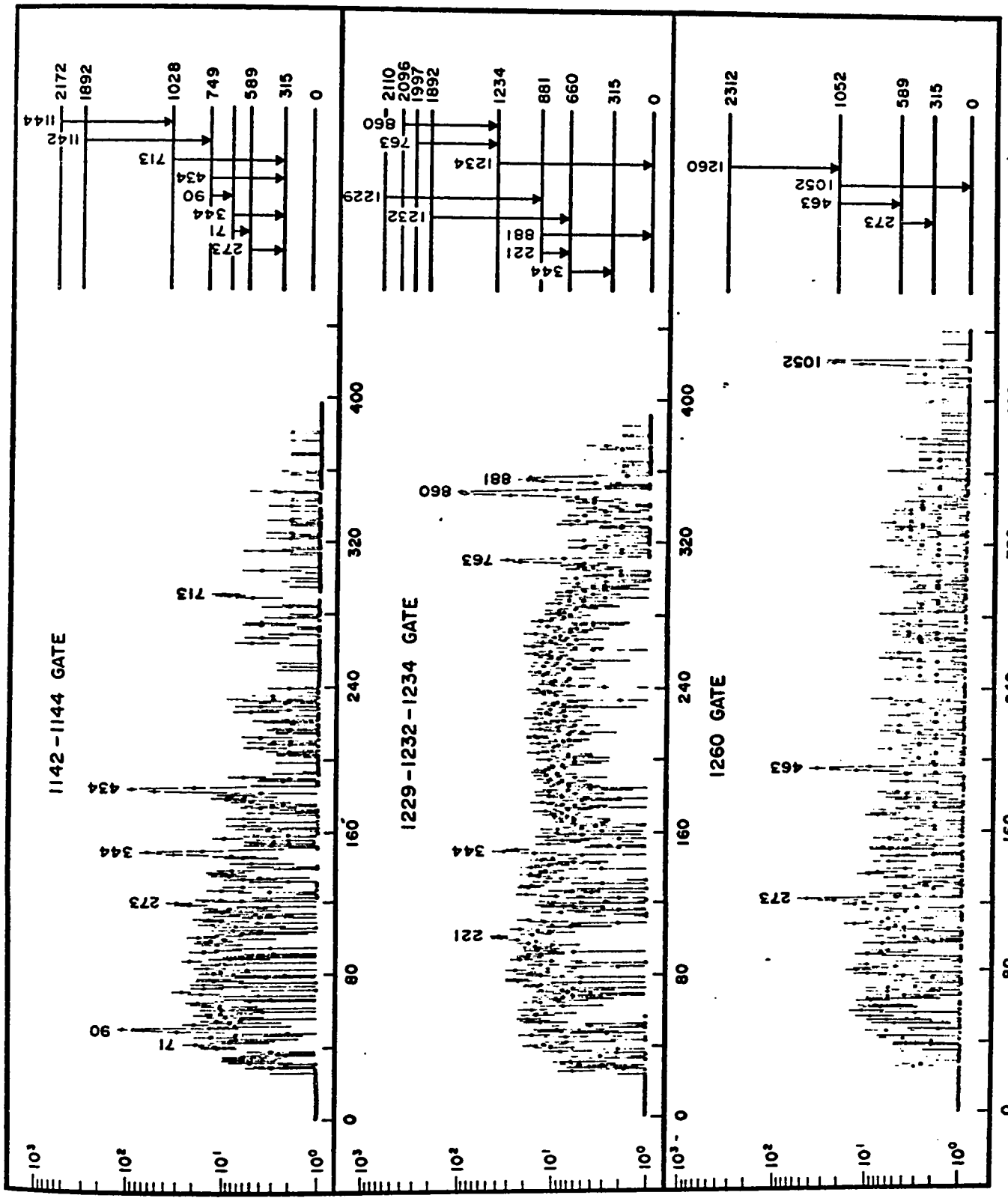

Figure 4.10 Coincidence spectra associated with the 1142-1144 keV, 1229-1232-1234 keV and 1260 keV gates

gate. None of these three spectra are shown.

The spectra associated with the three gates of Fig. 4.10 provide further evidence for many of the levels shown in earlier spectra and need no comment.

Coincidence probabilities were derived from all the coincidence spectra, used to test the decay scheme, and to deduce the intensities of a number of weak or unresolved transitions.

4.5 The Decay Scheme

The results of the measurements described above are incorporated into the decay scheme of figs.4.11 and 4.12. Transitions from the low spin states populated by the beta decay of the $1/2^+$ ground state of ^{117}Cd are shown in fig. 4.11. The dashed level is populated mainly from the isomer. Fig. 4.12 shows the high spin states populated from the $11/2^-$ isomer. The gamma ray intensities, shown in parentheses in figs. 4.11 and 4.12 are relative to 100 for the strong 273 keV transitions. Fig. 4.12 also presents the log ft values for all levels , the deduced spins and parities, which will be discussed in the next section. and the states populated in the (^{3}He,d) and (α,t) reactions.

The beta feeding from the $11/2^-$ isomer of ^{117}Cd to the ground state of ^{117}In has not been observed. The lower limit for the log ft value for this transition is based on

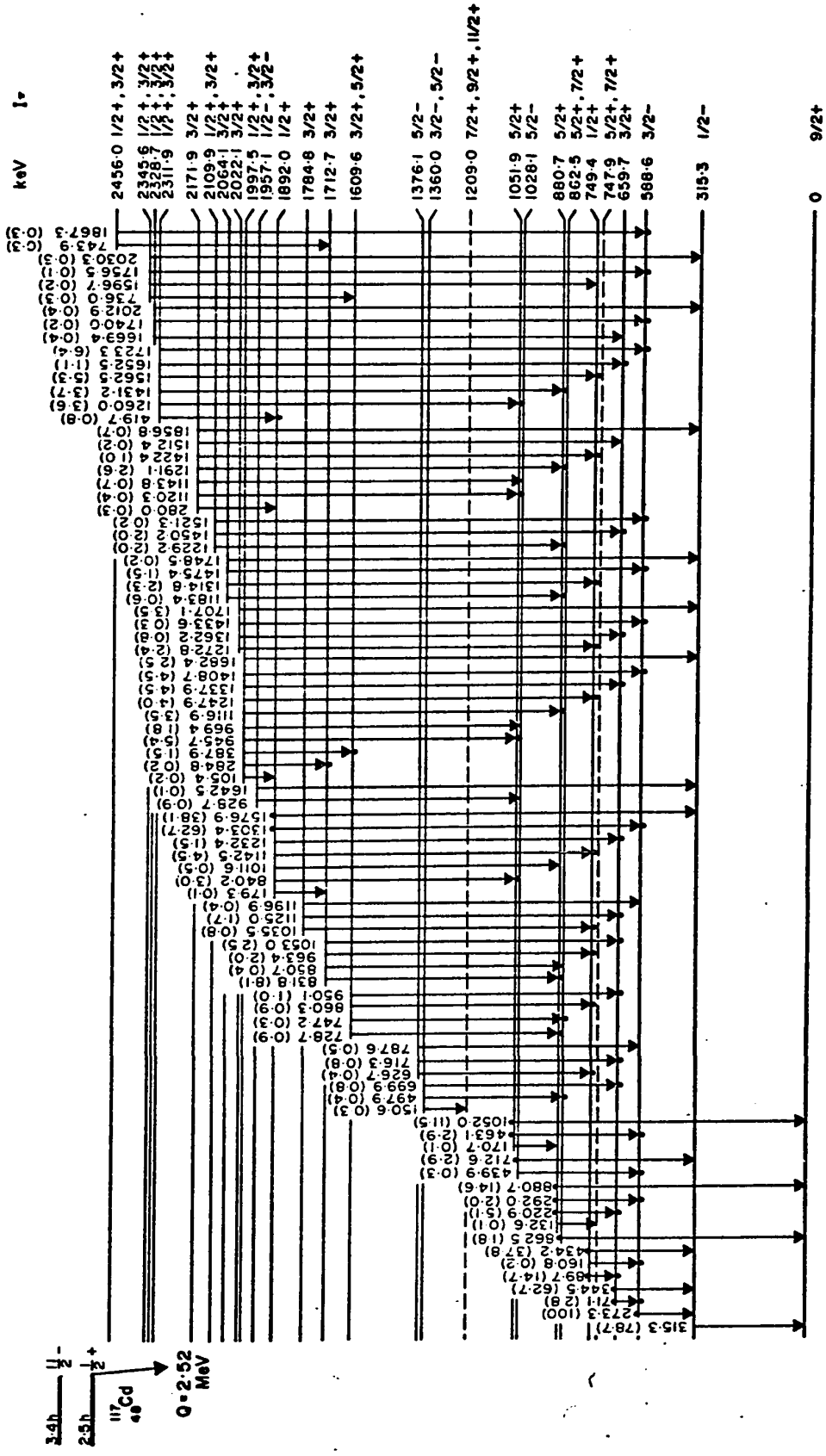

Figure 4.11 The decay scheme of ^{117g}Cd

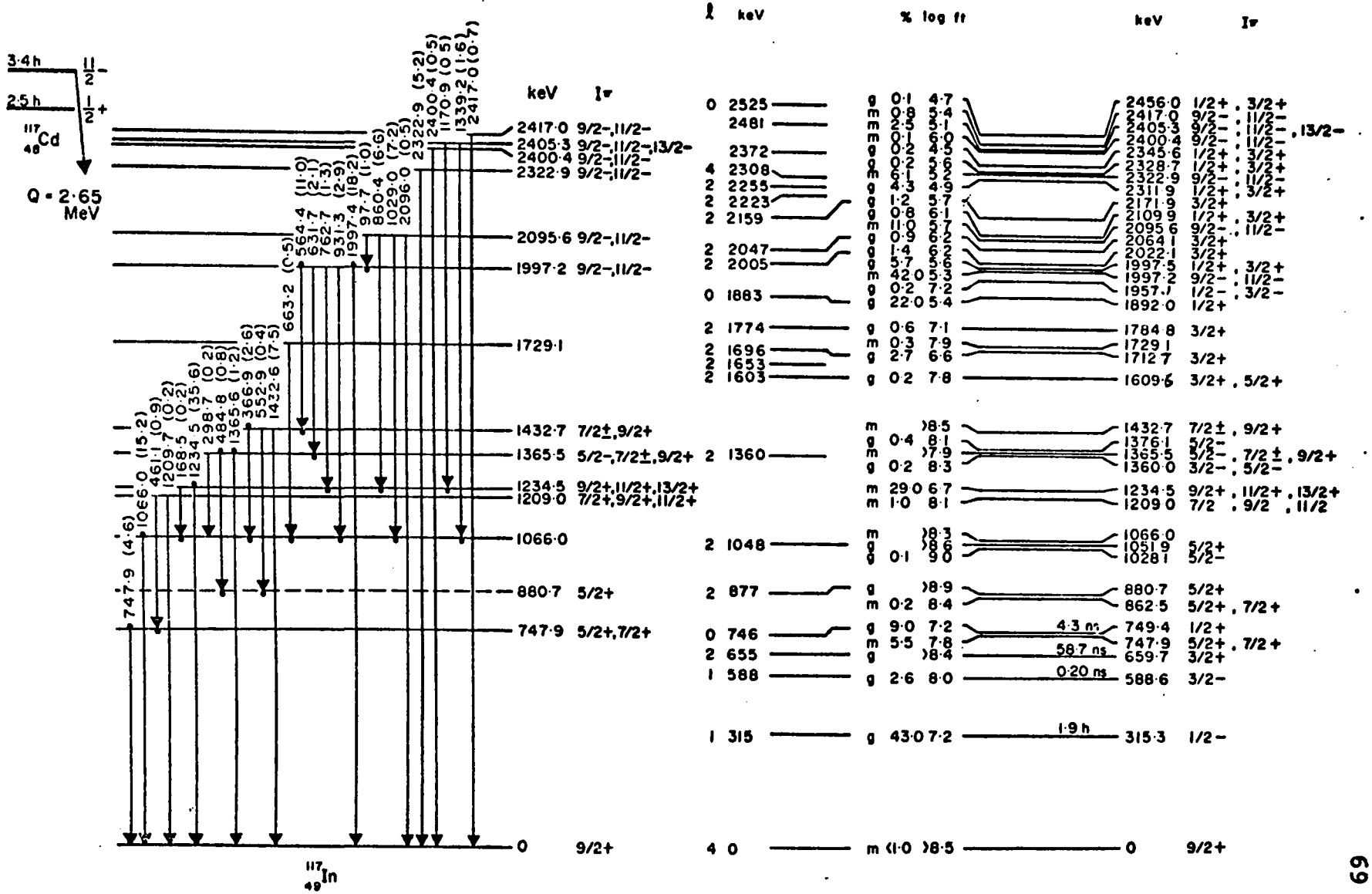

Figure 4.12 Left: The decay scheme of ^{117m}Cd, Centre: States populated in the (^{3}He,d) and (α,t) reaction studies, Right: Properties of states in ^{117}In

the assumption that its intensity cannot be greater than 1% of the total beta intensity (Sharma et al, 1964; Moret, 1969). The energies and ℓ-transfer values obtained from the single particle transfer reaction studies of Harar and Horoshko (1972) are also shown in Fig. 4.12. The correlation between the states which they observe and those of the present work is excellent if one accepts a systematic difference in the energy calibration of $\sim$ 0.8%. Except for levels above 2 MeV, this adjustment lies within their quoted experimental errors.

As is expected, the present work confirms the previously well established levels at 315.3, 588.6, 659.7 and 749.4 keV; the spins, parities, and lifetimes shown for these levels are those of Backlin et al. (1967).

Above 800 keV the results of the present work are in disagreement with those of earlier workers whose conclusions cannot be reconciled with the present coincidence measurements.

The levels at 862.5, 880.7, 1051.9, 1066.0 keV, identified by Pandharipande et al (1968) are now defined by many transitions and a large body of coincidence data. We find no evidence for the 950 keV state proposed by earlier workers. The present coincidence data shows the transition of that energy to be in direct coincidence with the 345 keV line, thus defining a new level at 1609.6 keV. We have also placed new levels at 747.9 and 1028.1 keV each defined by observed coincidence cascades.

Above 1066 keV the agreement with earlier workers becomes very poor. The levels at 1066.0, 1209.0, 1234.5, 1365.5 and 1432.7 keV must all have spins greater than 5/2 since they are fed from the ^{117}Cd isomer, while those at 1360.0 and 1376.1 must have spins less than or equal to 5/2 since they are fed from the ground state. Each of these states is established by the energy fit of several gamma rays and at least one piece of coincidence information.

Between 1600 and 2000 keV there are many low spin states (1609.6, 1712.7, 1784.8, 1892.0 and 1997.5 keV) all supported by many gamma rays and a large amount of coincidence data. There is also a strongly populated high spin state at 1997.2 keV which can be clearly differentiated from the low spin 1997.5 keV level by the fact that the transitions from it decay with a 3.4 hour half life. These two levels were not resolved in earlier work. In addition to these states there is probably a low spin state at 1957.1 keV and weak evidence for a high spin state at 1729.1 keV.

Above 2000 keV, there are many states defined by weak transitions. Those at 2022.1, 2064.1, 2109.9, 2171.9, 2311.9, 2328.7 and 2345.6 keV are securely established states of low spin, while the level at 2095.6 keV is a firmly established high spin state. Of the remainder the levels shown at 2405.3, and 2456.0 keV are each placed on the basis of an energy fit of a pair of gamma transitions while those at 2322.9, 2400.4 and 2417.0 keV are each de-excited by just one gamma transition

to the ground state. The parentage measurements and energy considerations forbid these transitions being placed elsewhere. There are four other weaker transitions of this category shown in table 4.1 which have not been placed in the decay scheme.

4.6 Spin and Parity Assignments

The spins and parities of five low lying states may be uniquely assigned using published data and form a secure base from which other spin-parity assignments may be deduced. The $9/2^+$ and $1/2^-$ assignments for the ground state and 315 keV isomer rest on atomic beam spin determinations (Cameron and Summers-Gill, 1962, 1963) and $^{118}Sn(d,^3He)^{117}In$ studies (Weiffenback and Tickle, 1971) and are in good agreement with shell model predictions. The $3/2^-$ assignment to the 588.9 keV state is uniquely determined from the M1+E2 character of the 273 keV transition (Backlin et al, 1967). The E1 character of the transitions from the 659.7 and 749.4 keV states to the $1/2^-$ isomeric state (Backlin et al, 1967) requires that both these states have positive parity and spins of 1/2 or 3/2. The anisotropic angular distribution pattern of the 89.7 - 344.5 keV gamma-gamma cascade (Mancuso and Arns, 1965; Begzhanov et al, 1969) makes the $3/2^+$ assignment to the 659.7 keV state mandatory. The angular distribution of the deuterons in the $^{116}Cd(^3He,d)^{117}In$ reaction (Harar and Horoshko, 1971) show that the 749.4 keV state is populated in

an $\ell = 0$ transfer and must therefore have a spin of 1/2. In addition to these five levels, one may also regard the spin-parity of the 1892.1 keV level to be certainly $1/2^+$. This conclusion is based on the log ft value of 5.4 for the beta feed of this state, the 1303-273 gamma-gamma angular correlation pattern (Mancuso and Arns, 1965; Begzhanov et al, 1969; Pandharipande et al, 1966) for the strongest cascade de-exciting this state, and the $\ell = 0$ transfer associated with this state in the (^{3}He,d) reaction.

Many of the high lying states have log ft values ≤ 6 characteristic of allowed transitions thus implying J^π values of $1/2^+$, $3/2^+$ for those levels fed from the ^{117}Cd ground state and $9/2^-$, $11/2^-$ or $13/2^-$ for those fed from the isomer. For states in the energy range 800 to 2000 keV the log ft values can be quite unreliable because they result from small differences between the intensities of the incoming and outgoing gamma rays.

The results of the (^{3}He,d) angular distributions (Harar and Horoshko, 1972) when used in conjunction with the present results, lead to unique assignments of $3/2^+$ for the 2022.1, 2064.1 and 2171.9 keV levels.

Since no $\ell = 5$ states were observed in the reaction data we cannot uniquely determine the spin for any of the states fed by allowed transitions from the $11/2^-$ isomer. However, for those of this group which deexcite to the $9/2^+$ ground state, the $13/2^-$ alternative can be rejected, as this

would require an M2 transition to be competing strongly with E1 and M1 transitions. States which fall into this category are those at 1997.2, 2095.6, 2322.9, 2400.4 and 2417.0 keV. The states at 1609.6, 1712.7 and 1784.8 keV are fed from the ^{117}Cd ground state with log ft values of 7.8, 6.6 and 7.1 respectively. They feed a number of low spin and parity states but not the $9/2^+$ ground state and are excited by $\ell = 2$ transfers in the reaction work. These facts strongly suggest that they are $3/2^+$ states. A $5/2^+$ choice for the 1609.6 keV state is also possible because of the high log ft value.

The 880.7 and 1051.9 keV levels are probably not beta fed, are populated from many states of $1/2^+$ or $3/2^+$, and deexcite to the $9/2^+$ ground state and to $3/2^+$ and $3/2^-$ excited states. Since they are also excited by $\ell = 2$ transfers in the reaction work, their spins and parities must be $5/2^+$.

It is not easy to identify either the 1360.0 or 1365.5 keV states with the 1360 keV $\ell = 2$ state in the reaction work. The 1365.5 keV state would be the natural choice but it is not fed in the beta decay. It is fed from the $(9/2^-, 11/2^-)$ state at 1997.2 and deexcites to a $5/2^+$ state at 880.7 keV and to the $9/2^+$ ground state. It could thus have a spin of $5/2^-$, $7/2^\pm$ or $9/2^+$. Neither $3/2^+$ or $5/2^+$ is acceptable. The 1360.0 keV level, which is the other possibility, is weakly beta fed from the ground state, deexcites to a $5/2^+$ state but not to the $9/2^+$ ground state. This data can readily be reconciled with assignments of $3/2^-$ and $5/2^-$ but not with $5/2^+$.

We conclude that the 1360 keV state of the reaction work is not populated in the decay process.

The 1028.1 and 1376.1 keV levels are also probably not fed in the beta decay, however, they decay to the low lying 1/2 and 3/2 states and not to the $9/2^+$ ground state. This suggests that they have spins of $5/2^-$ though other low spin choices are not ruled out. The 862.5 keV level is not appreciably beta fed, deexcites only to the $9/2^+$ ground state and is fed from $3/2^+$ and $5/2^+$ states at 1712.7 and 1360.0 keV respectively. Its spin can therefore be $5/2^+$ or $7/2^+$. The level at 1957.1 is fed by a first forbidden decay from the ^{117}Cd ground state and decays to $1/2^-$ and $3/2^-$ states; thus its spin and parity assignment is expected to be $1/2^-$ or $3/2^-$.

The states at 1066.0, 1234.5 and 1432.7 keV are fed from the 1997.2 keV, $9/2^-$, $11/2^-$ state and feed the $9/2^+$ ground state. The 1066.0 keV state is not beta fed and its spin can only be deduced as being between 7/2 and 13/2. The beta feed to the 1234.5 keV state is apparently first forbidden thus restricting the J^π values to $9/2^+$, $11/2^+$ and $13/2^+$. Weiffenbach and Tickle (1971) observe a state at 1.43 MeV with an $\ell = 3$ or $\ell = 4$ angular distribution in the (d,^{3}He) reaction. If this level is identified with our 1432.7 keV state, it restricts its J^π assignment to $7/2^+$ or $9/2^+$. The weakly populated 1209.0 keV level is apparently fed by a first for-

bidden transition from the isomer and feeds the ground state and the 747.9 keV state. Since the 747.9 keV level is also fed from a $5/2^+$ state and feeds the $9/2^+$ ground state, its spin and parity are restricted to $5/2^+$ or $7/2^+$. The J^π assignments for the 1209.0 keV level can therefore be $7/2^+$, $9/2^+$ or $11/2^+$.

4.7 Discussion

The low lying states of ^{117}In have been extensively studied by many workers and the present situation is clearly presented by Backlin et al (1967). The ground state and the 315.2 keV level are well described as $g_{9/2}{}^+$ and $p_{1/2}{}^-$ hole states, while the 587 keV state appears to be a mixture of the $p_{3/2}{}^-$ hole state and a coupling of the $p_{1/2}{}^-$ particle to the 2^+ core of ^{118}Sn. As these authors point out, positive parity states may be formed by coupling the $g_{9/2}$ hole to one or more of the several quadrupole vibration phonons, by coupling the negative parity particle states to an octupole vibration, or through many particle states. However all these mechanisms would place such states at energies of $\sim$ 1 MeV or higher. They therefore proposed that the $3/2^+$ and $1/2^+$ states at 659.7 and 749.4 keV were members of a rotational band based on the $1/2^+[431]$ Nilsson state which would occur at low excitation if the ^{117}In nucleus, which is expected to be spherical in its ground state, could take up a deformed shape at somewhat higher excitations. They based their suggestion on

the observation of an enhanced E2 transition between the $1/2^+$ and $3/2^+$ levels in ^{117}In and retarded E1 transitions to the low lying states. Similar evidence for the population of the Nilsson state appears in ^{115}In (Backlin et al, 1967) and ^{111}Ag (Berzins et al, 1969). Furthermore, the measured quadrupole moment of the 660 keV level (Raghavan and Raghavan, 1972) is in excellent agreement with the predictions of the rotational model.

Pandharipande et al (1968) and Moret (1969) made an attempt to identify the higher spin members of this band. Their proposal that the 880.7 keV state of spin $5/2^+$ be the next member of the sequence is consistent with our observation of a strong 880.7→659.7 keV transition and the presence of a retarded E1 transition to the $3/2^-$ hole state. The high spin state at 747.9 keV may well be the $7/2^+$ member of the band since it is fed from the $5/2^+$ state at 880.7 keV.

The $3/2^+$, $1/2^+$ and $5/2^+$ members of the proposed rotational band are all strongly populated in both the (^{3}He,d) and (α,t) reactions. The observed 746 keV peak would include both the $1/2^+$ state at 749.7 keV and the proposed $7/2^+$ state at 747.9 keV. This peak is much stronger in the (α,t) reaction than one would expect; and the excess intensity may well be due to the contribution of the $7/2^+$ component of the doublet, which would not be strongly excited in the (^{3}He,d) reaction.

Attempts to reproduce the energies of these states

from the rotational energy relationship for a K = 1/2 band have been made by regarding the inertial factor $h^2/2\mathcal{I}$ and the decoupling factor "a" as free parameters to make a fit to the experimental energies of the first four states in the band. Reasonable agreement between the experimental level energies and those derived from theory can be obtained with $h^2/2\mathcal{I}$ = 14 keV and a = -2.7. The theoretical predictions corresponding to these parameters, with the experimental energies given in brackets are as follows: $3/2^+$ 660 keV (660 keV), $7/2^+$ 752 (748), $1/2^+$ 731 (749), $5/2^+$ 919 (881), $11/2^+$ 957 (no candidate) and $9/2^+$ 1218 (1209). The values of $h^2/2\mathcal{I}$ and "a" chosen are not very critical and values of $h^2/2\mathcal{I}$ in the range 10 to 16 keV with values of "a" in the range -3.5 to -2.2 all give a reasonable fit to the observed level structure. The main argument for the identification of these levels with the rotational band must rest on the character of the intraband transitions. The 9/2→7/2, 5/2→7/2, 5/2→3/2 and 1/2→3/2 transitions in the proposed band seem relatively intense, but in the absence of knowledge concerning reduced transition probabilities, the identification of these levels with a band based on the $1/2^+$[431] state must be regarded as quite tentative. It should also be noted that in the case of ^{115}In, which has a very similar level structure, a hole-vibration coupling calculation (Dietrich et al, 1970) successfully explained many of the observed experimental results,

but failed to account for the low spin, low energy positive parity states. Recently, Alzetta et al (1972), in a quasi-particle calculation also failed to account for these low lying positive parity states.

The simplest core particle coupling approach predicts a multiplet of five positive parity levels with spins 5/2, 7/2, 9/2, 11/2 and 13/2 arising from the coupling of the 2^+ state of the core with the $9/2^+$ state of the proton hole. The level energies expected for this multiplet have been calculated by Pandharipande (1967) using a simple residual reaction. Although the candidates proposed for this multiplet by Pandharipande (1967) can no longer be accepted, the present work suggests possible alternatives. The spins and level energies predicted by Pandharipande's calculation together with our proposed candidates in parentheses are as follows: $7/2^+$ 829 (862), $5/2^+$ 1020 (1051), $13/2^+$ 1040 (1066), $9/2^+$ 1220 (1234) and $11/2^+$ 1440 (no candidate). The first four states proposed have spins and parities consistent with these assignments. We have no candidate to propose for the 11/2 member of the multiplet, although it is perhaps worth noting that there is a fairly strong unclassified transition of 1486.2 keV which could define a level at this energy and which could thus be considered as the fifth member. The proposed members of a 1/2+[431] rotational band and the $(9/2^+, 2^+)$ multiplet are shown in fig. 4.13.

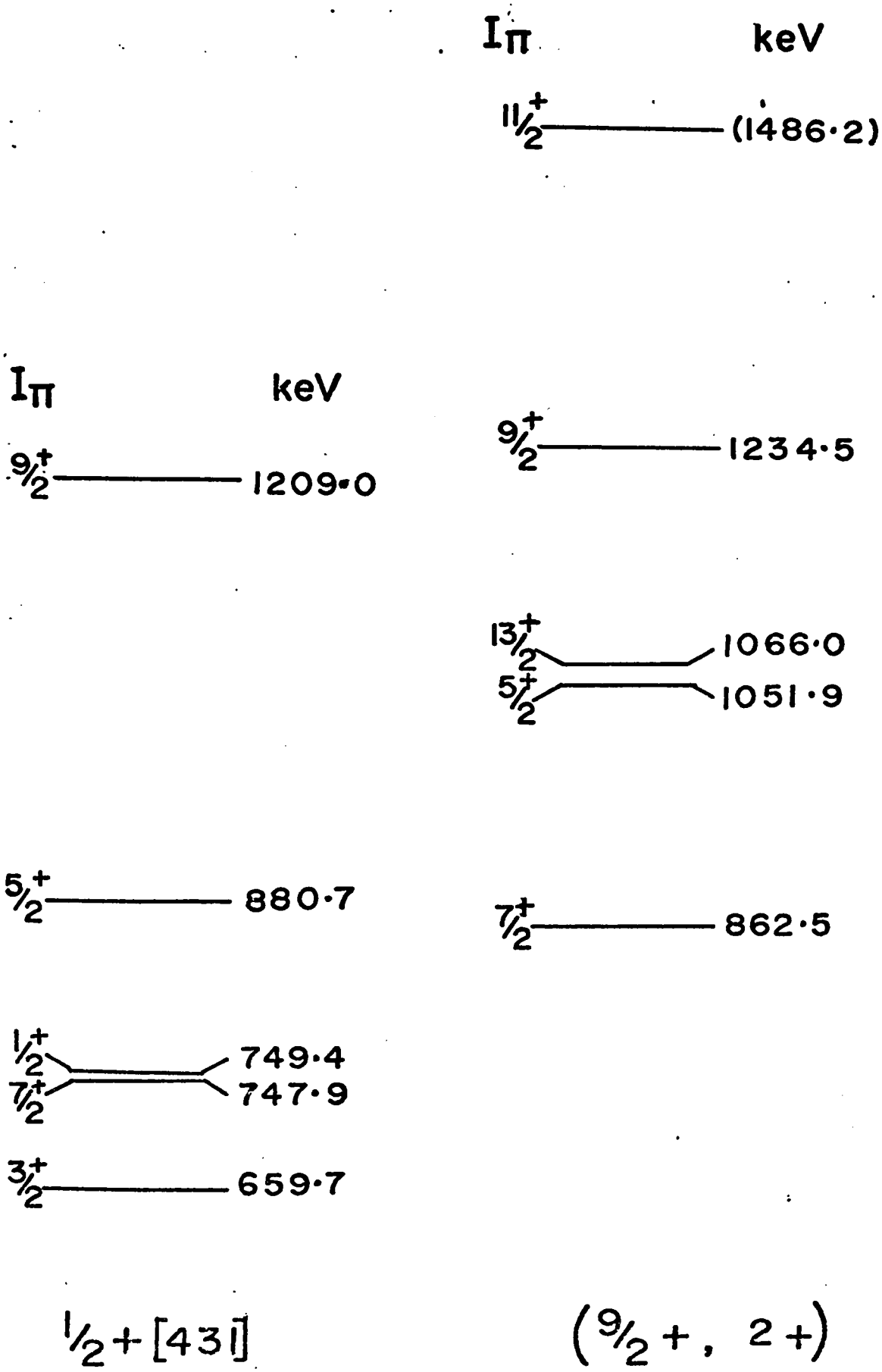

Figure 4.13 Proposed members of a 1/2+[431] rotational band and a (9/2+,2+) multiplet in ^{117}In

4.8 Summary

The energy levels of ^{117}In have been investigated following the beta decay of 3.4 h ^{117m}Cd and 2.5 h ^{117g}Cd. Using high resolution Ge(Li) detectors singly and in coincidence, one hundred and twenty-seven gamma transitions have been observed. Eighty-five of these transitions have been classified by both coincidence data and energy fit, twenty-nine weak transitions by energy fit alone, and twelve remain unclassifed. Thirty-seven levels in ^{117}In have been established; of these, twenty-four are low spin states fed from the ground state and thirteen are high spin states fed from the isomer. Spin and parity assignments for the newly established levels were discussed. Discussion of a possible interpretation in terms of a rotational band and in terms of core particle coupling is made.

CHAPTER 5

ENERGY LEVELS IN ^{171}Lu

5.1 Introduction

The single nucleon stripping reaction has been shown to be a very useful tool for studying the intrinsic states of deformed nuclei. Recently this technique has been used to study the proton particle states in the odd lutetium isotopes ^{173}Lu, ^{175}Lu and ^{177}Lu (O'Neil et al. 1971). The present work extends this investigation to ^{171}Lu.

The single particle reaction work has been complemented by means of gamma ray and conversion electron measurements following the reaction ^{169}Tm(α,2n)^{171}Lu. The gamma spectrum has been studied from the decay of ^{171}Hf by Harmatz and Handley (1966) and more recently by Gizon et al (1970). In addition there have been a number of in beam studies. Bjørnholm et al. (1965) studied isomeric decay following the ^{171}Yb(p,n)^{171}Lu reaction and reported a 70.4 keV, E3 transition with a 76 sec half life. They assign this as depopulating the 1/2-[541] Nilsson state to the 7/2+[404] ground state. Concurrent studies using the ^{169}Tm(α,2n)^{171}Lu reaction, (Noma et al. 1970, Hjorth et al. 1972 and Barnéoud et al 1972) and also the ^{171}Yb(d,2n)^{171}Lu reaction (Kemnitz et al. 1971) have resulted in a level scheme which includes rotational bands based on the 7/2+[404], 1/2-[541],

1/2+[411], 5/2+[402] and 9/2-[514] Nilsson orbitals. The single particle reaction work was undertaken to confirm these assignments and to search for further single particle states in the energy region between 0 and 1600 keV. The procedure and results of this study are described in sections 5.2 to 5.4 below.

The gamma ray studies were undertaken to establish rotational bands up to high spin for each of the above mentioned Nilsson orbitals. With high resolution Ge(Li) detectors in the coincidence mode it was possible to assign some interesting K forbidden interband transitions. By means of a conversion electron spectrum conversion coefficients for 27 transitions have been measured leading to M1:E2 mixing ratios for many cascade transitions. This work is described in sections 5.5 to 5.7 below.

5.2 Particle Spectrograph Experiments

The general features of the experimental procedures for the (^{3}He,d) and (α,t) exposures follow those of O'Neil et al. (1971). The F.N. accelerator was used to produce beams of 24 MeV ^{3}He particles and 26 MeV α particles. The beam intensity was typically 1 μA through 1 mm × 2.5 mm slits. The reaction products were analyzed with the Enge magnetic spectrograph, and recorded on 50 μm thick photographic emulsions. For the (^{3}He,d) exposures an aluminum absorber 0.5 mm thick was placed in front of the emulsion to stop tritons produced

in (α,t) reactions from reaching the plates. Similarly, a 0.05 mm thick aluminum absorber was used when recording the triton spectra in order to stop the carbon ions which recoil from the target backing, and singly charged α particles. The ytterbium targets were ∿ 60 μg/cm^2 thick on carbon backing of ∿ 50 μg/cm^2 thickness. The isotopic composition of the target material is given in table 5.1. It can be seen that the enrichment is not particularly good. In order to be

Table 5.1

Isotopic composition of the ^{170}Yb target

Abundance of Yb Isotope with Mass						
168	170	171	172	173	174	176
<0.07%	81.4%	7.8%	4.8%	2.3%	3.1%	0.73%

able to make allowance for the main isotopic impurity an exposure was made for the (^{3}He,d) reaction on a ^{171}Yb target. For the ^{172}Yb target impurity the shape of the spectrum is known from the work of O'Neil et al. (1971).

Spectra were recorded at θ = 38° and 48° for the (^{3}He,d) reaction and at θ = 90° and 120° for the (α,t) reaction. These angles were chosen to avoid as far as possible high mass impurity peaks in the region of interest. In the case of the (α,t) reaction backward angles were required because, for beam

energies near the target Coulomb barrier, tritons preferentially come out at backward angles.

Fig. 5.1 shows the deuteron spectrum from the (^{3}He,d) reaction at $\theta=38^\circ$ and the triton spectrum from the (α,t) reaction at $\theta = 90^\circ$. The measured resolutions (F.W.H.M.) were approximately 18 keV and 17 keV respectively.

The analyses of the spectra were carried out with the aid of the peak fitting program referred to by Burke et al. (1971). The average of the excitation energies from each reaction together with the observed (^{3}He,d) and (α,t) cross sections are presented in Table 5.2. For the strongly populated states the uncertainties are about 2 keV in the excitation energies and 15% in the relative intensities, for others the error in the intensity is greater than this due to the underlying background arising from isotopic impurities in the target.

5.3 The D.W.B.A. and Nilsson Calculations

In a single nucleon transfer reaction the cross section for any particular state depends in a simple way on $C_{j\ell}$, the spherical expansion coefficient for that state. In many cases, the distribution of strength among members of a band provides a characteristic "fingerprint" by which the band may be identified. In other cases the value of $C_{j\ell}^2$ is nearly unity for one particular rotational band member. In either case the observed populations can be predicted quite well by calculations which use the stripping theory of Satchler (1958), nuclear

Figure 5.1

The deuteron spectrum obtained from the $^{170}Yb(^{3}He,d)^{171}Lu$ reaction at $\theta = 39°$ and the triton spectrum from the $^{170}Yb(\alpha,t)^{171}Lu$ reaction at $\theta = 90°$.

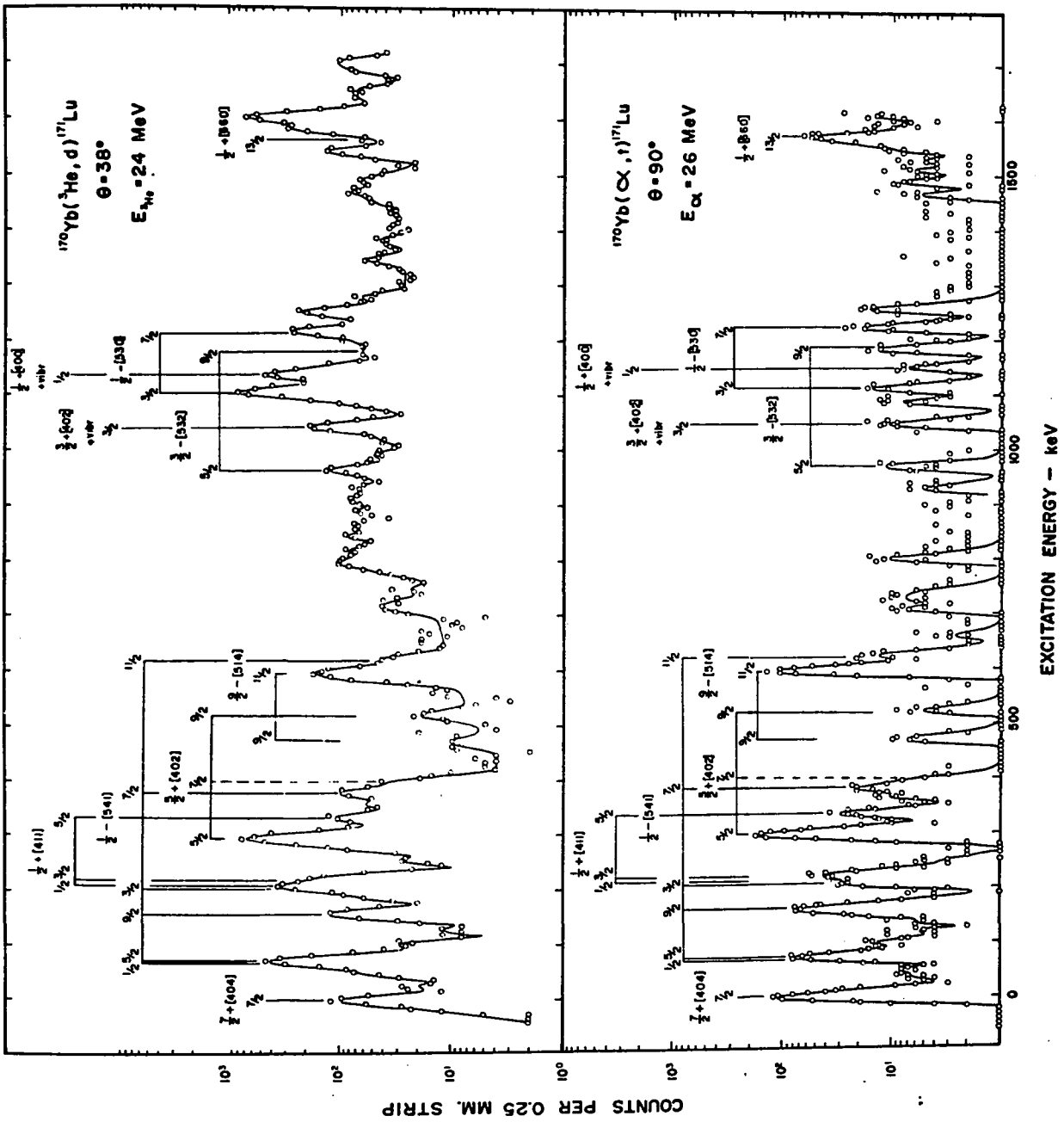
^{170}Yb(^{3}He, d)^{171}Lu
θ = 38°
$E_{^3He}$ = 24 MeV
^{170}Yb(α, t)^{171}Lu
θ = 90°
E_α = 26 MeV
COUNTS PER 0.25 MM. STRIP
EXCITATION ENERGY – keV

TABLE 5.2

Levels Populated in ^{171}Lu by the Single Particle Transfer Reactions

Energy (keV) gamma	Energy (keV) deuteron	Energy (keV) triton	Assignment $IK^{\pi}[Nn_z\Lambda]$	$(d\sigma/d\Omega$ (μb/sr) (^{3}He,d) at θ=38°	$(d\sigma/d\Omega$ (μb/sr) (α.t) at θ=90°
0	0	0	7/2 7/2+[404]	12	18
71.1	73	73	1/2 1/2-[541]	54	13
72.9			5/2 1/2-[541]		
159.2	159	160	9/2 1/2-[541]	16	14
206.4	209	207	3/2 1/2-[541]	38	4.6
208.1			1/2 1/2+[411]		
220.6	224	222	3/2 1/2+[411]	18	6.6
295.6	297	295	5/2 5/2+[402]	87	27
333.6	335	335	5/2 1/2+[411]	14	4.8
379.3	380	382	7/2 1/2-[541]	12	2.9
394.7	399	394	7/2 5/2+[402]	3.7	0.8
469.3	471	472	9/2 9/2-[514]	0.8	1.1
519.3	521	523	9/2 5/2+[402]	1.6	0.7
593.7	598	596	11/2 9/2-[514]	26	19
619.8	624	625	11/2 1/2-[541]	3.8	1.8
	799	802		12	1.6
	967	968	5/2 3/2-[532]	13	0.8
	1045	1049	(3/2 3/2+[402]25%+γ vib)	21	1.6
	1087	1090		7	∿1
	1107	1114	3/2 1/2-[530]	93	2.4
	1139	1151	(1/2 1/2+[400]28%+γ vib)	55	∿1
	1156		(1/2 1/2+[400]5% +β vib)	11	
	1178	1185	9/2 3/2-[532]	∿3	2.2
	1218	1224	7/2 1/2-[530]	32	3.1
	1253	1258		25	2.5
	1542	1549		14	1.2
	1565	1572	13/2 1/2+[660]	2.9	8.5
	1583	1594		31	1.0
	1603	1609		84	1.9

wave functions given by Nilsson (1955) and the intrinsic particle cross sections from the distorted wave Born approximation (Bassel et. al. 1962). The predicted spectroscopic factors with and without Coriolis coupling are presented in table 5.3.

The cross sections for the (^{3}He,d) and for the (α,t) reactions were calculated using the computer code DWUCK (Kunz 1967). The optical model parameters used for these calculations were the same as those used in a number of earlier studies, in particular that of O'Neil et al. (1971), on the odd mass lutetium isotopes ^{173}Lu, ^{175}Lu and ^{177}Lu. Following this work a local zero-range potential is used together with a lower cut-off of 9.6 fm for both the reactions. The standard zero range normalization factors of N = 4.42 for the (^{3}He,d) reaction and N = 46 for the (α,t) reaction were used. No renormalization has been performed, although it should be noted that the value of the normalization factor for the (α,t) reaction is subject to considerable uncertainty.

It has been observed that the ratio of the experimentally measured (^{3}He,d) and (α,t) cross sections can be a useful indicator of ℓ value. In studies of levels in rhenium isotopes (Lu and Alford 1971) this ratio was often found to be more useful than a complete angular distribution for the determination of ℓ values. The present results, for the ratios of the (^{3}He,d) cross sections measured at 38° to the (α,t) cross sections measured at 90°, are shown in Fig. 5.2. The solid lines are values obtained from the DWBA calculations plotted as a function of excitation energy. The experimental

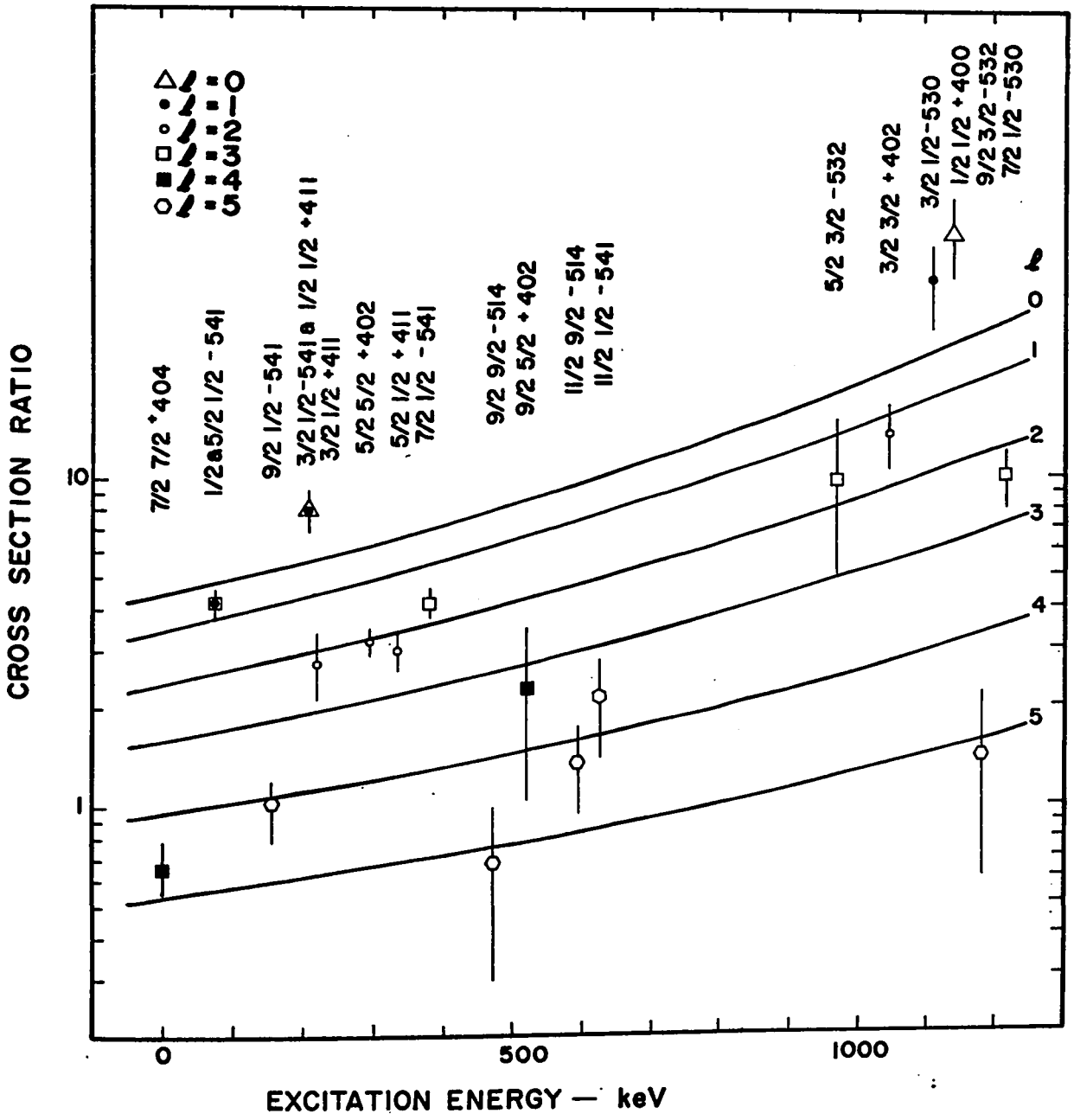

Figure 5.2 Experimental and theoretical (^{3}He,d) and (α,t) cross section ratios.

points are identified according to the ℓ value assigned on the basis of all the data. With a few exceptions, these assigned values are in good agreement with the predictions of fig. 2.

Table 5.2 lists the experimental (^{3}He,d) to (α,t) cross section ratios together with the assigned ℓ values and the calculated cross section ratio for that ℓ value. In addition, in columns 6 to 9 are listed the spectroscopic factors extracted for the two reactions and in order to provide an indication of the expected value for that assignment, the spectroscopic factors, $U^2C_{j\ell}{}^2$ given by a Nilsson model calculation which includes Coriolis coupling. Well parameters for $\kappa = 0.0637$ and $\mu = 0.600$ were used in the calculation as recommended by Lamm (1969). These parameters are simply related to the parameters C and D presented in Chapter 2. The Fermi surface was placed 0.3 MeV below the unperturbed 7/2+[404] band head, with a diffuseness parameter of 0.8 MeV. The deformation δ was assumed to be 0.29. Coriolis matrix elements were reduced by a factor of 0.65. This last assumption will be discussed more fully in section 5.8. Coriolis mixing between the following negative parity orbitals was considered: 1/2-[541], 3/2-[532], 1/2-[530], 9/2-[514], 7/2-[523], 1/2-[550], 3/2-[541], 5/2-[532], 5/2-[523] and 11/2-[505]; and also between the 7/2+[404], 5/2+[402], 1/2+[411], 1/2+[400], 3/2+[402], 1/2+[420], 3/2+[411], 5/2+[413] and 3/2+[422] positive parity orbitals, and between the 1/2+[660] and 3/2+[651] states. Mixing of states for which ΔN=2 was not included.

TABLE 5.3

Predicted spectroscopic factors with and without the inclusion of Coriolis coupling

Orbital	Spin	Spectroscopic factor - $C_{j\ell}^2 U^2$	
		Unperturbed	Perturbed
7/2+[404]	7/2	0.67	0.69
	9/2	<0.01	<0.01
1/2-[541]	1/2	0.03	0.03
	3/2	0.04	0.05
	5/2	0.17	0.20
	7/2	0.04	0.07
	9/2	0.45	0.70
	11/2	0.02	0.05
1/2+[411]	1/2	0.02	0.02
	3/2	0.09	0.09
	5/2	0.03	0.03
	7/2	0.03	0.03
	9/2	<0.01	<0.01
5/2+[402]	5/2	0.80	0.82
	7/2	0.04	0.03
	9/2	0.02	0.02
9/2-[514]	9/2	<0.01	<0.01
	11/2	0.89	1.18
3/2-[532]	3/2	0.01	<0.01
	5/2	0.12	0.10
	7/2	0.05	0.02
	9/2	0.73	0.67
	11/2	0.03	0.01
1/2-[530]	1/2	0.02	0.02
	3/2	<0.01	<0.01
	5/2	0.44	0.44
	9/2	0.18	0.12
	11/2	0.10	0.10

TABLE 5.4

Spectroscopic Information for ^{174}Lu

Assignment $IK^{\pi}[Nn_z\Lambda]$	Energy (keV)	Ratios of (^{3}He,d) and (α,t) cross sections	Assigned ℓ	Calculated cross section ratio for assigned ℓ	U^2C^2 from (^{3}He,d) reaction	U^2C^2 from (α,t) reaction	U^2C^2 predicted with Coriolis coupling
7/2 7/2+[404]	0	0.7	4	1.0	0.78	0.73	0.69
1/2 1/2-[541]	71	} 4.2	1	3.8	0.27[a]	0.23[a]	0.03
5/2 1/2-[541]	73	}	3	1.7	0.79[a]	0.33[a]	0.20
9/2 1/2-[541]	159	1.1	5	0.6	1.8	1.06	0.70
3/2 1/2-[541]	206	} 8.2	1	4.4	0.18[a]	0.10[a]	0.05
1/2 1/2+[411]	208	}	0	5.6	0.18[a]	0.12[a]	0.02
3/2 1/2+[411]	220	2.8	2	3.0	0.20	0.17	0.09
5/2 5/2+[402]	296	3.2	2	3.3	0.85	0.86	0.82
5/2 1/2+[411]	336	3.0	2	3.4	0.14	0.15	0.03
7/2 1/2+[541]	379	4.2	3	2.3	0.14	0.08	0.07
7/2 5/2+[402]	394	4.6	2	3.7	0.03	0.03	0.03
9/2 9/2-[514]	469	0.7	5	0.7	0.08	0.10	<0.01
9/2 5/2+[402]	519	2.3	4	1.5	0.07	0.05	0.02
11/2 9/2-[514]	594	1.3	5	0.8	2.4	1.3	1.18
11/2 1/2-[541]	619	2.1	5	8.7	0.19	0.13	0.05
	800	7.3					
5/2 3/2-[532]	967	15	3	4.9	0.15	0.05	0.10
(3/2 3/2+[402])	1046	13	2	9.4	0.19	0.14	0.22
	1087	6.5					
3/2 1/2-[530]	1108	39	1	17	0.30	0.14	0.22
(1/2 1/2+[400])	1139	~55	0	21	0.18	~0.1	0.18
(1/2 1/2+[400]	1156	~11	0	22	0.04		0.03
9/2 3/2-[532]	1180	~ 1.4	5	1.6	~0.29	0.39	0.67
7/2 1/2-[530]	1219	10	3	7.4	0.31	0.20	0.44
13/2 1/2+[660]	1570	0.3	6	0.9	0.46	1.51	1.38
	1584	31					
	1604	44					

a) Spectroscopic factor if the entire cross section of this multiplet is assumed to be of the assigned ℓ.

5.4 Interpretation of the Single Particle Transfer Results

5.4.1 The 7/2+[404] orbital

This Nilsson orbital has been assigned as the ground state of all of the odd mass lutetium isotopes previously studied. This is in accordance with the strict level order of the Nilsson diagram (Lamm, 1969) and is in agreement with the present single particle transfer results. The only rotational member which has a large spectroscopic factor is the I = 7/2 band head for which $C_{j\ell}^2 = 0.98$. The values of $U^2C_{j\ell}^2$ deduced from the measured (^{3}He,d) and (α,t) cross sections are shown in table 5.4 and imply a value of U^2 for this state between one half and unity. Thus the Fermi surface in the target nucleus must lie below the 7/2+[404] orbital. As mentioned above the value used for the Nilsson calculation was -300 keV.

5.4.2 The 1/2-[541] orbital

The ground state of this orbital decays to the 7/2+[404] state via an isomeric 71.1 keV, E3 transition first observed by Bjørnhòlm et al. (1965). The rotational band is expected to be strongly decoupled and the single particle transfer results confirm this. The value for the decoupling parameter predicted by the Nilsson model calculation is 3.2. This results in the I = 5/2 band member being depressed to an energy very close to the I =1/2 band head. Thus in the single particle spectra the peak at 71 keV is assigned as an unresolved doublet composed

of these states. In addition peaks at 158, 208, 380 and 624 keV in the particle spectra are assigned as the I = 9/2, 3/2, 7/2 and 11/2 rotational band members. The calculated spectroscopic factors are in reasonable agreement with the experimental values.

5.4.3. The 1/2+[411], 5/2+[402] and 9/2-[514] orbitals

These orbitals at band head energies of 208, 295 and 469 keV respectively have been previously assigned in ^{171}Lu as a result of gamma-ray studies. The spectroscopic factors observed in the present work places these assignments on a secure basis.

The 1/2+[411] orbital appears as a proton hole state with a calculated emptiness factor $U^2 = 0.3$. The contribution from the I = 1/2 state is unresolved from the I = 3/2 state of the 1/2-[541] orbital. Peaks are assigned to the I = 3/2 and 5/2 band members at 220 and 333 keV.

The I = 5/2 band head of the 5/2+[402] orbital is observed to be populated strongly. The spectroscopic factor is seen to be in excellent agreement with the predicted value. The higher spin members of this band are all predicted to have very small cross sections. The only one assigned in the single particle reactions is the I = 9/2 member at 519 keV.

According to the Nilsson model the 9/2-[514] orbital should appear as a low-lying particle state in the odd mass lutetium nuclei. It originates from the $h_{11/2}$ shell-model

configuration and thus even at large deformation it has a value of $C_{j\ell}^2 \approx 0.99$ for I = 11/2. The Coriolis coupling calculation predicts that the value of the spectroscopic factor for this state should be slightly greater than unity due to admixtures of the 11/2 7/2-[523] and 11/2 11/2-[505] states. This is in fact observed, the predicted admixtures to the wave functions from the two states mentioned above being 9% and 1% respectively. The observed spectroscopic factors for the I = 9/2 state are quite small but still much larger than the predicted value. The discrepancy has not been explained. However these results do confirm the assignment of the state at 469 keV as the band head of the 9/2-[514] orbital and not as the 7/2-[523] hole state as suggested by Norma et al. (1969).

5.4.4 The 3/2-[532] and 1/2-[530] orbitals

In the study of the odd mass lutetium isotopes ^{173}Lu, ^{175}Lu and ^{177}Lu (O'Neil et al. 1971) by single particle stripping reactions new assignments were made for band members of the 3/2-[532] and 1/2-[530] orbitals. These are proton particle states expected at around 1 MeV in the odd mass isotopes of lutetium. The model predicts that the most strongly populated states will be the I = 5/2 and 9/2 states of the 3/2-[532] band and the I = 3/2 and 7/2 states of the 1/2-[530] band. Because of background arising from isotopic impurities in the target

it is harder to make these assignments in the present work. However, the deformation and therefore the band head energy of excited states is expected to vary smoothly with mass, so an extrapolation of the energies of the states observed in the other lutetium isotopes should be a reasonable guide, fig. 5.3. This procedure predicts energies of ∿ 950 and 1175 keV for the I = 5/2 and 9/2 members of the 3/2-[532] band and ∿ 1110 and ∿ 1220 keV for the I = 3/2 and 7/2 members of the 1/2-[530] band in ^{171}Lu. The obvious candidates for the I = 3/2 and 7/2 members of the 1/2-[530] band are the peaks at 1107 and 1218 keV. The assignments for the 3/2-[532] band members are a little more tentative. The 5/2, 7/2-[532] state is probably at 967 keV; the (^{3}He,d) and (α,t) cross sections are reasonably close to the predicted values for this case. The 9/2, 3/2-[532] state is predicted by the Nilsson calculation to lie about 260 keV higher. The only candidate for this state is the peak 1185 keV, it has about the right strength and has a (^{3}He,d) to (α,t) ratio characteristic of a high ℓ value.

5.4.5. The 1/2+[660] and 3/2+[651] orbitals

Two positive parity bands 1/2+[660] and 3/2+[651], both arising from the $i_{13/2}$ spherical state, might be expected in the neighbourhood of the observed 3/2-[532] and 1/2-[530] bands. In the absence of Coriolis mixing, each of these positive parity bands would give rise to a strong ℓ = 6 transition

Figure 5.3

Energy dependence of the 3/2-[532] and 1/2-[530] states with mass.

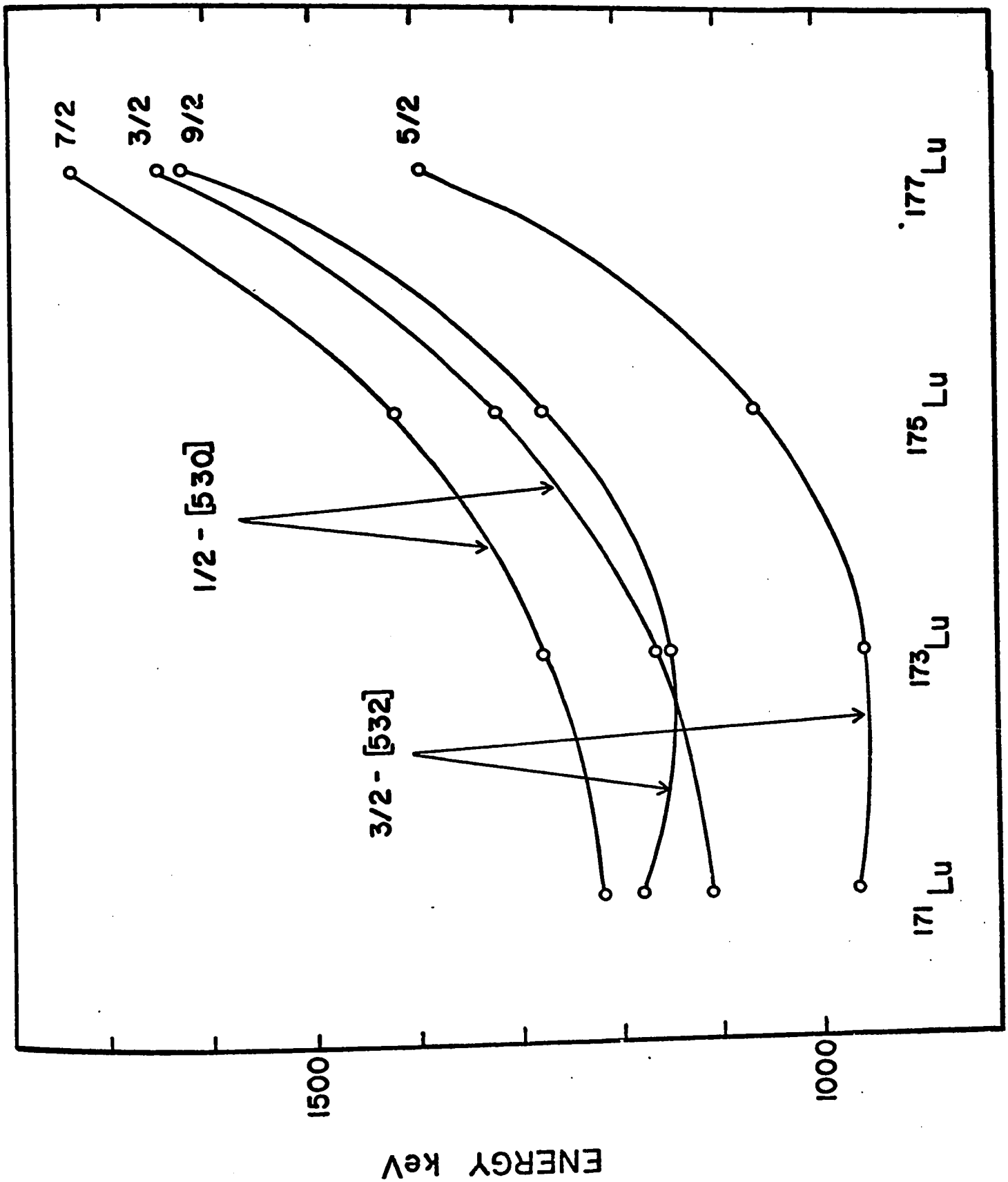
ENERGY keV
1500
1000
7/2
3/2
9/2
5/2
1/2 - [530]
3/2 - [532]
177Lu
175Lu
173Lu
171Lu

to the spin 13/2 member of the band. The Coriolis mixing is expected to be very strong, with the result that most of the ℓ=6 strength from both bands should be concentrated in the spin 13/2 member of the lower band. Thus these bands would be characterized by a single ℓ=6 transition with a spectroscopic factor greater than unity at an excitation between 1.5 and 2 MeV. Such an ℓ=6 state exists at 1565 keV and has been tentatively assigned to the 1/2+[660] band, on the grounds that this band is expected to be lower in energy than the 3/2+[651] Since in the heavier lutetium isotopes this state is expected to occur at still higher excitation, it is not surprising that it has not been identified.

5.4.6 Other States

Soloviev et al. (1966) have made a calculation for ^{171}Lu where the interaction of the quasi-particle states with phonons is considered. The results are presented in Table 5.5. The values given in the column for experimental energies are taken from the present work. It can be seen that, apart from the hole states which will not be populated very strongly in the single particle stripping reaction, all the predicted "pure" single particle states below 1.5 MeV have been observed, where "pure" is taken to mean that the single particle state forms more than 80% of the mixture. Unfortunately the values of the spectroscopic factors are not sensitive enough to test whether the calculated admixtures are reasonable.

TABLE 5.5

Proposed Non Rotational States in ^{171}Lu Resulting from a Consideration of the Interaction of Quasiparticles with Phonons Soloviev et al. 1966).

K^{π}	Energy (keV) present	expt.	cal.	Structure
7/2+	0		0	404↓ 93%; 404↓ $+Q_1(20)$ 3%; 402↓$+Q_1(22)$ 3%
1/2-	71		160	541↓ 81%; 541↓ $+Q_1(20)$ 14%
1/2+	208		200	411↓ 88%; 411↑ $+Q_1(22)$ 6%; 413↓ $+Q_1(22)$ 4%
9/2-	469		270	514↑ 97%
5/2+	295		310	402↑ 88%; 402↑ $+Q_1(20)$ 6%; 400↑ + $Q_1(22)$ 5%
3/2+			750	411↑ 58%; 411 $+Q_1(22)$ 39%
7/2-	662		850	523↑ 98%
5/2+			1000	413↓ 37%; 411↓ $+Q_1(22)$ 61%
3/2+	1046	?	1050	402↓ 25%; 404↓ $+Q_1(22)$ 72%
3/2-			1200	532↓ 81%
1/2+	1138	?	1350	400↑ 28%; 402↑ $+Q_1(22)$ 41%; 411↓ $+Q_1(20)$ 25
1/2+	1156	?	1370	400↑ 5%; 411↓ $+Q_1(20)$ 65%; 402↑ $+Q_1(22)$ 15%
11/2+			1400	404↓ $+Q_1(22)$ ∿ 100%
7/2+			1500	404↓ 3%; 404↓ $+Q_1(20)$ 97%

In addition to the "pure" single particle states it may be seen that the calculation predicts that at around 1 MeV there should be states which are mixtures of single particle state and γ and β vibrational phonons. Specifically, we might expect to observe a state which is predicted to be 25% 3/2+[402] and states which are 28% and 5% of the 1/2+[400] state. As a guide the predicted spectroscopic factors can be reduced by these fractions. The energy dependence introduced by the U^2 term is neglected. Peaks in the single particle spectra at 801 and 1046 keV are candidates for the 3/2+[402], 25% state, 1046 keV being the most likely choice. The 1/2+[400] 28% and 5% states might be at 1138 and 1156 keV. The agreement obtained is shown in Table 5.4. The values of the predicted spectroscopic factor shown in column 8 are those given by the Nilsson calculation reduced by the appropriate factor, as shown in column 4 of table 5.5

5.5 Measurement of Electron and Gamma Spectra

The $(\alpha,2n)$ experiments were carried out at beam energies of 21 MeV for the conversion electron measurements and at 21 and 23.5 MeV for the gamma ray measurements. Targets were of natural Tm and were prepared by cold rolling the metal (Westgaard and Bjørhholm 1966). Typical beam currents and target thicknesses were 500 nA and 0.9 mg/cm^2 for the conversion electron measurements and 2 nA and 3 mg/cm^2 for the gamma-ray studies.

For the electron measurements a beam of α particles was focussed onto a target at the source position of the orange electron spectrometer which was adjusted to give a resolution $\Delta p/p \sim 0.8\%$. Fig. 5.4 shows the electron spectrum from bombardment of a ^{169}Tm target with 21 MeV alpha particles. The electron lines observed and their assignments are presented in Table 5.6. The multipolarity assignments for the stronger transitions are shown in table 5.7. These are determined from the K conversion coefficients and in some cases confirmed from the α_L, α_M and K to L ratios. The gamma intensities for these ratios were obtained from a run with a 21 MeV alpha particle beam using a Ge(Li) detector placed at 54^o to the beam direction to minimize angular distribution effects. The normalization factor was determined by assuming the calculated α_K conversion coefficient of Hager and Seltzer (1968) for the strong 269-270 keV E2 doublet. The K to L ratios are of course independent of this factor and for Bρ values less than 1500 are very sensitive functions of multipolarity. The multipolarity assignments proved to be a very useful complement to the gamma-gamma coincidence results in making assignments to the level scheme. The E1 assignment of the 137.0 keV transition confirms the Nilsson assignment of the 1/2+[411] band obtained from the single particle transfer results.

A gamma spectrum taken at 23.5 MeV beam energy with a 0.9 cm^3, planar Ge(Li) counter at 90^o to the beam direction

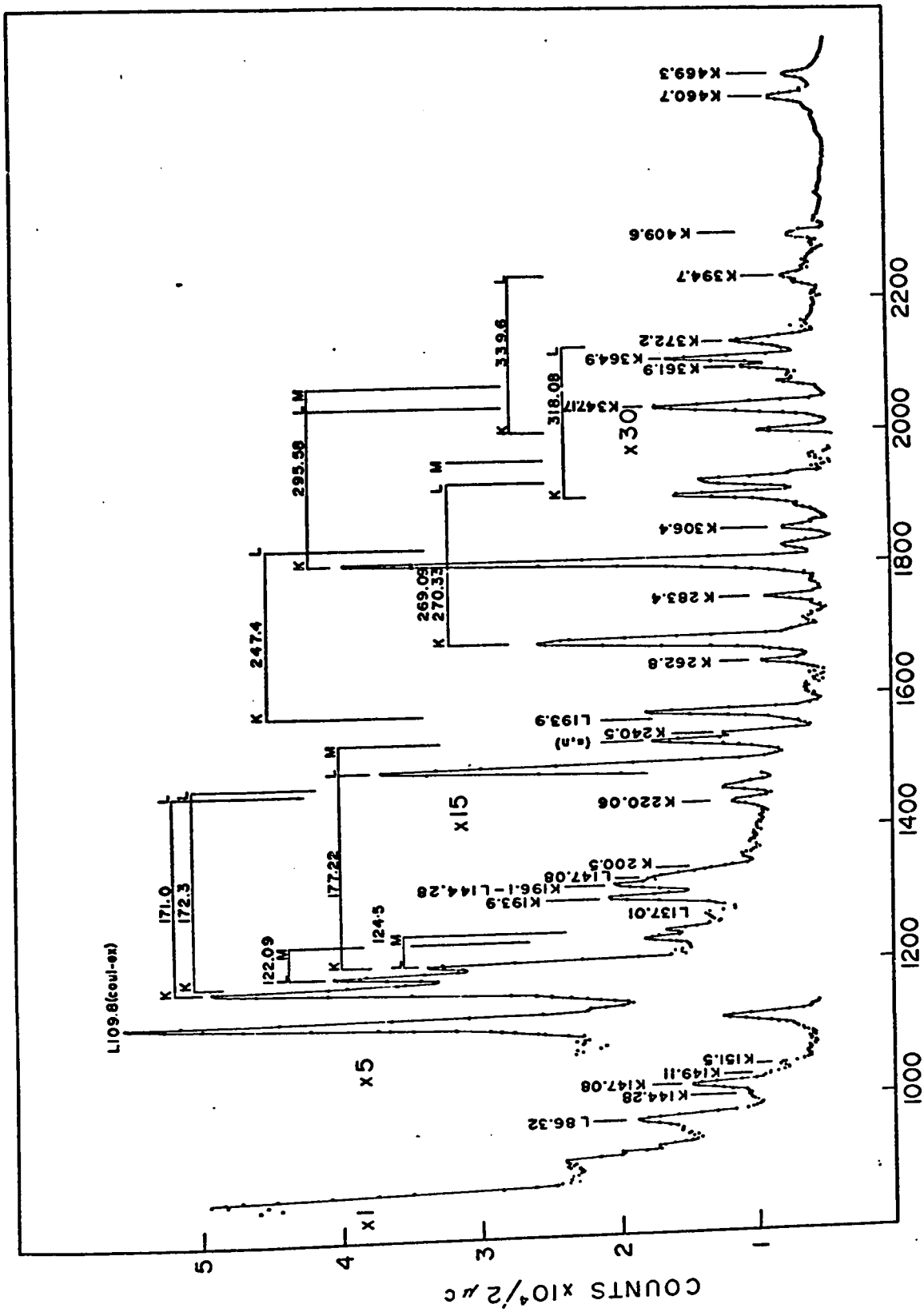

Figure 5.4 Spectrum of in beam conversion electrons from the reaction $^{169}Tm(\alpha,2n)^{171}Lu$

TABLE 5.6

Conversion Electrons Following the Reaction $^{169}Tm(\alpha,2n)^{171}Lu$ at 21 MeV Bombarding Energy

Electron Energy (keV)	Electron Intensity	Assignment	Gamma Intensity
75.4	56 ±23	L 86.32	34.9
81.2	12.9±0.9	K 144.28	34.8
84.1	43.6±3.1	K 147.08	51.7
86.0	11.1±1.6	K 149.11	18.4
87.9	8.0±0.5	K 151.5	12.6
107.8	$18.5^{+11.2}_{-2.3}$	K 171.0	40.2
109.4	4.0±0.8	K 172.3	15.1
111.4	22.1±2.7	L 122.09	100
113.6	$14.5^{+1.0}_{-0.8}$	K 177.22	79.6
119.8	4.5±0.8	M 122.09	100
121.9	2.5±0.5	M 124.5	36.6
126.0	1.4±0.3	L 137.01	177.7
130.8	9.9±1.5	K 193.1	7.6
		K 193.9	25.2
		L 141.0	-
133.8	8.9±1.3	K 196.1	5.0
		L 144.28	34.8
		L 147.08	51.7
137.3	8.3±1.2	K 200.0	7.7
		K 200.5	3.0
138.5	2.2±0.9	L 149.11	18.4
157.1	4.1±0.4	K 220.06	15.1

TABLE 5.6 (continued)

Electron Energy (keV)	Electron Intensity	Assignment	Gamma Intensity
161.4	4.6 ±0.7	L 171.0	40.2
162.5	0.96±0.4	L 172.3	15.2
167.7	14.2 ±1.4	L 177.22	79.6
		M 171.0	40.2
		M 172.3	15.1
177.0	0.15±0.05	K 240.5	15.9
182.4	0.8 ±0.1	L 193.1	7.6
		L 193.9	25.2
183.8	1.38±0.4	K 247.4	30.2
199.0	1.25±0.09	K 262.8	7.1
205.8	5.18±0.4	K 269.09	41.2
		K 270.33	33.3
219.7	0.79±0.8	K 283.4	9.8
284.9	9.68±0.7	K 295.58	84.6
236.8	0.56±0.13	L 247.4	33.2
242.8	0.83±0.06	K 306.4	21.9
254.5	1.92±0.14	K 318.08	48.5
258.9	1.66±0.12	L 269.09	41.2
		L 270.33	33.3
256.9	0.37±0.05	M 269.09	41.2
		M 270.33	33.3
276.6	0.40±0.06	K 339.6	10.2
284.9	1.96±0.14	L 295.58	84.6
		K 347.17	55.0

TABLE 5.6 (continued)

Electron Energy (keV)	Electron Intensity	Assignment	Gamma Intensity
293.2	0.69±0.06	M 295.58	84.6
301.5	0.20±0.11	K 361.9	5.2
302.0	0.84±0.12	K 364.9	25.9
307.6	0.5 ±0.26	L 318.08	40.5
309.0	0.76±0.2	K 372.2	5.6
330.0	0.42±0.09	K 394.7	5.8
346.0	0.29±0.06	K 409.6	13.7
397.2	0.61±0.2	K 460.7	18.1

TABLE 5.7

Multipolarity Assignments in ^{171}Lu by Conversion Coefficients and K/L Ratios

Transition Energy (keV)	Experimental Conversion Coefficient	Theoretical Coefficients M1	E2	E1	Assignment
86.32	α_L = 1.7 ±0.8	0.70	3.0	0.076	M1 + E2 or E2
122.09	α_L = 0.23±0.05	0.28	0.72	0.028	M1(>95%) + E2
	α_M = 0.05±0.01	0.062	0.21	0.0064	
124.51	α_M = 0.07±0.01	0.057	0.19	0.006	M1(>90%) + E2
137.0	α_L = 0.01±0.005	0.19	0.44	0.02	E1
144.28	α_K = 0.39±0.04	1.1	0.42	0.11	E2
147.08	α_K = 0.89±0.08	0.99	0.39	0.10	M1(>70%) + E2
149.11	α_K = 0.64±0.08	0.98	0.38	0.10	M1(60±20)% + E2
	α_L = 0.13±0.06	0.15	0.32	0.016	
	K/L= 4.91±0.3	6.6	1.2	6.2	
151.5	α_K = 0.67±0.08	0.97	0.37	0.09	M1(50±15)% + E2
171.0	$\alpha_K = 0.46^{+0.28}_{-0.07}$	0.68	0.26	0.07	M1(50±30)% + E2
	α_L = 0.12±0.02	0.10	0.19	0.01	
	K/L= 3.83±1.7	6.5	1.5	6.3	
172.3	α_K = 0.28±0.07	0.68	0.26	0.07	M1(50±30)% + E2
	α_L = 0.07±0.03	0.10	0.19	0.01	
	K/L= 4.15±0.9	6.5	1.5	6.3	

(continued next page)

TABLE 5.7 (continued)

Transition Energy (keV)	Experimental Conversion Coefficient	Theoretical Coefficients M1	E2	E1	Assignment
177.22	α_K = 0.19±0.04	0.61	0.23	0.063	E2
	α_L = 0.19±0.04	0.09	0.15	0.010	
	K/L= 1.1 ±0.6	6.5	1.6	6.3	
220.06	α_K = 0.29±0.02	0.34	0.13	0.036	M1(75±15)% + E2
240.5	α_K = 0.10±0.05	0.27	0.08	0.03	E2
247.4	α_K = 0.05±0.01	0.25	0.09	0.025	E2
	α_L = 0.02±0.01	0.036	0.035	0.004	
	K/L= 2.46±0.4	6.5	2.4	6.5	
262.8	α_K = 0.19±0.01	0.22	0.08	0.024	M1(80±10)% + E2
269.09 / 270.33	α_K = 0.074 [a]	0.20	0.074	0.02	E2
	α_L = 0.024±0.002	0.03	0.026	0.033	
	α_M = 0.053±0.005	0.0060	0.062	0.007	
	K/L= 3.1 ±0.4	6.5	2.7	6.6	
283.4	α_K = 0.086±0.007	0.18	0.06	0.02	E2 or M1 + E2
295.58	α_K = 0.11±0.01	0.16	0.057	0.017	M1(50±10%) + E2

(continued next page)

TABLE 5.7 (continued)

Transition Energy (keV)	Experimental Conversion Coefficient	Theoretical Coefficients M1	E2	E1	Assignment
306.4	α_K = 0.040±0.005	0.15	0.05	0.016	E2
318.08	α_K = 0.042±0.006	0.14	0.05	0.015	
	α_L = 0.013±0.002	0.019	0.014	0.002	E2
	K/L= 3.8 ±0.29	6.5	3.2	6.7	
339.6	α_K = 0.04 ±0.02	0.11	0.038	0.3	E2
347.17	α_K = 0.007±0.004	0.10	0.036	0.012	E1
361.9	α_K = 0.04 ±0.02	0.092	0.033	0.011	E2
364.9	α_K = 0.034±0.008	0.090	0.032	0.011	E2
372.2	α_K = 0.05 ±0.03	0.084	0.030	0.01	E2 or M1 + E2
394.7	α_K = 0.08 ±0.02	0.073	0.026	0.009	M1
409.6	α_K = 0.022±0.005	0.066	0.023	0.008	E2
460.7	α_K = 0.035±0.01	0.048	0.018	0.006	M1(55±30)% + E2
469.3	α_K = 0.01 ±0.005	0.046	0.017	0.006	E1 or E2

a) Normalization

is shown in fig. 5.5. The resolution was 0.7 keV (F.W.H.M.) at 122 keV. Those gamma rays assigned to ^{171}Lu are labelled with their energy in keV. Of the remaining transitions some arise from Coulomb excitation of the target, others from the (n,n') reaction on materials surrounding the target and detector and the majority from competing reactions such as (α,n). In order to study the gamma radiation with energy above ∿ 400 keV a number of runs were made using a 50 cm^3 Ge(Li) detector system having an energy resolution of 2.5 keV (F.W.H.M.) at 1332 keV.

In order to determine isotopic assignments from excitation functions and to distinguish lines arising from target impurities the reaction ^{168}Er(^{7}Li,4n)^{171}Lu was used. The accelerator was able to provide ^{7}Li beam energies in a range over the maximum of the (^{7}Li,4n) probability curve. This curve was not directly determined, but could be inferred from the Q value relationships for the reaction and the known shape of such cross section curves. The beam energies used were 32, 34 and 36 MeV. Some of the results are shown in fig. 5.6. Intensity ratios, relative to the intensity of the 137.0 keV transition, are plotted against the ^{7}Li bombarding energy. States of high spin are populated more strongly with higher beam energy and so for such states the excitation curve has an upward slope. Lines from the (^{7}Li, 5n) reaction would also have an upward slope, but the beam energies for both reactions were such that such lines were not expected.

Figure 5.5

Spectrum of in beam gamma rays from the reaction $^{169}Tn(\alpha,2n)^{171}Lu$. Peaks arising from other reactions are unlabelled.

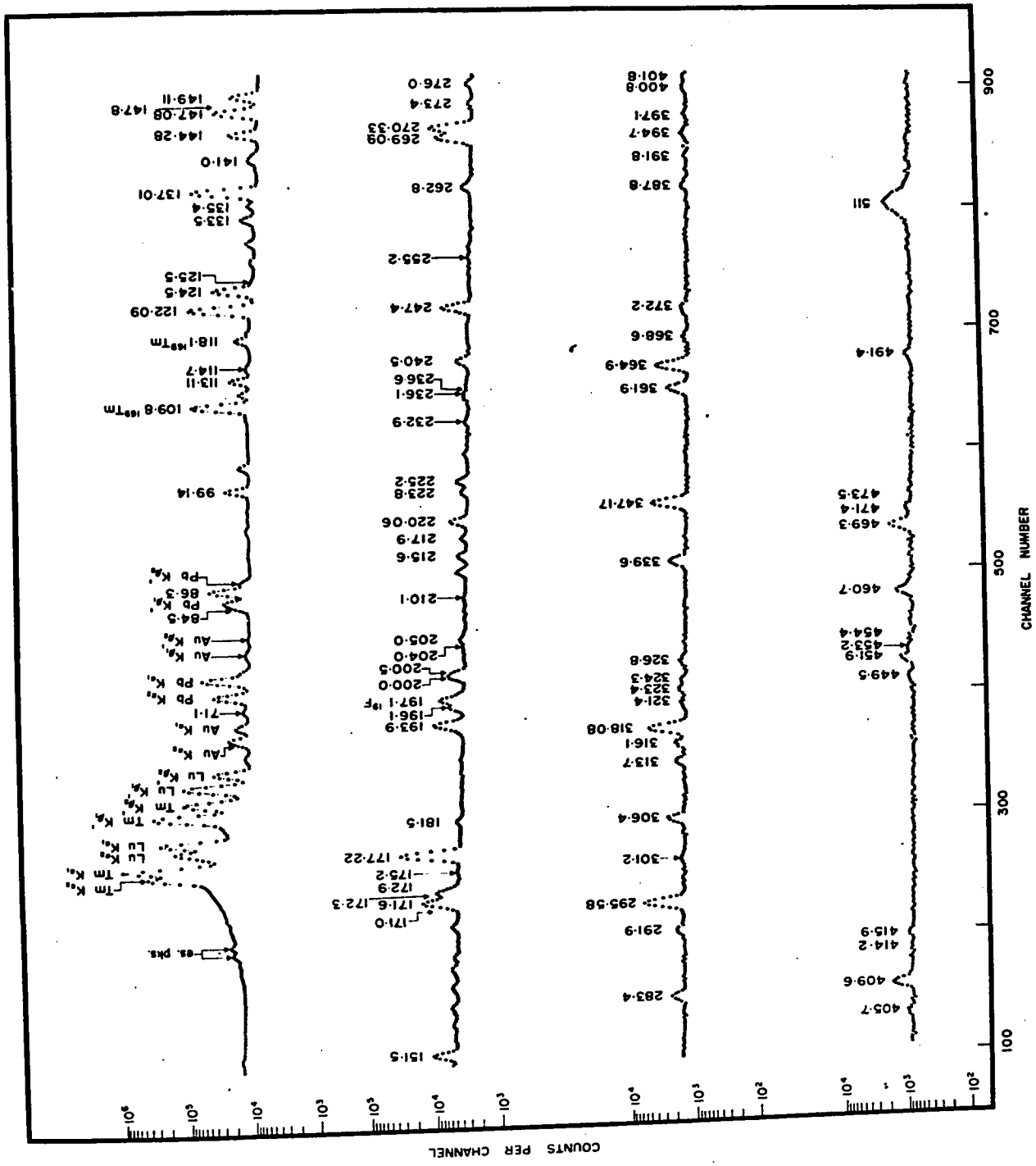
COUNTS PER CHANNEL
CHANNEL NUMBER
100
300
500
700
900
151·5
171·0
172·3
171·6
172·9
175·2
177·22
181·5
193·9
196·1
197·1 19F
200·0
204·0
205·0
210·1
215·6
217·9
220·06
223·8
225·2
232·9
236·1
236·6
240·5
247·4
255·2
262·8
269·09
270·33
273·4
276·0
283·4
291·9
295·58
301·2
306·4
313·7
316·1
318·08
321·4
323·4
324·3
326·8
339·6
347·17
361·9
364·9
368·6
372·2
387·8
391·8
394·7
397·1
400·8
401·8
405·7
409·6
414·2
415·9
449·5
451·9
453·2
454·4
460·7
469·3
471·4
473·5
491·4
511
99·14
109·8 155Tm
113·11
114·7
118·1 155Tm
122·09
124·5
125·5
133·5
135·4
137·01
141·0
144·28
147·08
147·8
149·11
Pb Kα2
86·3
Pb Kβ1
84·5
Au Kα1
Au Kα2
Pb Kα1
Pb Kα2
71·1
Au Kα1
Au Kα2
Lu Kβ1
Lu Kβ2
Tm Kβ1
Lu Kα1
Lu Kα2
Tm Kα1
Tm Kα2
es. pks.

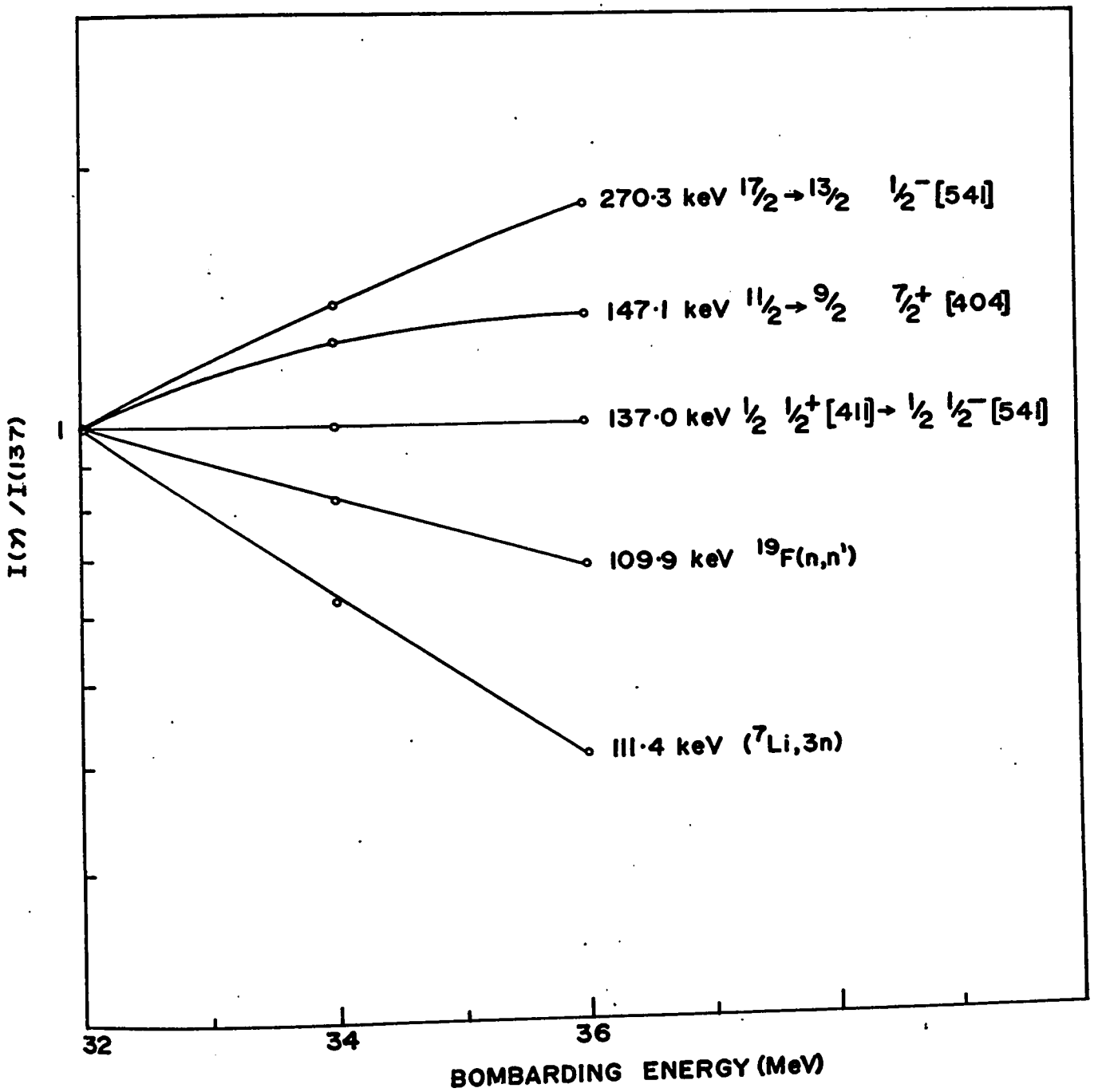

Figure 5.6

Ratio of gamma-ray intensity to that of the 137.0 keV line as a function of ^{7}Li bombarding energy

Lines from the (^{7}Li, 3n) reaction and impurity lines are observed to have a downward sloping excitation curve relative to the 137.0 keV transition.

The energies and relative intensities of transitions assigned to ^{171}Lu are given in columns one and two of table 5.8 These values compare well with the results of similar experiments done by Kemnitz et al. (1971), Hjorth et al. (1972) and Barneoud et al. (1972). The intensities of unresolved lines have been determined from the coincidence probabilities as described below. The intensities of transitions following the α-induced reaction to the ^{7}Li-induced reaction can be indicative of spin assignments since the (^{7}Li,4n) reaction preferentially populates high spin states. These ratios normalized to one for the 122.1 keV transition are given in column 3 of table 5.8 Column 4 shows the transition assignment within the nucleus. Fig. 5.7 shows the ratios $I_{\gamma}(E_{\alpha}=23.5$ Mev)$/I_{\gamma}(E_{^{7}Li} = 36$ MeV) plotted against the spin of the de-exciting state. In obtaining this ratio, the total photon intensity de-exciting the state was used wherever possible. It is apparent that these results give a useful indication of the spin value of the populated state. However the dependence is not quite the same for each band since each level may be populated in two ways; that is directly or by gamma transitions from other states.

TABLE 5.8

Gamma rays following the reaction $^{169}Tm(\alpha,2n)^{171}Lu$ at 23.5 MeV bombarding energy at 90° to the beam direction.

E_γ (keV)	I_γ (E_α=23.5 MeV)	$\frac{I_\gamma(E_\alpha=23.5\ MeV)}{I_\gamma(E_{^7Li}=36\ MeV)}$	Assignment I_i	K_i^π	I_f	K_f^π
71.1 ± 0.1	1.7 ± 0.3	1.2	1/2	1/2-	7/2	7/2+
75.0 ± 0.5[b]	1.1 ± 0.6[c]		5/2	5/2+	3/2	1/2+
84.5 ± 0.3	5.6 ± 3.1					
86.32 ± 0.05	34.9 ± 5.0	0.8	9/2	1/2-	5/2	1/2-
99.14 ± 0.05	11.3 ± 1.0	1.1	7/2	5/2+	5/2	5/2+
113.11 ± 0.08	12.2 ± 1.8	1.6	5/2	1/2+	3/2	1/2+
114.7 ± 0.3	2.4 ± 0.4	0.2				
122.09 ± 0.03	100[a]	1.0[a]	9/2	7/2+	7/2	7/2+
124.5 ± 0.1	11.0 ± 3.0[c]		9/2	5/2+	7/2	5/2+
	24.7 ± 5.0[c]		11/2	9/2-	9/2	9/2-
125.5 ± 0.3	1.4 ± 0.5		5/2	1/2+	1/2	1/2+
133.5 ± 0.2	8.4 ± 1.1	1.3	3/2	1/2-	5/2	1/2-
135.4 ± 0.2	4.5 ± 0.8	1.3	3/2	1/2-	1/2	1/2-
137.01 ± 0.03	107.5 ± 6.0	1.2	1/2	1/2+	1/2	1/2-

TABLE 5.8 (continued)

E_γ (keV)	I_γ (E_α=23.5 MeV)	$\frac{I_\gamma(E_\alpha=23.5\ MeV)}{I_\gamma(E_{^7Li}=36\ MeV)}$	Assignment I_i	K_i^π	I_f	K_f^π
141.0 ± 0.3	4.6 ± 1.0	0.5				
144.28 ± 0.05	21.7 ± 2.2	0.5	7/2	1/2+	3/2	1/2+
147.08 ± 0.05	49.0 ± 4.9	0.8	11/2	7/2+	9/2	7/2+
147.8 ± 0.3	2.3 ± 1.0		3/2	1/2+	5/2	1/2-
149.11 ± 0.05	23.1 ± 2.5	0.8	13/2	9/2-	11/2	9/2-
151.5 ± 0.1	14.0 ± 1.8	0.6	11/2	5/2+	9/2	5/2+
171.0 ± 0.1	27.9 ± 3.8	0.6	13/2	7/2+	11/2	7/2+
171.6 ± 0.3	10.9 ± 1.3		13/2	5/2+	11/2	5/2+
172.3 ± 0.1	14.3 ± 2.0		15/2	9/2-	13/2	9/2-
172.9 ± 0.2	2.7 ± 2.0		7/2	1/2-	3/2	1/2-
175.2 ± 0.3	1.3 ± 1.0					
177.22 ± 0.03	97.9 ± 9.6	0.5	13/2	1/2-	9/2	1/2-
181.5 ± 0.2	2.2 ± 0.8	0.1				
193.9 ± 0.1	16.0 ± 5.0[c]		15/2	7/2+	13/2	7/2+
	11.6 ± 6.0[c]		9/2	1/2+	7/2	1/2+
196.1 ± 0.2	7.6 ± 1.0	0.7	17/2	9/2-	15/2	9/2-

TABLE 5.8 (continued)

E_γ (keV)	I_γ (E_α=23.5 MeV)	$\frac{I_\gamma(E_\alpha=23.5\ MeV)}{I_\gamma(E_{^7Li}=36\ MeV)}$	Assignment I_i	K_i^π	I_f	K_f^π
200.0 ± 0.2	7.9 ± 2.0	1.1	9/2	9/2-	11/2	7/2+
200.5 ± 0.2	6.6 ± 1.9	0.7	15/2	5/2+	13/2	5/2+
204.0 ± 0.3	3.1 ± 1.0					
205.0 ± 0.3	3.0 ± 1.0		17/2	5/2+	15/2	5/2+
210.1 ± 0.3	1.1 ± 0.4		19/2	1/2-	17/2	9/2-
215.6 ± 0.1	5.3 ± 1.0	0.5	17/2	7/2+	15/2	7/2+
217.9 ± 0.1	3.1 ± 0.6	0.5	19/2	9/2-	17/2	9/2-
220.06 ± 0.05	15.0 ± 2.7	2.3	7/2	1/2-	9/2	1/2-
223.8 ± 0.2	4.0 ± 1.1	0.6	9/2	5/2+	5/2	5/2+
225.2 ± 0.2	6.8 ± 1.4	0.9	9/2	1/2+	5/2	1/2+
232.9 ± 0.2	1.9 ± 0.7		17/2	1/2+	15/2	5/2+
236.1 ± 0.2	2.3 ± 0.8		19/2	7/2+	17/2	7/2+
236.6 ± 0.2	1.8 ± 1.1		21/2	9/2-	19/2	9/2-
240.5 ± 0.1	8.7 ± 1.2	0.5	11/2	1/2-	7/2	1/2-
247.4 ± 0.1	27.5 ± 2.6	1.0	11/2	1/2+	7/2	1/2+
255.2 ± 0.4	1.4 ± 1.0	0.2	21/2	7/2+	19/2	7/2+

TABLE 5.8 (continued)

E_γ (keV)	I_γ (E_α=23.5 MeV)	$\frac{I_\gamma(E_\alpha=23.5\ MeV)}{I_\gamma(E_{^7Li}=36\ MeV)}$	Assignment I_i	K_i^π	I_f	K_f^π
262.8 ± 0.2	6.8 ± 0.8	0.4	13/2	1/2+	11/2	1/2+
269.09 ± 0.07	44.2 ± 4.8	0.8	11/2	7/2+	7/2	7/2+
270.33 ± 0.07	61.5 ± 6.5	0.4	17/2	1/2-	13/2	1/2-
273.4 ± 0.3	2.7 ± 0.4	0.5	13/2	9/2-	9/2	9/2-
276.0 ± 0.2	4.1 ± 0.5	1.4	11/2	5/2+	7/2	5/2+
283.4 ± 0.1	10.1 ± 1.1	1.0	11/2	1/2-	13/2	1/2-
291.9 ± 0.1	5.5 ± 0.7	0.3	7/2	1/2+	5/2	1/2-
295.58 ± 0.06	62.0 ± 6.1	1.2	5/2	5/2+	7/2	7/2+
296 ± 1[b]	3.2 ± 1.9[c]		17/2	5/2+	15/2	1/2+
301.2 ± 0.3	2.4 ± 0.8					
306.4 ± 0.1	15.0 ± 1.8	1.9	7/2	1/2-	5/2	1/2-
313.7 ± 0.2	6.4 ± 0.9		15/2	1/2-	11/2	1/2-
316.1 ± 0.2	7.2 ± 1.0		13/2	1/2+	9/2	1/2+
318.08 ± 0.08	53.4 ± 6.2	0.7	13/2	7/2+	9/2	7/2+
321.4 ± 0.2	4.2 ± 0.9	0.5	15/2	9/2	11/2	9/2-
323.4 ± 0.3	5.5 ± 1.0	0.2	13/2	5/2+	9/2	5/2+

TABLE 5.8 (continued)

E_γ (keV)	I_γ (E_α=23.5 MeV)	$\frac{I_\gamma(E_\alpha=23.5\ MeV)}{I_\gamma(E_{^7Li}=36\ MeV)}$	Assignment I_i	$K_i\pi$	I_f	$K_f\pi$
324.3 ± 0.3	1.0 ± 0.4[c]		11/2	9/2-	11/2	7/2+
	2.0 ± 0.8[c]		17/2	1/2+	15/2	1/2+
326.8 ± 0.2	4.9 ± 0.8		15/2	1/2-	17/2	1/2-
339.6 ± 0.1	17.6 ± 1.9	0.6	15/2	1/2+	11/2	1/2+
347.17 ± 0.08	54.8 ± 5.6	1.1	9/2	9/2-	9/2	7/2+
361.9 ± 0.1	22.8 ± 2.3	0.3	21/2	1/2-	17/2	1/2-
364.9 ± 0.1	43.3 ± 4.4	0.7	15/2	7/2+	11/2	7/2+
368.6 ± 0.2	4.2 ± 0.8		17/2	9/2-	13/2	9/2-
372.2 ± 0.3	5.2 ± 0.9		15/2	5/2+	11/2	5/2+
387.8 ± 0.3	5.6 ± 0.8		19/2	1/2-	15/2	1/2-
391.8 ± 0.4	2.0 ± 1.0			?	17/2	7/2+
394.7 ± 0.3	5.7 ± 1.8		7/2	5/2+	7/2	7/2+
397.1 ± 0.4	2.8 ± 1.6		9/2	5/2+	9/2	7/2+
400.8 ± 0.4	3.4 ± 1.8		17/2	1/2+	13/2	1/2+
401.8 ± 0.4	1.6 ± 0.9		11/2	5/2+	11/2	7/2+
405.7 ± 0.3	3.0 ± 1.1[c]		17/2	5/2+	13/2	5/2+
	1.8 ± 0.9[c]		19/2	1/2-	15/2	9/2-

TABLE 5.8 (continued)

E_γ (keV)	I_γ (E_α=23.5 MeV)	$\frac{I_\gamma(E_\alpha=23.5\ MeV)}{I_\gamma(E_{^7Li}=36\ MeV)}$	Assignment I_i	$K_i\pi$	I_f	$K_f\pi$
409.6 ± 0.1	28.1 ± 3.3	0.5	17/2	7/2+	13/2	7/2+
414.2 ± 0.3	2.2 ± 1.3		19/2	9/2-	15/2	9/2-
415.9 ± 0.2	5.3 ± 0.9		19/2	1/2+	15/2	1/2+
449.5 ± 0.3	6.3 ± 2.1	0.1	25/2	1/2-	21/2	1/2-
451.9 ± 0.2	15.7 ± 2.8	0.4	19/2	7/2+	15/2	7/2+
453.2 ± 0.4	7.5 ± 2.4		11/2	1/2+	9/2	1/2-
454.4 ± 0.4	4.3 ± 2.1		21/2	9/2-	17/2	9/2-
460.7 ± 0.2	25.2 ± 2.9		11/2	1/2-	9/2	1/2-
469.3 ± 0.2	40.3 ± 4.4		9/2	9/2-	7/2	7/2+
471.4 ± 0.3	8.0 ± 3.0		11/2	9/2-	9/2	7/2+
473.5 ± 0.4	4.8 ± 2.5		13/2	9/2-	11/2	7/2+
491.4 ± 0.2	8.2 ± 1.4		21/2	7/2+	17/2	7/2+
512 ± 2 [b]	2.0 ± 1.0 [c]		29/2	1/2-	25/2	1/2-
517.8 ± 0.4	5.3 ± 1.2					
527.9 ± 0.4	4.8 ± 1.1					
539.9 ± 0.4	4.4 ± 1.3		7/2	7/2-	9/2	7/2+
597.2 ± 0.3	25.5 ± 4.0		15/2	1/2-	13/2	1/2-

TABLE 5.8 (continued)

E_γ (keV)	I_γ (E_α=23.5 MeV)	$\frac{I_\gamma(E_\alpha=23.5\ MeV)}{I_\gamma(E_{^7Li}=36\ MeV)}$	Assignment I_i	K_i^π	I_f	K_f^π
607.5 ± 0.4	5.8 ± 1.8			?	15/2	7/2+
610.4 ± 0.4	5.1 ± 1.9					
615.3 ± 0.5	3.6 ± 1.0		15/2	1/2+	13/2	1/2-
661.9 ± 0.4	8.6 ± 1.8		7/2	7/2-	7/2	7/2+
709.1 ± 0.4	19.7 ± 4.3					
714.8 ± 0.5	9.2 ± 2.1		19/2	1/2-	17/2	1/2-
722 ± 2 [b]	3.3 ± 1.7 [c]		19/2	9/2-	17/2	1/2-
748.7 ± 0.6	4.4 ± 1.2					
760 ± 2 [b]	3.5 ± 1.8 [c]		19/2	1/2+	11/2	1/2-
801.4 ± 0.4	22.8 ± 3.4			?	13/2	7/2+
814.6 ± 0.5	9.5 ± 1.9					
837.1 ± 0.6	1.0 ± 0.6					
871.9 ± 0.5	7.3 ± 1.9					

(a) Normalization

(b) Transition is seen only in coincidence, the energy is determined from coincidence spectra

(c) Unresolved or weak line, the intensity is determined from the coincidence probabilities.

Figure 5.7

The ratios $I_\gamma(E_\gamma = 23.5\ \text{MeV})I/(E_{^7\text{Li}} = 36\ \text{MeV})$ plotted against the spin of the de-exciting state.

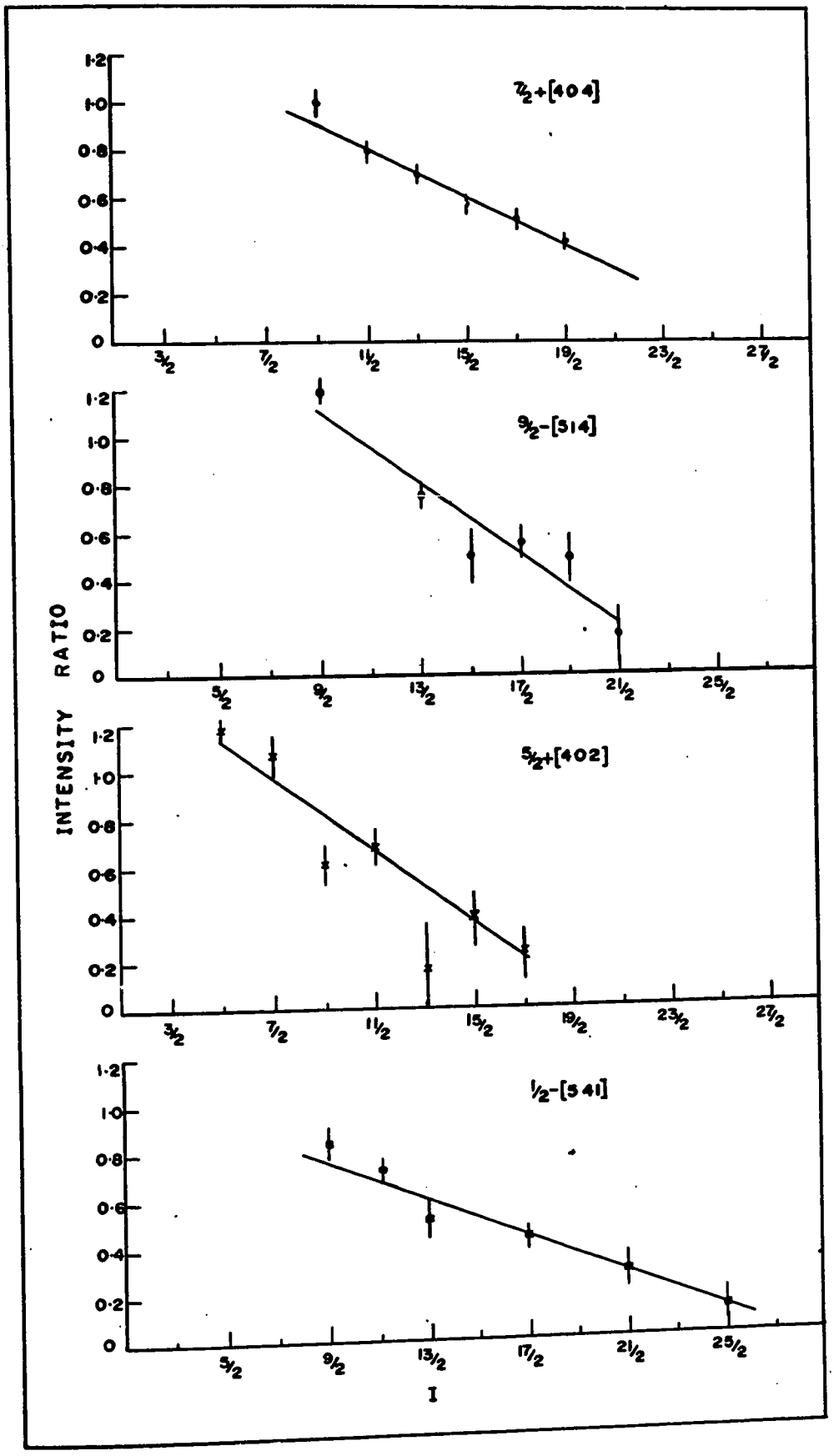
7/2+[404]
9/2-[514]
5/2+[402]
1/2-[541]
INTENSITY RATIO
I
1·2
1·0
0·8
0·6
0·4
0·2
0
3/2
7/2
11/2
15/2
19/2
23/2
27/2
5/2
9/2
13/2
17/2
21/2
25/2

5.6 Gamma-gamma coincidence measurements

A two parameter coincidence experiment was performed in which approximately six million pairs of coincidence events were recorded. The Ge(Li) detectors used had volumes of 0.9 cm^3 and 37 cm^3. They were mounted at 90° with respect to the beam direction and to each other. A special beam line arrangement allowed the detectors to be placed within 2cm of the target position. The resolution of the detectors at 200 keV, as measured from the coincidence projections was 1.1 keV and 2.5 keV. Although the small detector had very poor efficiency above 200 keV its good resolution made it possible to set clean gating windows on each of the photopeaks of the group 144, 147, 149 and 151 keV. The data were analyzed by setting gates on photopeaks from both axes of the coincidence matrix. Events due to background underlying the gating photopeak are subtracted off in each case. No correction was made for chance but the excellent true to chance ratio ($\sim$ 20:1) ensured that chance peaks were not troublesome. The resolving time of the coincidence system was approximately 80 nsec. Coincidence spectra associated with 52 gates were obtained. Each was analyzed to obtain the coincidence probability between a gating transition and each transition appearing in coincidence with it. The values obtained were compared with those predicted for the assigned level scheme except for the cases of close doublets where this procedure was used to calculate

the strength of the transition.

5.7 The Level Scheme

The level scheme of ^{171}Lu proposed on the basis of the experiments described above is shown in fig. 5.8. The rotational bands built on the 7/2+[404], 1/2-[541], 1/2+[411], 5/2+[402] and 9/2-[514] Nilsson orbitals are established to high spin by firm coincidence evidence. Part of the coincidence data is shown in figs. 5.9 to 5.11. Figure 5.9 shows the 147, 171 and 177 keV gated spectra. Most of the peaks observed in coincidence with the 147 and 171 keV photopeaks are assigned to the 7/2+[404] band, together with interband transitions from the 9/2-[514] band. In addition an 801.4 keV transition is observed to feed the ground state band at the I = 13/2 level, thus defining a new level at 1241.6 keV. This state apparently feeds both the I = 15/2 and 17/2 members of the ground state band by means of the 607.5 and 391.8 keV transitions which have been assigned on the basis of energy fit. The transition to the I = 11/2 level is not observed, an upper limit of 3 (relative to the intensity of the 122.09 keV transition) being placed on its intensity. The structure above the 801 keV line in the 147 keV gated spectrum corresponds in energy to known impurity peaks.

The 177 keV gated spectrum presents evidence for a number of assignments within the 1/2-[541] band. Also a number of interband transitions are observed. The 615 and 760 keV transitions feed the 1/2-[541] band from the I = 15/2 and 17/2

Figure 5.8

Level scheme of ^{171}Lu. Levels drawn double width are observed in the single particle transfer spectra.

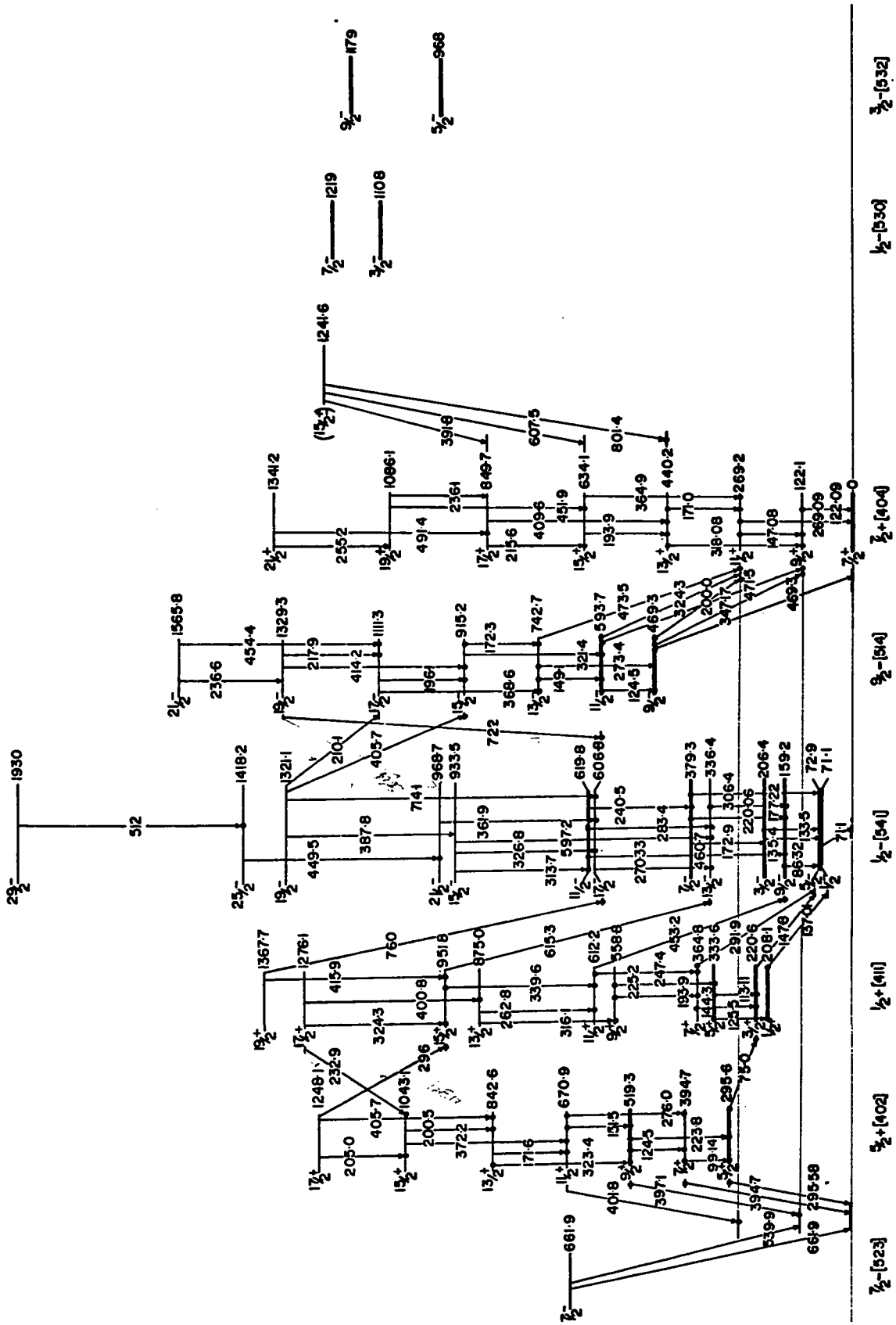
171 71 Lu 100
7/2-[523]
7/2+[402]
1/2+[411]
1/2-[541]
9/2-[514]
1/2+[404]
1/2-[530]
3/2-[532]

Figure 5.9

Coincidence spectra associated with the 147.08, 171.0-171.6-172.3 and 177.22 keV gates.

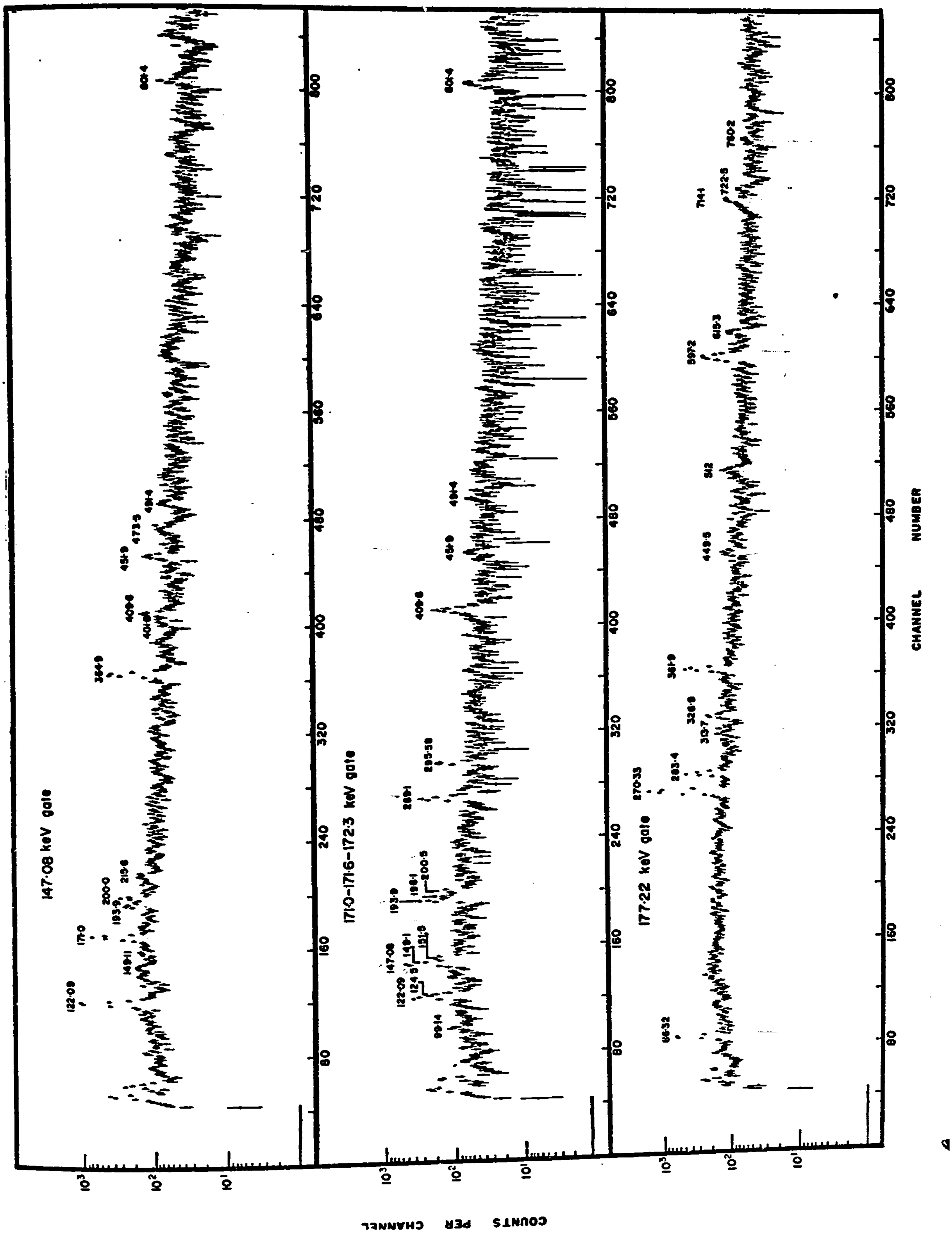
147·08 keV gate
171·0-171·6-172·3 keV gate
177·22 keV gate
CHANNEL NUMBER
COUNTS PER CHANNEL
80
160
240
320
400
480
560
640
720
800
10^3
10^2
10^1
122·08
149·11
171·0
193·9
200·0
215·6
364·9
401·9
409·6
451·9
473·5
491·4
801·4
99·14
122·09
124·8
147·08
149·1
151·5
193·9
198·1
200·5
269·1
295·58
409·6
491·4
86·32
270·33
283·4
313·7
328·9
361·9
449·5
512
597·2
615·3
714·1
722·5
760·2

states of the 1/2+[411] band. The 722 keV transition observed in the 177 keV gated spectrum feeds the 1/2-[541] band from the I = 19/2 state of the 9/2-[514] band. This, and other K forbidden transitions, will be discussed in section 5.8.

Figure 5.10 shows the 149, 144 and 295 keV gated coincidence spectra. Lines in coincidence with the 149 keV transition are assigned to the 9/2-[514] band with the exception of a number of interband transitions to the 7/2+[404] band and a K forbidden interband transition from the 19/2, 1/2-[541] state to the 15/2, 9/2-[514] state.

Evidence for another K hindered interband transition is shown in the 295 keV gated coincidence spectrum. The 295.6 keV transition depopulates the 5/2+[402] band and most of the lines observed are assigned to this band. However the 247 and 339 keV transitions are assigned to the 1/2+[411] band. They arise from coincidences with a weak 296 keV transition from 17/2, 5/2+[402] to 15/2, 1/2+[411].

Figure 5.11 presents coincidence spectra recorded with the 1 cm^3 detector. The 151 keV gated spectrum contains lines assigned to the 5/2+[402] band and also two interband transitions: a 232.9 keV transition between 17/2, 1/2+[411] and 15/2, 5/2+[402] and a 75.0 keV transition from the band head of the 5/2+[402] band to the 3/2, 1/2+[411] state in competition with the 295.5 keV transition to the ground state. The 137 keV transition de-excites the 1/2+[411] band to the ground state.

Figure 5.10

Coincidence spectra associated with the 149.11, 144.28 and 295.58-296.2 keV coincidence gates.

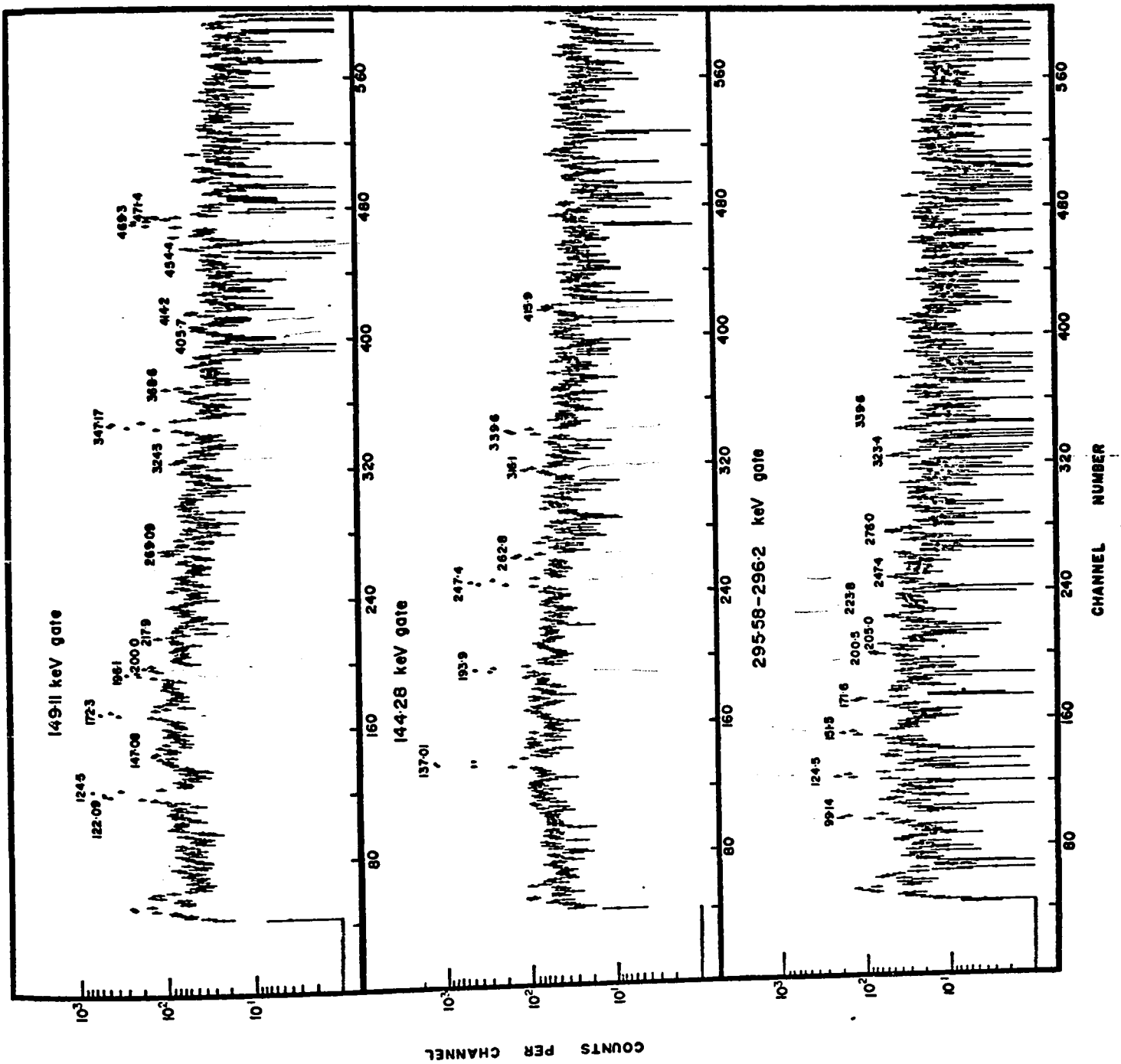
149·11 keV gate
144·28 keV gate
295·58–296·2 keV gate
COUNTS PER CHANNEL
CHANNEL NUMBER

Figure 5.11

Coincidence spectra associated with the 137.01 and 151.5 keV gates. Windows set on the 37 cm^3 detector spectrum.

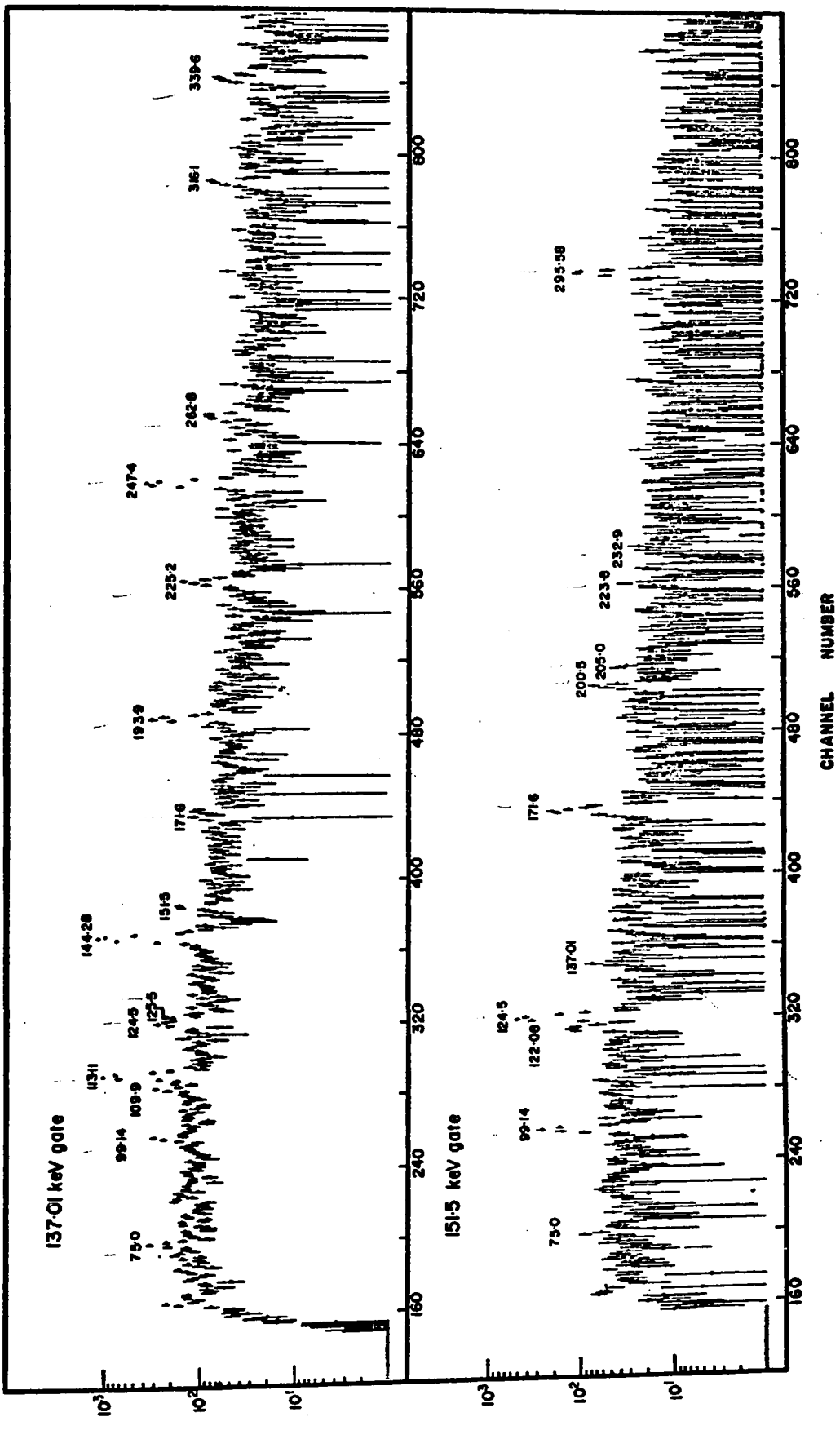
137-01 keV gate
151-5 keV gate
COUNTS PER CHANNEL
CHANNEL NUMBER
160
240
320
400
480
560
640
720
800
10^3
10^2
10^1
75-0
99-14
109-9
113-11
124-5
125-5
144-28
151-5
171-6
193-9
225-2
247-4
262-8
316-1
339-6
122-09
137-01
200-5
205-0
223-6
232-9
295-58

Consequently, the 137 keV gated coincidence spectrum contains most of the lines assigned to the 1/2+[411] band and also, because of the 75 keV interband feeding, transitions in the 5/2+[402] band. Because of the recognition of the interband feeding and the excellent resolution of the 1 cm^3 detector it is now possible to assign the 125.5 keV transition to the 1/2+[411] band. Previously it was thought that the 5/2→1/2 1/2[411] transition was one of an unresolved triplet at energy 124.5 keV. As a consequence the energies of the levels in the 1/2+[411] and 1/2-[541] have all been shifted up by 1 keV from previous assignments. This shift has made possible the fitting of three $\Delta K=2$ interband transitions. As this manuscript was in preparation a paper appeared in Physics Letters (Kemnitz et al. 1972) in which the authors report seeing a number of interband transitions with $\Delta K=2$ and 4 for which evidence is presented above. There appears to be good agreement between their result and ours.

The 109 keV line seen in the 137 keV gated coincidence spectrum is not assigned.

The band head of the 7/2-[523] band was placed at 662 keV by Gizon et al. (1970) who studied the gamma spectrum following the decay of ^{171}Hf. Levels in this band are too far from the Yrast line to be strongly populated by the $(\alpha,2n)$ reaction. Consequently we observe only the 661.9 and 539.9 keV transitions depopulating this band. For the same reason

we have no gamma ray evidence to support the single particle reaction assignments to the 1/2-[530] and 3/2-[532] bands.

5.8 Discussion

5.8.1 Introduction

The single particle transfer results and the on line gamma and conversion electron data, when used in conjunction, provide secure assignments for a number of Nilsson orbitals upon which rotational bands may be constructed to high spin. It is interesting to examine the predictions of the rotational model for this case where there is sufficient data to test the limitations of the model. It is also worthwhile to consider what other states might be present at low excitation.

5.8.2 A possible three quasi-particle state at 1241.6 keV

It would seem that the most probable assignment of the high spin state at 1241.6 keV would be that of a three quasi-particle state. In odd A spectra one expects three quasi-particle states to occur at an excitation energy of approximately twice the diffuseness parameter, Δ. Such states have been cbserved in ^{177}Hf and ^{177}Lu (Alexander et al. 1964) and in ^{177}Ta (Skanberg et al. 1970).

It is possible to make a tentative assignment for the spin of this state from the relative intensities of the de-exciting transitions. To a first approximation one would

expect the relative intensities of gamma transitions de-exciting a state to vary as $E_\gamma^{2\lambda+1}$. The intensity ratios of the three transitions feeding the I = 13/2, 15/2 and 17/2 levels of the 7/2+[404] band are 1:0.25:0.09, in reasonable agreement with the ratios 1:0.43:0.11 expected for dipole transitions. Thus 15/2 seems the most probable spin for the 1241.6 keV state. In ^{171}Lu the most probable configurations at low energies are the 7/2+[404] proton state coupled with two low lying neutron states. The available single particle orbitals are shown in fig. 5.12. In the present case a likely configuration is

$$\{\pi 7/2+[404],\ \nu 7/2+[633],\ \nu 1/2-[521]\}15/2- \ .$$

5.8.3 Gyromagnetic factors

Assuming pure configurations the rotational model allows the calculation of the gyromagnetic factor g_K from the cascade to cross-over gamma transition intensities within a rotational band (Winter et al 1970). The results which are obtained by using the neighbouring ^{170}Yb quadrupole moment Q_o = 7.55b (Stelson and Grodzins 1966) and g_R = 0.3, are listed in table 5.8 and are compared with the g_K values for the 7/2+[404], 5/2+[402] and 9/2-[514] orbitals, predicted by the classical Nilsson model (Nilsson 1955). For an unmixed band the value of the gyromagnetic ratio g_K is given by

$$g_K = \frac{1}{2K}\,(g_s - g_\ell)\sum_\ell (a^2_{\ell,K-1/2} - a^2_{\ell,K+1/2}) + g_\ell$$

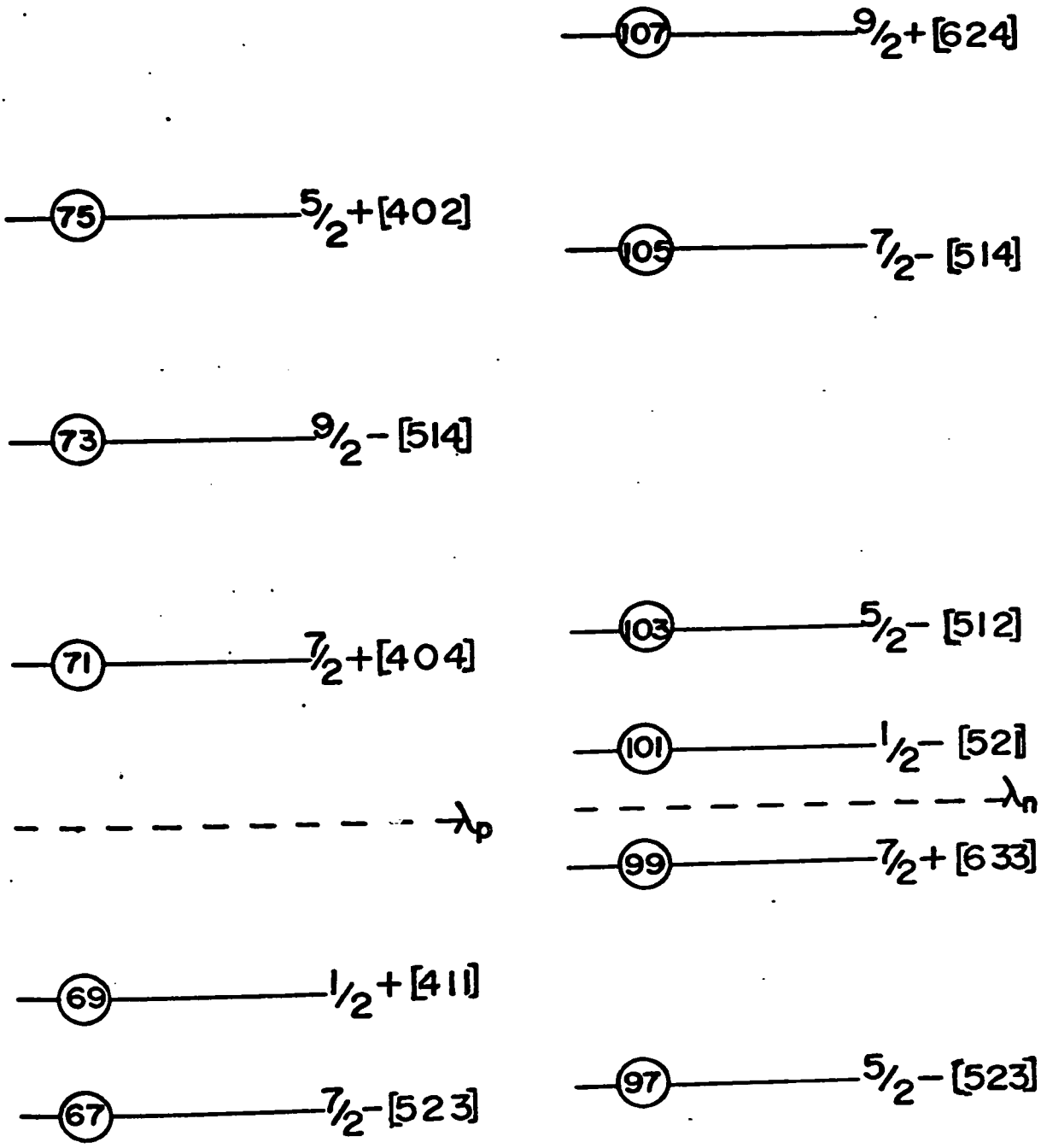

Figure 5.12

Available proton and neutron single particle orbitals for ^{171}Lu

for $K \neq 1/2$, the $a_{\ell,n}$ terms are the Nilsson expansion coefficients which are related to the coefficients of Chi by

$$C_{j\ell} = \sum_{\lambda} \langle \ell\lambda \tfrac{1}{2} K-\lambda \,|\, jK \rangle a_{\ell\lambda}.$$

For free nucleons one has $g_s = \binom{5.585}{3.826}$ and $g_\ell = \binom{1}{0}$ for protons and neutrons respectively. In practice it is found that better agreement with experiment is obtained using $g_s = 0.6\ g_s$ free. This value was used in the present calculation.

It may be noted that the agreement is best for the 7/2+[404] band for which the effects of Coriolis coupling are expected to be least. These data are more extensive but are in general agreement with those of Hjorth et al. (1972) and Kemnitz et al. (1971). It may be noted also that values of $1/\delta^2$ presented in table 5.8 are derived using a model dependent approach, and furthermore it is assumed that there are no Coriolis coupling effects. The results are in good agreement with those given by angular distribution measurements (Hjorth et al.1972) One may conclude that the rotational model approach is valid and that the results are not very sensitive to the effects of Coriolis coupling.

The next two sections present a discussion of an attempt to calculate rotational energy spacings and branching ratios in a way which properly takes the effects of Coriolis coupling into account.

TABLE 5.9

Gyromagnetic factors of the 7/2+[404], 5/2+[402], 9/2-[514] 1/2+[411] and 1/2-[541] rotational bands in ^{171}Lu

Orbital	Initial Spin	$1/\delta^2$	g_K branching ratios	g_K Nilsson Model
7/2+[404]	11/2	3.8±0.6	±0.67±0.10	
	13/2	4.7±0.8	±0.71±0.11	
	15/2	5.5±1.8	±0.73±0.24	
	17/2	3.8±0.8	±0.65±0.14	0.70
	19/2	5.4±2.1	±0.75±0.29	
	21/2	5.5±4.0	±0.70±0.51	
5/2+[402]	9/2	16 ±6	±1.10±0.4	
	11/2	49 ±8	±1.68±0.3	
	13/2	55 ±12	±1.70±0.4	1.46
	15/2	48 ±9	±1.31±0.2	
	17/2	47 ±18	±1.24±0.5	
9/2-[514]	13/2	22 ±4	±1.1 ±0.2	
	15/2	24 ±6	±1.1 ±0.3	
	17/2	21 ±5	±1.0 ±0.2	1.23
	19/2	25 ±15	±1.1 ±0.7	
	21/2	10 ±7	±0.8 ±0.6	

5.8.4 Description of the rotational bands

When the energy spacings of the rotational bands in ^{171}Lu are presented in a plot of the effective moment of inertia against $2I^2$ (fig. 5.13) it is apparent that a number of different mechanisms must be taken into account in order to provide a complete description of the rotational energy levels. An excellent discussion of this point has recently appeared (Hjorth et al. 1972). These workers suggest that $\Delta K = 2$ coupling is necessary to account for the oscillating behavior of the 5/2+[402] band. Also they examine the predictions of the Harris (1965) variable moment of inertia model and fit the 1/2+[411] band by making a separate variable moment of inertia fit for those levels for which I+1/2 is even or odd. In the present work the approach has been to attempt a complete description with one general calculation. To this end a Nilsson model calculation which includes Coriolis mixing and an approximation to a variable moment of inertia has been performed. The general philosophy has been to describe the energy spacings within the rotational bands with a minimum of parameters and to use values of the variable parameters which are physically reasonable rather than letting the program make a search on all the available parameters. The results of the fit to the energy spacings are presented in table 5.9. The Nilsson parameters used are as described in section 5.3. The expressions for the unperturbed energy

Figure 5.13

The effective moment of inertia plotted against $2I^2$ for rotational bands in ^{171}Lu.

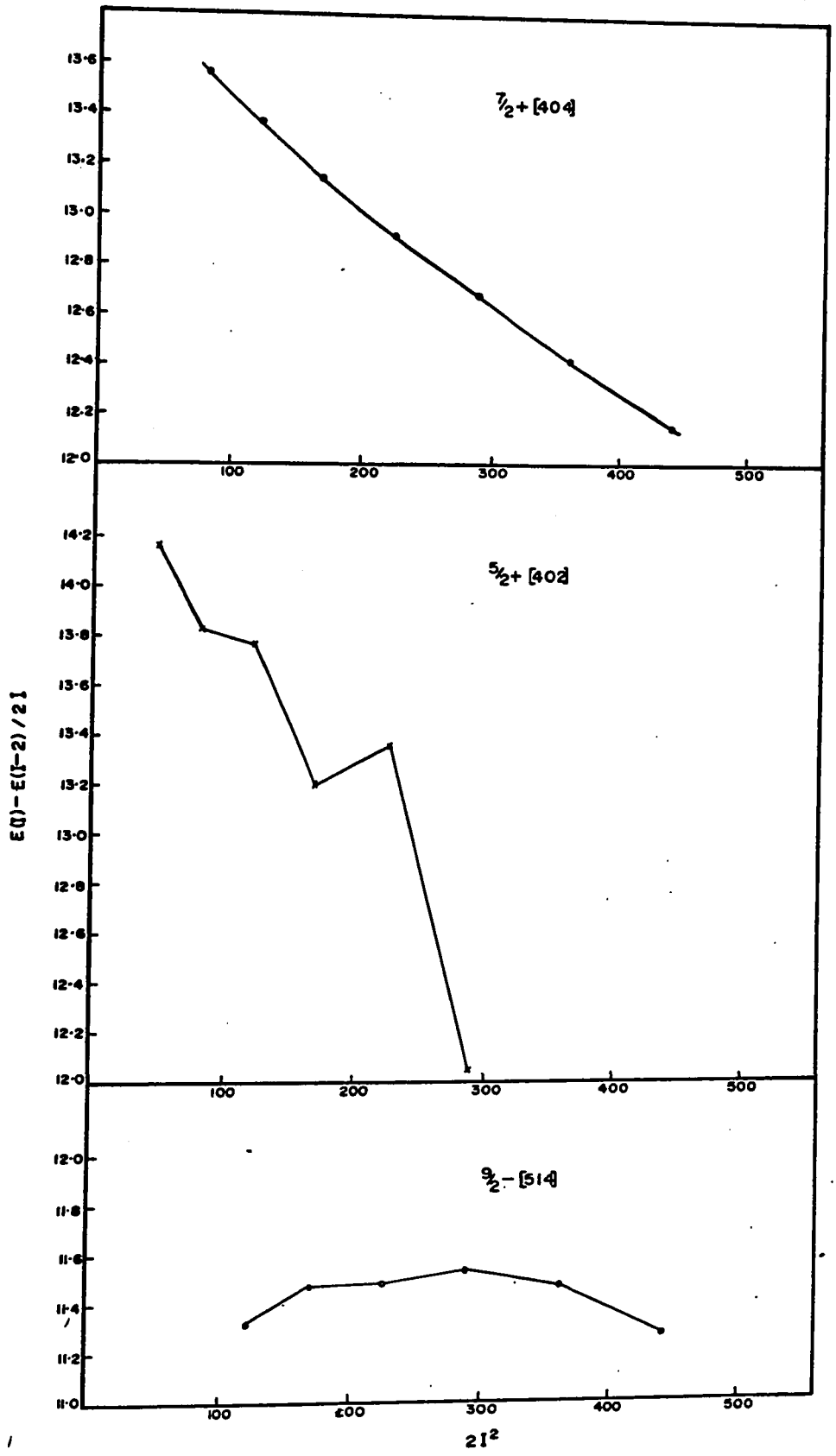
7/2+ [404]
5/2+ [402]
9/2− [514]
E(I) − E(I−2) / 2I
2I²
13·6
13·4
13·2
13·0
12·8
12·6
12·4
12·2
12·0
14·2
14·0
13·8
13·6
13·4
13·2
13·0
12·8
12·6
12·4
12·2
12·0
12·0
11·8
11·6
11·4
11·2
11·0
100
200
300
400
500

TABLE 5.10

Calculated Fit to the Energy Levels in ^{171}Lu

Orbital	Spin	Level Energy (keV)	
		expt.	predicted
7/2+[404]	7/2	0.0	0.0
	9/2	122.1	121.7
	11/2	269.2	268.7
	13/2	440.2	440.0
	15/2	634.1	634.2
	17/2	849.7	849.9
	19/2	1086.6	1085.6
	21/2	1341.2	1339.3
9/2-[514]	9/2	469.3	469.3
	11/2	593.7	593.9
	13/2	742.7	742.4
	15/2	915.2	914.7
	17/2	1111.3	1110.5
	19/2	1329.3	1329.3
	21/2	1565.8	1570.2
5/2+[402]	5/2	295.5	295.5
	7/2	394.7	393.7
	9/2	519.3	518.4
	11/2	670.9	669.6
	13/2	842.6	843.9
	15/2	1043.1	1044.8
	17/2	1248.1	1258.3
1/2+[411]	1/2	208.1	208.1
	3/2	220.6	226.6
	5/2	333.6	331.2
	7/2	364.8	365.0
	9/2	558.8	556.4
	11/2	612.2	609.6
	13/2	875.0	877.2
	15/2	951.8	949.0
	17/2	1276.1	1287.5
	19/2	1367.7	1373.0
1/2-[541]	1/2	71.1	71.1
	3/2	206.4	198.7
	5/2	72.9	83.8
	7/2	379.3	376.6
	9/2	159.2	177.0
	11/2	619.8	624.7
	13/2	336.4	350.6
	15/2	933.5	940.4
	17/2	606.8	602.2
	19/2	1321.1	1320.9
	21/2	968.7	927.4
	25/2	1418.2	1320.2

levels and for the Coriolis matrix elements are as given in chapter 2. The rotational energy matrix is constructed and diagonalized in the space of all the Nilsson orbitals which arise from the $g_{7/2}$, $d_{5/2}$, $h_{11/2}$, $d_{3/2}$ and $s_{1/2}$ shell model states, plus the 1/2-[530] Nilsson orbital from the $f_{7/2}$ state. When known, the band head energies are those found experimentally, otherwise the Nilsson model predictions are used.

It is found that the rotational parameters and decoupling parameters have to be treated as free parameters, although the necessary changes are small. The coriolis attenuation factor α is commonly given a value between 0.6 and 1.0 (Løvhøiden et al. 1972). It may be noted that the 17/2, 5/2+[402] and 17/2, 1/2+[411] states lie very close in energy. This energy separation was reproduced with $\alpha = 0.65$ and so this value was adopted for all the bands. A good fit to the 7/2+[404] band was obtained with $B_K = -8$ eV, accordingly this value was used for all the positive parity bands. It is suggested by fig. 5.13 that a smaller value for B_K must be used for the 9/2-[514] band. A good fit was obtained with $B_K = -3.5$ eV. This value was also used for the 1/2-[541] band. These values for B are of the same magnitude as that found by Rensfelt et al. (1970) for the 7/2-[523] band in ^{161}Ho. The rotational and decoupling parameters

which were used are presented in table 5.11

Table 5.11

Rotational parameters used in the unified model description of the rotational level energies of ^{171}Lu

Orbital	A_K (keV)	B_K (eV)	a
7/2+[404]	13.9	-8	
1/2-[541]	11.2	-3.5	2.95
1/2+[411]	13.8	-8	-0.62
5/2+[402]	14.25	-8	
9/2-[514]	13.9	-3.5	

By using a power series expansion, as presented in chapter 2, it is possible to make a fit to the energy spacings of a rotational band to better than 1%. However this leaves very few degrees of freedom (in general just two or three per band) and the physical significance of all the parameters is not clear. The approach outlined above represents an attempt to describe the rotational energy spacings in a more realistic way.

5.8.4 Unified model description of transition probabilities

A more stringent test of the model is its ability to correctly predict transition probabilities and branching

ratios especially in the case of the K forbidden transitions discussed in section 5.7. For these special cases the branching ratios will only be correctly predicted if the calculated admixtures of wave functions are correct. For the levels of greatest interest the predicted amplitudes are given in table 5.12

Using the predicted energies as shown in table 5.10 the transition probabilities are calculated between states

$$\psi^I = \sum_{i=1}^{N} C^I_{K_i} \psi_o^{I,K_i} \quad \text{and} \quad \psi^{I'} = \sum_{j=1}^{N} C^{I'}_{K_j} \psi_o^{I'K_j} .$$

Here, the quantity $C^I_{K_i}$ is the amplitude of the admixture of the wave function ψ_o^{I,K_i} into the state with spin I, and N is the number of mixed bands. The reduced transition probabilities between mixed states are given by Hjorth et al. (1970) as

$$B(E2,I\to I') = \frac{5}{16\pi} e^2 Q_o^2 \Big[\sum_{K_i=K_j} C^I_{K_i} C^{I'}_{K_j} \langle IK_i 20 | I'K_j\rangle \Big]^2$$

$$B(M1,I\to I') = \Big(\frac{e\hbar}{2Mc}\Big)^2 \frac{3}{4\pi} \frac{1}{4} \Big[\sum_{K_i=K_j\pm 1,K_j} C^I_{K_i} C^{I'}_{K_j} \{\langle IK_i 1, K_j-K_i | I'K_j\rangle$$

$$+ b_{M1}\delta_{K_i,\frac{1}{2}}\delta_{K_j,\frac{1}{2}}(-1)^{I'+\frac{1}{2}}\langle I\tfrac{1}{2}1\ -1|I'-\tfrac{1}{2}\rangle\}G_{M1}^{K_j K_i}\Big]^2$$

where for $K = \frac{1}{2}$

$$b_{M1}G_{M1}^{\frac{1}{2}\frac{1}{2}} = \sqrt{2}(-1)^{\ell+1} \sum_{\ell} \Big[a^2_{\ell_o}(g_S-g_R) + 2a_{\ell_o}a_{\ell_1}\sqrt{\ell(\ell+1)}\ (g_\ell - g_R)\Big] .$$

The diagonal elements $G_{M1}^{K_i K_j}$ $(K_i = K_j = K)$ are given by

$$G_{M1}^{KK} = \sum_{\ell\Lambda} a_{\ell\Lambda}^2 [(-1)^{\Sigma-\frac{1}{2}} (g_s - g_R) + 2\Lambda(g_\ell - g_R)],$$

and the off diagonal elements $(K_i + K+1, K_j = K)$ by

$$G_{M1}^{K+1,K} = G_{M1}^{K,K+1} = -\sqrt{2} \sum_{\ell\Lambda} [a_{\ell\Lambda}^{K_j} a_{\ell\Lambda}^{K_i} (g_S - g_R)$$

$$+ a_{\ell,\Lambda+1}^{K_j} a_{\ell,\Lambda}^{K_i} \sqrt{(\ell+\Lambda+1)(\ell-\Lambda)} \quad (g_\ell - g_R)],$$

where the coefficients $a_{\ell\Lambda}$ are the normalized amplitudes for the particle wave function taken from the Nilsson model calculation. The gyromagnetic ratios are taken to be $g_S = 0.6\, g_{S\ free}$ and $g_R = 0.3$ with the quadrupole moment $Q_o = 7.55b$. For in band E2 transitions Q_o is assumed to be constant. The transition rates are given by

$$T(E\lambda) = 4\pi \left(\frac{\lambda+3}{3}\right)^2 R^{-2\lambda} B(E\lambda)$$

and

$$T(M\lambda) = 4\pi \left(\frac{\lambda+3}{3}\right)^2 R^{-2\lambda} \left(\frac{\hbar}{mc}\right)^{-2} B(M\lambda)$$

where $R = 1.20\ A^{1/3}$ fm and $B(E\lambda)$ and $B(M\lambda)$ are in units of $fm^{2\lambda}$.

The results of the calculation are compared with experimental results in table 5.13 as branching ratios, normalized to 100 for each level. It may be noted that the calculation correctly predicts appreciable branching for the

TABLE 5.12

Admixtures of Orbitals for Highly Mixed States in ^{171}Lu

Spin	Level Energy (keV)	Amplitude of wave functions						
		1/2+[411]	1/2+[404]	3/2+[411]	3/2+[402]	3/2+[422]	5/2+[402]	7/2+[404]
17/2	1248.0	0.499	-0.145	-0.171	0.033	-0.015	0.833	0.075
17/2	1276.1	-0.830	0.171	-0.024	-0.025	0.025	0.528	0.045
		1/2-[541]	3/2-[532]	5/2-[532]	5/2-[523]	7/2-[523]	9/2-[514]	11/2-[505]
19/2	1321.1	0.891	-0.405	-0.023	0.054	-0.068	0.112	0.027
19/2	1329.3	0.123	-0.054	0.131	0.005	0.473	-0.836	-0.204

Table 5.13

Experimental and Calculated Branching Ratios for Gamma Transitions in ^{171}Lu

Orbital	Transition I_i	K_i^π	I_f	K_f^π	Transition Energy (keV)	Branching Ratio expt.	Branching Ratio theory	Comment
7/2+[404]	11/2	7/2+	7/2	7/2+	269.09	47	54	
			9/2	7/2+	147.08	53	46	
	13/2	7/2+	9/2	7/2+	318.0	66	73	
			11/2	7/2+	171.0	34	27	
	15/2	7/2+	11/2	7/2+	364.9	73	82	
			13/2	7/2+	193.9	27	18	
	17/2	7/2+	13/2	7/2+	409.6	85	87	
			15/2	7/2+	215.6	15	13	
	19/2	7/2+	15/2	7/2+	451.9	87	90	
			17/2	7/2+	236.1	13	10	
	21/2	7/2+	17/2	7/2+	491.4	85	92	
			19/2	7/2+	255.2	15	8	
1/2-[541]	3/2	1/2-	1/2	1/2-	135.4	35	12	
			5/2	1/2-	133.5	65	88	
	7/2	1/2-	3/2	1/2-	172.9	8	6	
			5/2	1/2-	306.4	46	15	
			9/2	1.2-	220.06	46	79	
	11/2	1/2-	7/2	1/2-	240.5	20	26	
			9/2	1/2-	460.7	57	45	
			13/2	1/2-	283.4	23	29	
	15/2	1/2-	11/2	1/2-	313.7	17	44	
			13/2	1/2-	597.2	69	29	
			17/2	1/2-	326.8	14	27	

(continued next Page)

Table 5.13 (continued)

Orbital	Transition I_i	K_i^π	I_f	K_f^π	Transition Energy (keV)	Branching Ratio expt.		Branching Ratio theory	Comment
	19/2	1/2-	15/2	1/2-	387.8	30		44	
			17/2	1/2-	714.8	49		37	
			21/2	1/2-	352.4	<5		17	
			15/2	9/2-	405.7	10		0.8	ΔK=4
			17/2	9/2-	210.1	6		0.6	ΔK=4
1/2+[411]	5/2	1/2+	1/2	1/2+	125.5	10		33	
			3/2	1/2+	113.1	90		67	
	7/2	1/2+	3/2	1/2+	144.29	79	a	6	
			5/2	1/2+	31.2	1		0.03	
			5/2	1/2-	291.9	20		94	
	9/2	1/2+	5/2	1/2+	225.2	37		70	
			7/2	1/2+	193.9	63		30	
	11/2	1/2	7/2	1/2+	247.4	79	a	32	
			9/2	1/2+	53.4	<1		<0.5	
			9/2	1/2-	453.2	21		68	
	13/2	1/2+	9/2	1/2+	316.1	51		84	
			11/2	1/2+	262.8	49		16	
	15/2	1/2+	11/2	1/2+	339.6	83		54	
			13/2	1/2-	615.3	17		46	
	17/2	1/2+	13/2	1/2+	400.8	63		92	
			15/2	1/2+	324.3	37		8	
	19/2	1/2+	15/2	1/2+	415.0	60		66	
			17/2	1/2-	760.2	40		34	
5/2+[402]	5/2	5/2+	7/2	7/2+	295.58	98		99.7	
			3/2	1/2+	75.0	2		0.3	ΔK=2
	7/2	5/2+	5/2	5/2+	99.1	66		70	
			7/2	7/2+	394.7	34		30	ΔK=1

(continued next page)

Table 5.13 (continued)

Orbital	Transition I_i	K_i^π	I_f	K_f^π	Transition Energy (keV)	Branching Ratio expt.	Branching Ratio theory	Comment
	9/2	5/2+	5/2	5/2+	223.8	22	18	
			7/2	5/2+	124.5	62	67	
			7/2	7/2+	519.3	<5	0.5	ΔK=1
			9/2	7/2+	397.1	16	14	ΔK=1
	11/2	5/2+	7/2	5/2+	276.0	21	36	
			9/2	5/2+	151.5	71	53	
			9/2	7/2+	548.8	<5	4	ΔK=1
			11/2	7/2+	401.8	8	7	ΔK=1
	13/2	5/2+	9/2	5/2+	323.4	66	53	
			11/2	5/2+	171.6	34	47	
	15/2	5/2+	11/2	5/2+	372.2	44	65	
			13/2	5/2+	200.5	56	35	
	17/2	5.2+	13/2	5/2+	405.7	43	69	
			15/2	5/2+	205.0	28	26	
			15/2	1/2+	296.2	29	5	ΔK=2
9/2-[514]	9/2	9/2-	7/2	7/2+	469.3	39	95	
			9/2	7/2+	347.1	53	5	
			11/2	7/2+	200.0	8	0.05	
	11/2	9/2-	9/2	9/2-	124.5	74	26	
			9/2	7/2+	471.5	24	69	
			11/2	7/2+	324.3	2	5	
	13/2	9/2-	9/2	9/2-	273.4	9	15	
			11/2	9/2-	149.11	75	45	
			11/2	7/2+	473.5	16	40	
	15/2	9/2-	11/2	9/2-	321.4	23	41	
			13/2	9/2-	172.3	77	59	

(continued next page)

Table 5.13 (continued)

Orbital	Transition I_i	K_i^π	I_f	K_f^π	Transition Energy (keV)	Branching Ratio expt.	Branching Ratio theory	Comment
	17/2	9/2-	13/2	9/2-	368.6	36	53	
			15/2	9/2-	196.1	64	47	
	19/2	9/2-	15/2	9/2-	414.2	26	63	
			17/2	9/2-	217.9	36	35	
			15/2	1/2-	395.8	<10	2	
			17/2	1.2-	722.5	38	0.6	
	21/2	9/2-	17/2	9/2-	454.4	71	68	
			19/2	9/2-	236.6	29	32	

a) Calculated using coincidence probabilities and the conversion coefficients of Hager and Seltzer (1968).

K forbidden transitions observed experimentally. For pure states transitions for which $\Delta K > \lambda$ are complete forbidden, such transitions proceed due to admixtures in the wave-function of states of different K.

5.9 Summary

A variety of experiments has been performed in order to establish and identify the states in the rare earth deformed nucleus ^{171}Lu. Proton particle states have been studied using (^{3}He,d) and (α,t) stripping reactions. The reaction products were analyzed with an "Enge" split pole magnetic spectrograph. The expected components of the following intrinsic proton states have been identified: 7/2+[404] (ground state), 1/2-[541], 1/2+[411] , 5/2+[402] and 9/2-[514]. In addition, tentative assignments are made for rotational states based on the 3/2-[532], 1/2-[530] and 1/2+[660] orbitals, and for states which are mixtures of β and γ vibrations and particle states. The cross section ratios of the two stripping reactions were used as an indication of ℓ value and spectroscopic factors were extracted using D.W.B.A. calculations. Gamma radiation and conversion electrons following the reaction $^{169}Tm(\alpha,2n)^{171}Lu$ have been studied, using high resolution Ge(Li) detectors in singles and coincidence mode, and an on line, doubly focussing, electron spectrometer. Coincidence probabilities have been calculated and have been used to determine the intensities of unresolved gamma transi-

tions. Excitation functions of gamma-rays following the $^{168}Er(^{7}Li,\alpha n)$ reaction were used to check isotopic assignments. The ratio of the relative intensities of gamma transitions following the ^{7}Li, and α induced reactions was found to be a good indicator of the spin of the de-exciting level. It was found that a rotational model calculation which included Coriolis coupling term and an approximation to a spin dependence of the moment of inertia was able to provide a satisfactory fit to the energies of the observed rotational levels and the gamma branching ratios. The emphasis was on performing a calculation which would give a reasonable description of the properties of all the rotational levels without making undue assumptions or introducing parameters with no physical significance. The problem has been, and remains, which parameters should be allowed to vary. The present calculation points out the striking effects of Coriolis coupling by predicting significant mixing for bands differing in K values by as much as four.

REFERENCES

Alaga, C., Alder, K., Bohr, A., and Mottelson, B.R. (1955), Mat. Fys. Mat. Fys. Medd. Dan. Vid. Selsk. 29, No. 9.

Alexander, P., Boehm, F. and Kankekit, E. (1964).Phys. Rev. 133B, 284.

Alzetta, R., Gmitros, M., and Gambhir, Y.K.(1972).Czech. J. Phys. B21, 768.

Backlin, A., Fogelberg, B., and Malmskog, S.G.(1967).Nuc. Phys. A96, 539.

Bardeen, J., Cooper, L.N. and Schrieffer, J.R. (1957). Phys. Rev. 108, 1175.

Barneond, D., Foin, C., Bandry, A., Gizon, A. and Valentin, J. (1972).Journal de Physique 33, 15.

Bassel, R.H., Drisko, R.M. and Satchler, G.R. (1962).ORNL Report 3240.

Begzhanov, R.B., Khodzhaev, M. Kh. and Sharipov, Sh.Sh.(1969). Sov. J. Nucl. Phys. 8, 142.

Berzins, G., Bunker, M.E. and Starner, J.W.(1969).Nucl. Phys. A126, 273.

Bjørnholm, S., Borggreen, J., Frahm, H.J. and Sigurd Hansen, N.J. (1965).Nucl. Phys. 73, 593.

Bohr, A. (1952). K. Danske Vidensk. Selsk, Mat.-Fys. Medd. 26, no. 14.

Bohr, A. and Mottelson, B.R. (1953). K. Danske Videnske. Selsk. Mat.-Fys. Medd. 27, no. 16.

Bohr, A., Mottelson, B.R. and Pines, D. (1958). Phys. Rev. 110, 936.

Burke, D.G., Alford, W.P. and O'Neil, R.A. (1971). Nucl. Phys. A161, 129.

Cameron, J.A. and Summers-Gill, R.G. (1962). Can. J. Phys. 40, 1041.

Cameron, J.A. and Summers-Gill, R.G. (1963). Can. J. Phys. 41, 823.

Chan, K.Y. (1966). Nucl. Phys. 85, 261.

Chasman, C., Jones, K.W. and Ristien, R.A. (1965). Nucl. Inst. and Meth. 37, 1.

Chi, B.E. (1967). State University of New York (Albany) publication.

Chilosi, G., Van Hise, J.R., and Tang, C.W. (1968). Phys. Rev. 168, 1409.

Davydov, A.S. and Filippov (1958). Nucl. Phys. 8, 237.

Dietrich, F.S., Herskind, B., Naumann, R.A., Stokstad, R.G., and Walker, G.E. (1970). Nucl. Phys. A155, 209.

Ejiri, H., Ishihara, M., Saki, M., Inamura, T. and Katori, K. (1966). Nucl. Phys. 89, 641.

Elliott, J.P. (1958). Rochester lecture notes, compiled by Macfarlane, H.M.

Enge, H.A. (1964). Nucl. Inst. and Meth. 28, 126.

Geiger, J.S. (1965). A.E.C.L. report CRGP-1214.

Gizon, J., Barneoud, D. and Valentin, J. (1970), J. Nucl. Phys. A148, 561.

Gregory, P.R., Preibisz, Z., Waddington, J.C. and Johns, M.W. (1970). Bull. Am. Phys. Soc. 15, No. 6, 783.

Gregory, P.R. and Taylor, T. (1972). Phys. Letts. To be published.

Grover, J.R. and Gilat, J. (1967). Phys. Rev. 157, 802.

Grover, J.R. and Gilat, J. (1967). Phys. Rev. 157, 814.

Hager, R.S. and Seltzer, E.C. (1968). Nucl. Data A4.

Hamamoto, I. and Igaguwa, T. (1969). Nucl. Phys. A126, 241.

Harar, S. and Horoshko, R.N. (1972). Nucl. Phys. 183, 161.

Harmatz, B. and Handley, T.H. (1966). Nucl. Phys. 81, 481.

Harris, S.H. (1965). Phys. Rev. 138, B509.

Haxel, O., Jensen, J.H.D. and Suess, H.E. (1949. Phys. Rev. 75, 1766.

Haxel, O., Jensen, J.H.D. and Suess, H.E. (1950). Z. Physik 128, 295.

Hjorth, S.A., Ryde, H., Hagemann, K.A., Løvhøiden, G. and Waddington, J.C. (1970). Nucl. Phys. A144, 513.

Hjorth, S.A., Ryde, H. and Shanberg, B. (1972). Journal de Physique 33, 23.

Kemnitz, P., Funke, L., Hohmuth, K., Kaun, K.-H, Sodan, H. and Winter, G. (1971). Nucl. Phys. A164, 513.

Kemnitz, P., Funke, L., Kaun, K.-H, Sodan, H. and Winter, G. (1972). Phys. Letts. 39B, 179.

Kerman, A.K. (1956). Mat. Fys. Medd. Dan. Vid. Selsk. 30, no. 15.

Kofoed-Hansen, O., Lindhard, J., and Nielsen, O.B. (1950). Dan. Mat. Fys. Medd. 25, No. 16.

Kunz, P.D. (1967). Private communication.

Kurz, H.E., Jasper, E.W., Fischer, K. and Hermes, F. (1971). Nucl. Phys. A168, 129.

Lamm, I.-L. (1969). Nucl. Phys. A125, 504.

Løvhøiden, G., Hjorth, S.A., Ryde, H. and Harms-Lingdahl, L. (1972). Nucl. Phys. A181, 589.

Lu, M.T. and Alford, W.P. (1971). Phys. Rev. C3, 1243.

Mancuso, R.V., and Arns, R.R. (1965). Nucl. Phys. 68, 504.

Mariscotti, M.J.A., Scharff-Goldhaber, G. and Buck, B. (1968). Phys. Rev. 178, 1864.

Mayer, M.G. (1949). Phys. Rev. 75, 1969.

Mayer, M.G. (1950). Phys. Rev. 78, 16.

Moret, R.,(1969). J. de Physique 30, 501.

Moringa, Cf. H. and Gugelot, P.C. (1963). Nucl. Phys. 46, 210.

Nathan, O. and Nilsson, S.G. (1965). Alpha, Beta and Gamma Ray Spectroscopy, ed. K. Siegbahn (North-Holland, Amsterdam).

Nielsen, O.B. and Kofoed-Hansen, O. (1955). Dan. Mat. Fys. Medd. 29, No. 6.

Nilsson, S.G. (1955). Dan. Mat. Fys. Medd. 29, No. 15.

Noma, H., Shibata, T. and Yoshisawa, Y. (1970). J. Phys. Soc. Japan 28, 546.

O'Neil, R. (1970). Private communication.

O'Neil, R.A., Burke, D.G. and Alford, W.P. (1971). Nucl. Phys. A167, 481.

O'Neil, R.A. (1972). Thesis, McMaster University.

Pandharipande, V.R., Prasad, K.G., Singru, R.M., and Sharma, R.P. (1966). Phys. Rev. 143, 740.

Pandharipande, V.R. (1967). Nucl. Phys. A100, 449.

Pandharipande, V.R., Prasad, K.G., Sharma, R.P. and Thosar, B.V. (1968). Nucl. Phys. A109, 81.

Raghavan, R.S., and Raghavan, P. (1972). Phys. Rev. Lett. 28, 54.

Rensfelt, K.-G., Johnson, A. and Hjorth, S.A. (1970). Nucl. Phys. A156, 529.

Robinson, H. (1969). Private communication.

Rowe, D.J. (1970). Nuclear Collective Motion. Methuen and Co. Ltd. Chap. 6.

Satcher, G.R. (1958). Ann. Phys. 3, 275.

Sharma, R.P., Gopinathan, K.P. and Amtey, S.R. (1964). Phys. Rev. B134, 730.

Skanberg, B., Hjorth, S.A. and Ryde, H. (1970). Nucl. Phys. A154, 641.

Soloviev, V.G., Vogel, P. and Jungklaussen, G. (1966). Dubna Report E4-3051.

Spencer, J.L. and Enge, H.A. (1967). Nucl. Inst. and Meth. 48, 181.

Stelson, P.H., Dickens, J.K., Raman, S. and Trammell, R.C. (1972). Nucl. Inst. and Meth. 98, 481.

Stephens, F.S., Lark, N.L. and Diamond, R.M. (1965). Nucl. Phys. 63, 82.

Tang, C.W., Coryell, C.D., and Gordon, G.E. (1965). Bull. Am. Phys. Soc. 10, 425.

Ungrin, J. and Johns, M.W. (1969). Nucl. Inst. and Meth. 70, 112.

Weiffenbach, C.V. and Tickle, R. (1971). Phys. Rev. C3, 1668.

Westgaard, L. and Bjørnholm, S. (1966). Nucl.Inst. and Meth. 42, 77.

Williams, G.N., McPherson, D. (1968). CRNL Report No. PLP76.

Winter, G., Funke, L., Hohmuth, K., Kaun, K.H., Kemnitz, P. and Sodan, H. (1970). Nucl. Phys. A151, 337.

APPENDIX

A variable moment of inertia description of bands in odd-even nuclei

(accepted for publication in Physics Letters)

A VARIABLE MOMENT OF INERTIA DESCRIPTION OF BANDS IN ODD-EVEN NUCLEI

P. R. Gregory and T. Taylor

Department of Physics, McMaster University
Hamilton, Ontario, Canada

Abstract

The advantages of extending a variable moment of inertia model to bands in odd-even nuclei are demonstrated. Calculations are performed for bands which are not significantly affected by Coriolis coupling.

The variable moment of inertia (VMI) model, as formulated by Mariscotti et. al. (1), yields excellent two parameter fits to the excitation energies of the ground state bands of even-even nuclei, over a wide mass range. The expression for the excitation energy, in the semiclassical model, contains a rotational energy term $I(I+1)/2\mathcal{I}_I$ and a potential energy term $C(\mathcal{I}_I-\mathcal{I}_0)^2/2$ where $\mathcal{I}_0$ corresponds to the ground state moment of inertia and C is a restoring force constant. The moment of inertia for a particular state of spin I is determined by the variational condition $\partial E_I/\partial\mathcal{I}_I = 0$. Deviations from the I(I+1) rule for energy spacings within a band are in this way attributed to an increase in the moment of inertia.

With the advent of very high resolution Ge(Li) detectors it has recently become possible to study high spin

members of bands in odd-even nuclei by (Heavy Ion,xn) reactions. In particular, data is now available for bands which are not expected to be significantly affected by Coriolis mixing, thus the feasibility of extending the VMI model to odd-even nuclei may be easily evaluated.

The specific cases considered are the 7/2+[404] valence proton band in ^{171}Lu (2) and the 11/2-[505] valence neutron band in ^{153}Gd(3). The experimentally derived gyromagnetic ratios (2,3) are found to be constant within each band. The observed values are $g_K = 0.70$ for the 7/2+[404] band and $g_K = -0.16$ for the 11/2-[505] band assuming the intrinsic quadrupole moments $Q_o = 7.55$ for ^{171}Lu (4) and $Q_o = 6.08$ for ^{153}Gd (4) and employing the gyromagnetic ratio $g_R = 0.30$ for the rotor. The values predicted by the Nilsson model are $g_K = 0.70$ for the 7/2+[404] band and $g_K = -0.19$ for the 11/2-[505] band. The constancy of the gyromagnetic ratios and the agreement with the theoretical predictions for pure bands implies that the effect of Coriolis mixing is negligible for the bands in question.

The spin dependence of the excitation energy spacings can be conveniently compared with that of neighbouring even-even nuclei in a plot of $\Delta I = 2$ transition energies versus I. This comparison is made in Fig. 1. Rezanka et. al. (5) have noted that for the case of ^{153,154}Gd the effective moments of inertia as well as their variation with angular momentum may be seen to be almost identical. Apparently the rotation-particle coupling does not significantly renormalize the effective moments of inertia in ^{171}Lu and ^{153}Gd.

Figure 1

The variation of the effective moment of inertia with angular momentum is seen to be almost identical for $^{171}Lu(^{153}Gd)$ and $^{170}Yb(^{154}Gd)$.

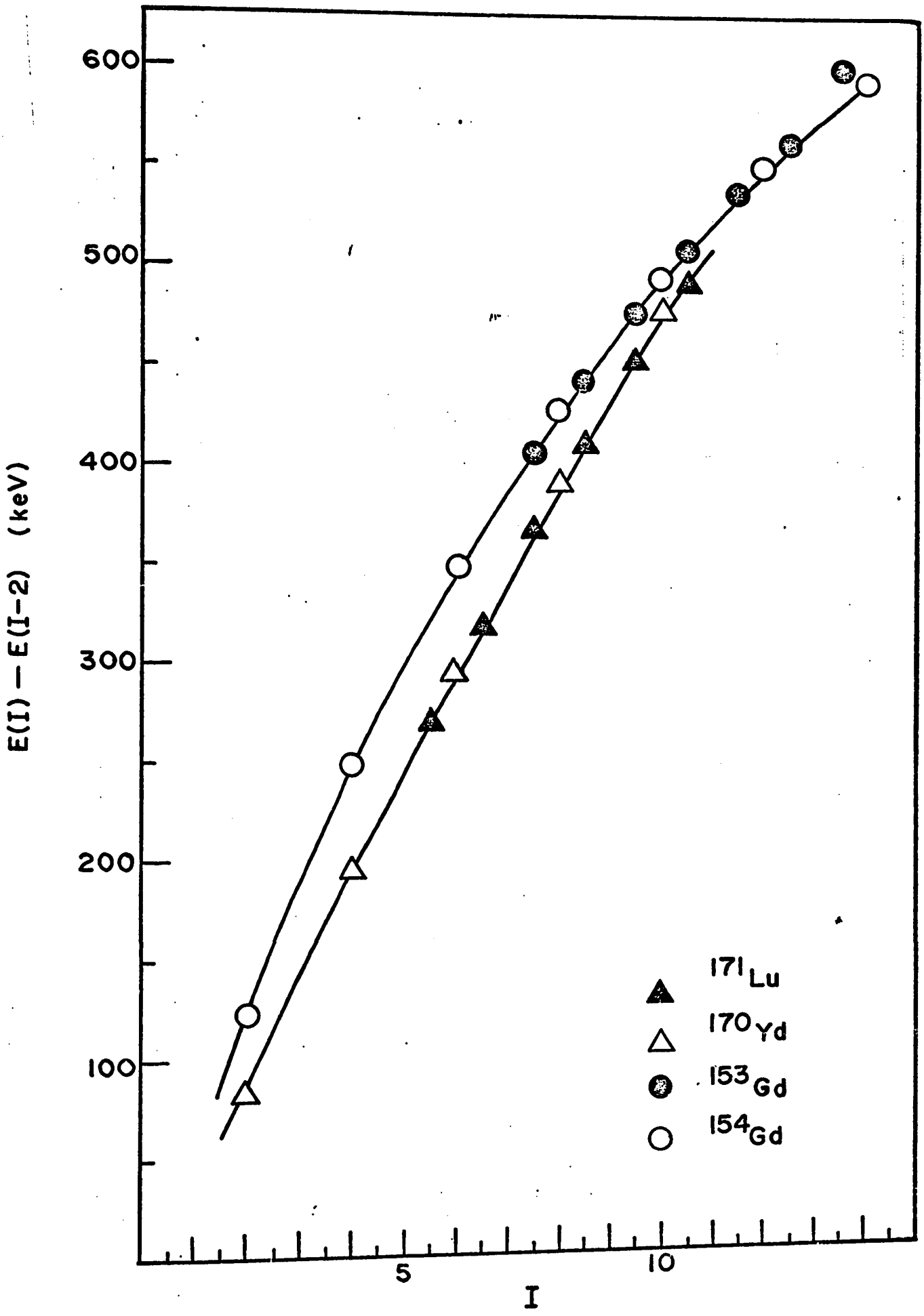
600
500
400
300
200
100
E(I) — E(I-2) (keV)
5
10
I
171Lu
170Yd
153Gd
154Gd

Table 1

Experimental and calculated energies and moments of inertia of bands in ^{153}Gd, ^{154}Gd ^{171}Lu and ^{170}Yb. Also shown are the values of I_K (keV^{-1}) and $C(keV^3)$ associated with each fit.

^{171}Lu (2)											
7/2+[404]	I	9/2	11/2	13/2	15/2	17/2	19/2	21/2	23/2	25/2	27/2
band	E_{expt}	122.1	269.2	440.2	634.1	849.7	1086.1	1341.2	(1613.8)		
$\mathcal{J}_{7/2}$=0.0365	E_{calc}	122.2	269.4	440.4	634.1	849.6	1085.7	1341.5	1616.2	1908.8	2218.6
C = 6.24 $\times 10^6$	$\mathcal{J}_I$	0.0371	0.0377	0.0383	0.0391	0.0398	0.0406	0.0414	0.0423	0.0431	0.0440
^{170}Yb (8)											
ground state	I	2	4	6	8	10	12	14	16	18	20
band	E_{expt}	84.2	277.7	572	962	1439	(1986)				
$\mathcal{J}_0$=0.0355	E_{calc}	84.0	276.9	572.3	962.3	1438.8	1994.1	2621.5	3315.0	4069.7	4881.1
C = 6.57 $\times 10^6$	$\mathcal{J}_I$	0.0359	0.0367	0.0378	0.0391	0.0406	0.0422	0.0438	0.0455	0.0472	0.0489
^{153}Gd (3)											
11/2-[505]	I	13/2	15/2	17/2	19/2	21/2	23/2	25/2	27/2	29/2	31/2
band	E_{expt}	363.4	575.0	804.7	1050.7	1311.8	1586.3	1872.3	≥2186.0		
$\mathcal{J}_{11/2}$=0.0330	E_{calc}	363.2	574.5	803.7	1049.6	1311.2	1587.6	1877.9	2181.6	2497.9	2826.3
C = 3.23 $\times 10^6$	$\mathcal{J}_I$	0.0347	0.0363	0.0379	0.0394	0.0409	0.0423	0.0438	0.0452	0.0465	0.0479
^{154}Gd (5)											
ground state	I	2	4	6	8	10	12	14	16	18	20
band	E_{expt}	122.9	371.1	717.9	1145.0	1638.4	2187.1	2780.5			
$\mathcal{J}_0$=0.0241	E_{calc}	119.2	369.6	719.1	1146.7	1638.6	2185.6	2780.9	3419.3	4096.9	4810.5
C = 2.08 $\times 10^6$	$\mathcal{J}_I$	0.0262	0.0296	0.0332	0.0368	0.0403	0.0437	0.0470	0.0501	0.0532	0.0561

Figure 2

The calculated moments of inertia for odd-even and even-even nuclei show the same variation with angular momentum.

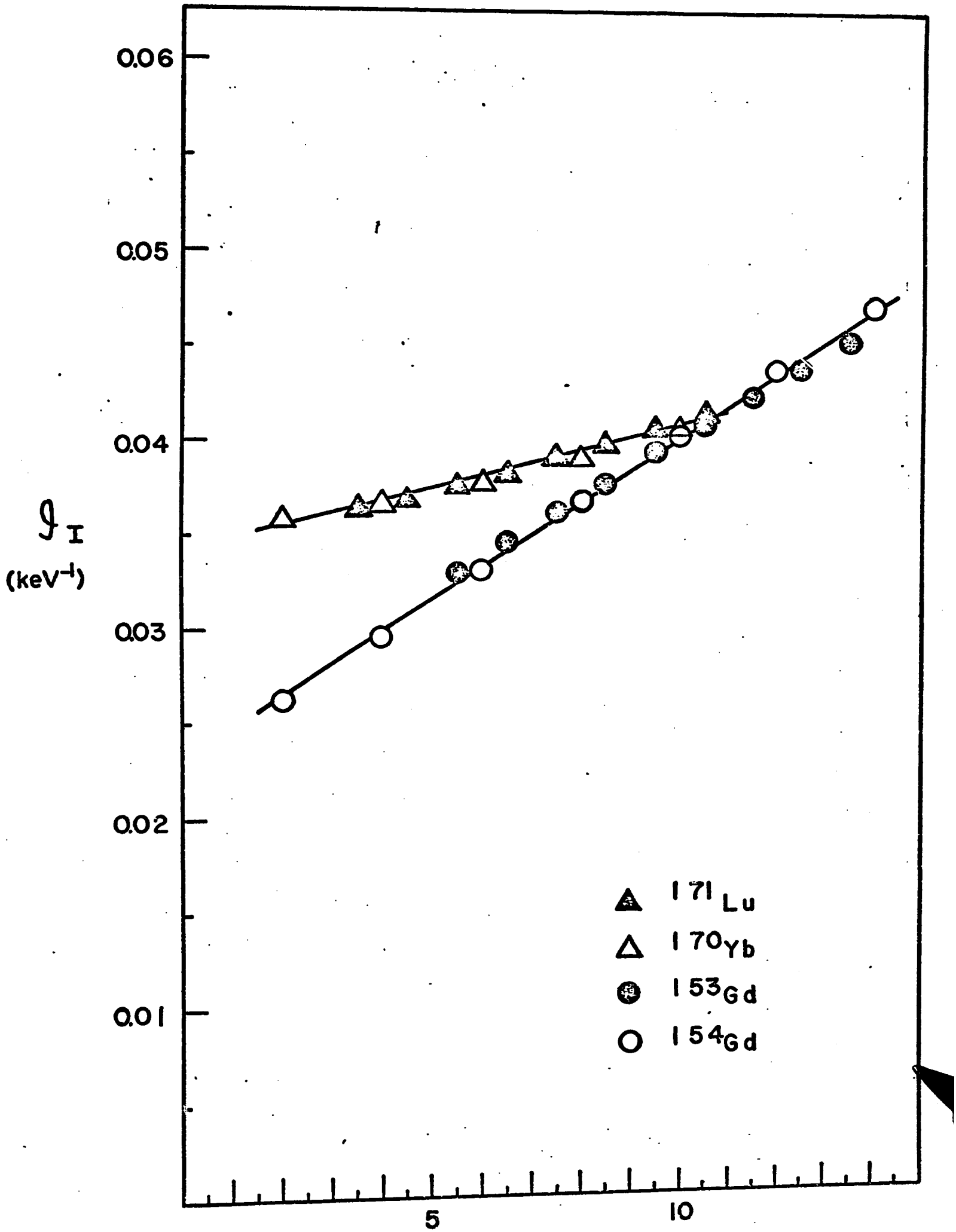
0.06
0.05
0.04
0.03
0.02
0.01
g_I
(keV^{-1})
5
10
^{171}Lu
^{170}Yb
^{153}Gd
^{154}Gd

The ad hoc expression originally formulated by Mariscotti et. al. (1) and recently theoretically justified by Volkov (6) is logically extended to odd-even nuclei by adopting the expression (7)

$$E_I(\mathcal{J}_I) = C(\mathcal{J}_I - \mathcal{J}_K)^2/2 + (I(I+1)-K(K+1))/2\mathcal{J}_I \ .$$

The parameters $\mathcal{J}_K$ and C are determined by a least squares fit to the equally weighted experimental excitation energies. The results are presented in Table 1. The variation of the moment of inertia as a function of spin is shown in Fig. 2. The qualitative similarity between neighbouring even-even and odd-even cases is impressive and suggests the desirability of including a variable moment of inertia in more sophisticated calculations.

The advantages of a variable moment of inertia model for bands in odd-even nuclei are now apparent and therefore the extension of the model to Coriolis mixed bands is under consideration. An inherent difficulty is that the variation of the moment of inertia implies the variation of the deformation which in turn gives rise to modified valence particle eigenfunctions and band head energies. Nonetheless such calculations may prove to be extremely fruitful.

The authors acknowledge useful discussions with A.B. Volkov and J. C. Waddington.

References

(1) M. A. J. Mariscotti, G. Scharff-Goldhaber, B. Buck, Phys. Rev. 178 (1969) 1864.

(2) P. R. Gregory, Z. Preibisz, J. C. Waddington and M. W. Johns, to be published.

(3) G. Løvhøiden, S. A. Hjorth, H. Ryde and L. Harms-Ringdahl, Nucl. Phys. A181 (1972) 589.

(4) P. H. Stelson and L. Grodzins, Nucl. Data (1965) 1, 21.

(5) I. Rezanka, F. M. Bemthol, J.O. Rasmussen, R. Stokstad, I. Fraser, J. Greenberg and D. A. Bromley, Nucl. Phys. A179 (1972) 51.

(6) A. B. Volkov, Phys. Lett. 35B (1971) 299.

(7) A. B. Volkov, to be published.

(8) H. Moringa, Nucl. Phys. 75 (1966) 385.